1-1-2018

The Biophysical Characterization of Caveolin-1

Sarah Plucinsky
Lehigh University, sarah.plucinsky@wagner.edu

The Biophysical Characterization of Caveolin-1

by

Sarah M. Plucinsky

A Dissertation

Presented to the Graduate and Research Committee

of Lehigh University

in Candidacy for the Degree of

Doctor of Philosophy

in

Chemistry

Lehigh University

January 2018

Approved and recommended for acceptance as a dissertation in partial fulfillment of the requirements for the degree of Doctor of Philosophy

Sarah Plucinsky
The Biophysical Characterization of Caveolin-1

11/14/17

Defense Date

Dissertation Director
Kerney J. Glover

Approved Date

Committee Members:

Robert A. Flowers, II

Damien Thévenin

Jim Roberts

Bryan Berger

ACKNOWLEDGMENTS

This dissertation would not have been possible without the contributions of several outstanding individuals who offered support and scientific discussion. First, I would like to thank Dr. Glover for his continued support throughout my graduate work and for his mentorship and guidance. The knowledge that I have acquired while working in the Glover lab has truly advanced my scientific career and that is in large part because of the motivation and guidance of Dr. Glover. I would also like to thank Dr. Jinwoo Lee who taught me everything I know about protein NMR and was instrumental in my first year of graduate school in introducing me to the field of caveolin-1 research. I would like to thank my committee members, Dr. Flowers, Dr. Roberts, Dr. Thevenin and Dr. Berger, for their mentorship throughout my graduate work. I want to thank the previous and current members of the Glover Lab for many years of scientific discussion and enjoyment in the lab. I have had the pleasure of interacting with several outstanding undergraduate researchers that have helped me with laboratory assistance. This dissertation is dedicated to my family for their unwavering support and motivation throughout my graduate career.

Table of contents

List of Figures

List of Tables

List of Appendices

List of abbreviations

GlyA: Glycophorin A

GST: glutathione S-transferase

Biotin maleimide: Nα-(3-Maleimidylpropionyl)Biocytin

NMR: Nuclear magnetic resonance

HSQC: Heteronuclear Single Quantum Coherence

TROSY-HSQC: Transverse relaxation optimized spectroscopy

PFOA: Perfluorooctanoic acid

CD: Circular dichroism spectroscopy

LMPG: lyso-myristoylphosphotidalglycerol

CSI: Chemical shift indexing plot

CHS: Cholesteryl hemisuccinate

CMC: critical micelle concentration

CRAC: Cholesterol recognition amino acid consensus

TCEP: *tris*(2-carboxyehtyl)phosphine

DMPC: 1,2-dimyristoyl-sn-glycero-3-phosphocholine

DHPC: 1,2-dihexanoyl-sn-glycero-3-phosphocholine

eNOS: endothelial nitric oxide synthase

PBS: Phosphate buffered salt

PEG: polyethylene glycol

SDS-Page: Sodium dodcylsulfate polyacrylamide gel electrophoresis

TBS: Tris bufferes saline

TBST: Tris buffered saline with tween

eNOS: endotheilial nitric oxide synthase

Abstract

The main topic of this doctoral dissertation is the biophysical characterization of caveolin-1. Caveolin-1 is an integral membrane protein that has been shown to be essential for the formation of caveolae. Caveolae are 50-100 nm invaginations in the plasma membrane that have a plethora of cellular functions including signal transduction, relieving mechano-stresses on the cell, and endocytosis. Caveolin-1 is at the center of all of the functions of caveolae and has been shown to play a predominant role in disease states. However, while there are a large number of biological studies on caveolin-1, there are few biophysical studies, leading to a lack of understanding of the structure, topology and oligomerization of caveolin-1. The progress made in these three main areas of caveolin-1 research as well as introducing a novel in vitro functional assay for caveolin-1 and a broadly applicable membrane protein isolation technique are introduced. In chapter 1, background and general information about caveolin-1 and the biophysical techniques that were utilized for its characterization are discussed. Chapter 2 discusses the structural characterization of a caveolin-1 construct containing residues 62-136 using NMR spectroscopy revealing that the N-terminal residues (62-85) were dynamic and caveolin-1 contains a helix-break-helix motif with two approximately equal length helices. Chapter 3 discusses the structural characterization of caveolin-1 residues (62-178) using NMR spectroscopy. Caveolin-1(62-178) is the longest construct of caveolin-1 to be structurally characterized and encompasses the previously uncharacterized C-terminal domain which formed a long helix. Additionally, caveolin-1 contains a helix-break-helix-break-helix motif. In chapter 4, alanine and phenylalanine scanning mutagenesis of caveolin-1 82-136, was utilized to identify key structural residues within both helix-1 and helix-2. In

chapter 5, the efforts to establish an in vitro functional assay for caveolin-1 utilizing the inhibition of endothelial nitric oxide synthase is presented. In chapter 6, cysteine scanning mutagenesis was utilized to evaluate the exposure of single residues in the caveolin-1 scaffolding domain to determine the topology of caveolin-1. Additionally, an evaluation of several different maleimide probes is presented. In chapter 7, a novel method to measure membrane protein oligomerization utilizing homo-FRET in liposomes is presented. Finally, in chapter 8 a purification method utilizing perfluorooctanoic acid (PFOA) to solubilize inclusion bodies is presented. This method has a three-fold advantage over conventional solubilization methods because: 1) PFOA can completely solubilize inclusion bodies, 2) PFOA is compatible with Ni-NTA chromatography and 3) PFOA is easily removed by detergent dialysis. Overall, this work represents significant advancements in understanding of the caveolin-1 protein.

Chapter 1: Caveolae, caveolin-1 and biophysical characterization of membrane proteins

Caveolae

The plasma membrane is a complex barrier which separates the interior of the cell from the extracellular environment. It is responsible for several vital biological functions such as the movement of molecules in and out of the cell. The membrane is composed of a variety of lipids and has been shown to contain 50% (w/w) protein (1). These proteins are called membrane proteins and are defined by their highly insoluble domains that interact with the membrane and participate in many of the functions that occur at the cell surface. These functions include transport of molecules across the membrane, cell-cell signaling, and enzymatic reactions (2). The fluid mosaic model was the original hypothesis of how the membrane was organized. The Fluid mosaic model states that the molecules in the plasma membrane diffuse freely in the membrane (3). However, over that last several decades several considerations have been taken into account that call into question the validity of this model. One major aspect is the high density of membrane proteins that cause a significant amount of crowding at the membrane surface which would hinder the free diffusion of molecules (4). In recent years, lipid segregation into distinct domains designated as lipid rafts has been observed. These “raft-like” domains are defined by their unique composition compared to the bulk plasma membrane and are often more rigid with higher concentrations of cholesterol and sphingomyelin (5).

While the existence of these rafts and their prevalence *in vivo* has been called into question, one well defined "raft-like" domain is called caveolae. Caveolae were first identified using electron microscopy in the 1950's (6). Caveolae are 50-100 nm invaginations within the plasma membrane that play a multifaceted role in cellular function. Most notably, they are involved in: mechano-protection, recruiting and concentrating signaling molecules, and endocytosis (7, 8, 9) (Figure 1-1). When there is pressure exerted on the membrane, it has been shown that caveolae will begin to flatten and increase the surface area of the cell, relieving the pressure to avoid cell lysis (10). When the pressure is removed caveolae reform at the cell surface. Caveolae have been shown to undergo non-clatharin dependent endocytosis. The highly curved nature of caveolae

facilitate vesicle formation and transport cargo across the cell (11). Finally, signaling molecules have been found at high levels within caveolae (12). Caveolae have been observed in several differentiated cell types but are found most predominantly in adipocytes and endothelial cells (13, 14). The loss of caveolae on the cell surface has been observed in several disease phenotypes such has heart disease, cancer, and muscular dystrophy and is often an indication of cellular dysfunction (15).

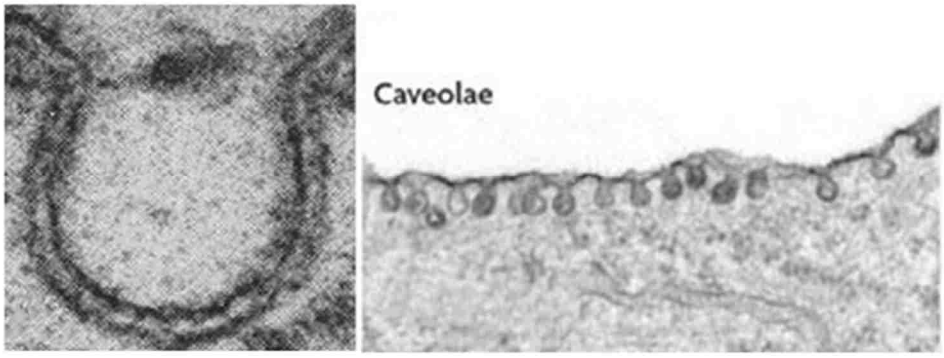

Nature Reviews Molecular Cell Biology **8**, 185-194 (March 2007)

Figure 1-1. A TEM image of a single caveolae. B) An image of the membrane surface showing a number of caveolae. (8, 16).

Cavoelae are enriched in cholesterol, sphingomyelin and an integral membrane protein called caveolin (17, 18) (Figure 1-2). The concentration of cholesterol within caveolae is found to be twice that of the bulk plasma membrane (8). The role of cholesterol in these microdomains has not been definitively characterized however the rigidity of cholesterol may stabilize the highly curved nature of caveolae. The role of cholesterol in caveolae stabilization is supported by a recent study of cells treated with cholesterol depleting drugs, which had significant changes in caveolae morphology (19). It is important to note that caveolae can be formed in *E. coli* cells, however, these domains are unique from those observed in mammalian cells (20). This was an unexpected finding because bacteria lack the necessary machinery to perform post-translational modifications such as palmitoylation and additionally are devoid of cholesterol. therefore, the role of cholesterol in caveolae formation is unclear, and further investigation is needed to elucidate the true effects of cholesterol on caveolae.

Sphingomyelin is also found to be enriched in caveolae, however recently the extent of this enrichment has been called into question (21, 22).

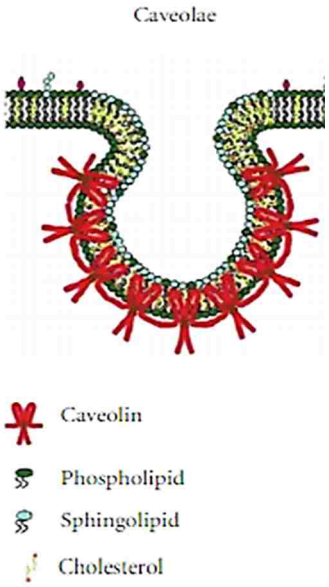

Figure 1-2. Cartoon representation of caveolae composition highlighting the enrichment of caveolin-1 and cholesterol (18).

Caveolin has been identified as the major protein component of caveolae. When the caveolin gene is silenced there is a complete loss of caveolae at the plasma membrane. Therefore caveolin is essential for the formation of caveolae. However, the cavin family of proteins that are also found in caveolae (23). There are four isoforms of cavin (cavin-1, -2, -3, -4) that have been shown to be targeted to the plasma membrane in the presence of cavolin-1 (23). The expression of cavin has been shown to have an effect on caveolae formation and morphology. Additionally, the cavin family has been shown to regulate several caveolae functions such as endocytosis (24). While there is evidence

that caveolin-1 and cavin interact at the plasma membrane, little is known about the formation of these complexes. It is therefore unclear what factors truly play a role in the formation and stabilization of caveolae. What is clear is that caveolin-1 is vital to normal caveolae formation and function.

Caveolin

There are three isoforms of the caveolin protein (-1, -2, and -3) with caveolin-1 being the most ubiquitous being found in most cell types (18) (Figure 1-3). Importantly, caveolin-1 has been shown to be essential for the formation of caveolae (25). All three proteins have significant sequence similarity both within the isoforms and also across species. Because of the high degree of conservation, the caveolin protein is crucial for cellular function. Often the functions of caveolin-1 are also applied to the other isoforms. However there are several stark differences within the isoforms that make it unlikely that these three proteins have similar structure and function. Of the three, caveolin-1 is the most ubiquitous, and is found in most terminally differentiated cell types, for example in adipocytes (13). Caveolin-2 is often co-expressed with caveolin-1 and it is thought that caveolin-1 and caveolin-2 form a hetero-oligomeric complex (26). It has been shown that when the expression of caveolin-1 is down regulated, caveolin-2 does not traffic to the membrane and is retained in the golgi (27). Therefore, caveolin-2 is unable to form caveolae in the absence of caveolin-1 (28). Caveolin-3 is expressed exclusively in muscles cells and has been shown to be related to muscular dystrophy and heart disease. Caveolin-3 is able to form caveolae in the absence of caveolin-1 (29, 30). The functional differences show that while there is significant sequence similarity

between the three isoforms, there may be structural differences that govern their overall function and distribution. In particular it should be noted that caveolin-1 contains only 3 C-terminal cysteines (C133, C143 and C156), which have been shown to be palmitoylated *in vivo* (31). Caveolin-2 and caveolin-3 contain 5 and 9 cysteine residues respectively (highlighted in Figure 1-3). It has been shown that caveolin-2 and caveolin-3 are palmitoylated, however there has not been an extensive study to show at which cysteines or if the palmitoylation has any effect on function (31). These major differences in expression and post translation modifications highlight the need for unique studies on caveolin-2 and caveolin-3 that explore their structure and function outside of the context of caveolin-1.

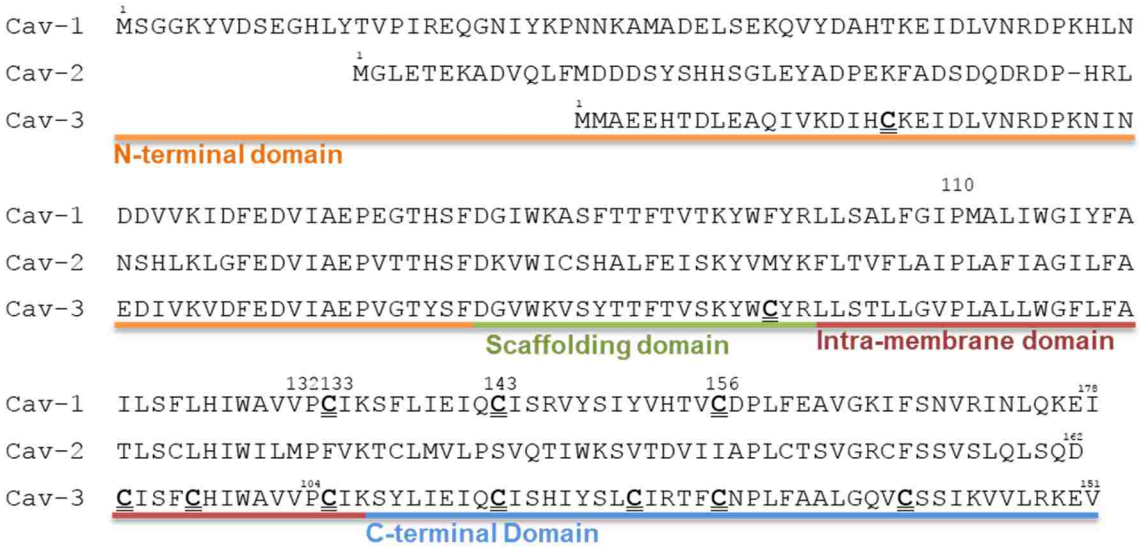

Figure 1-3. Sequence alignment of the three isoforms of caveolin-1. The cysteine residues are underlined to highlight differences in the sequence. The different domains are also highlighted to show where they start and stop in each of the isoforms.

Caveolin-1 is a 22 kDa protein that was first identified in 1992 by two separate groups. Initially the protein was labeled by one group as VIP21 and the other as caveolin (32, 33). Eventually, it was discovered that VIP21 and caveolin were in fact the same protein, with the consensus name being caveolin-1 (34). When the caveolin-1 gene is silenced it has been shown that caveolae completely disappear from the cell surface indicating that caveolin-1 is essential for the formation of caveolae (25) (Figure 1-4).

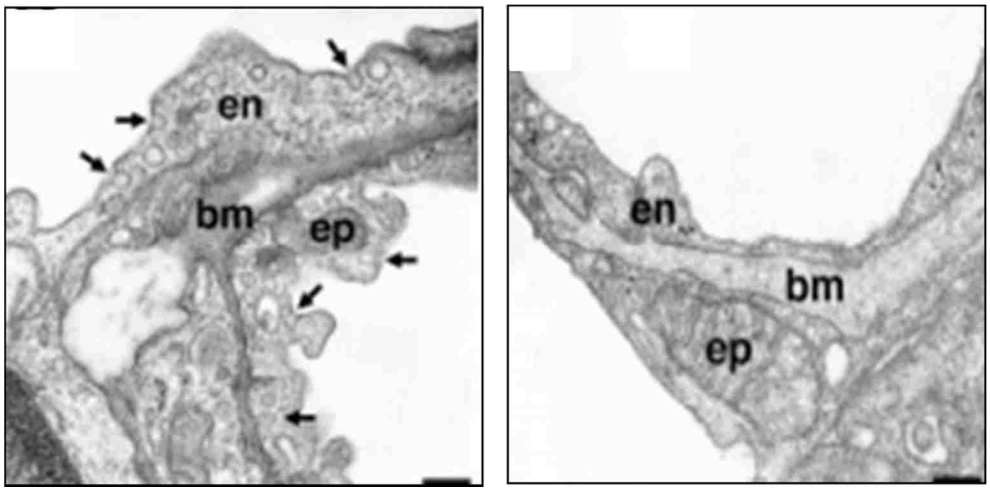

Figure 1-4. Left panel: lung tissue from mice that are expressing caveolin-1. Black arrows highlight caveolae. Right panel: lung tissue from mice with caveolin-1 gene silenced (25).

Caveolin-1 has been shown to be intimately related to several functions of caveolae (35). For example, caveolin-1 has been shown to regulate the endocytosis of molecules through caveolae. Caveolae endocytosis is markedly decreased in the presence of high levels of caveolin-1. therefore caveolin-1 is a negative regulator of caveolae

endocytosis (36). Caveolin-1 has been shown to interact both directly and indirectly with an array of signaling molecules such as endothelial nitric oxide synthase (eNOS), G-proteins, and Src-like kinases (35, 37, 38). Initially, these molecules were proposed to interact with caveolin-1 through a caveolin binding domain (CBM) (ΦXΦXXXXΦ, where Φ is an aromatic amino acid) (39). The role of this motif has been challenged in recent structural studies of several of the proposed caveolin-1 binding partners showed that many of the CBM domains were buried in the core of the protein structure (40, 41). While many of the interactions have been called into question, one established interaction has been identified between caveolin-1 and eNOS. Caveolin-1 has been shown to inhibit eNOS activity *in vivo* and *in vitro* (37). When the caveolin-1 gene is silenced or a frameshift mutation is present in the C-terminal domain, there is a buildup of nitric oxide within endothelial cells that leads to disease-type phenotypes (42).

When caveolin-1 is isolated using detergents such as triton X-114 it has been found in large oligomeric complexes (200, 400, and 600 kDa). Therefore the accepted hypothesis is that caveolin-1 oligomerizes *in vivo* (43). These large oligomeric complexes are thought to stabilize the highly curved nature of caveolae by forming a scaffold which inserts into the plasma membrane. However, in vitro reconstitution into both detergent micelles and bilayers have shown that caveolin-1 is monomeric (44)and unpublished results). The true oligomeric state of caveolin-1 *in vivo* is unclear. The use of mild detergents to extract caveolin-1 complexes may induce non-native oligomerization due to the highly insoluble nature of caveolin-1. Additionally, it is difficult to isolate what is the main factor in oligomer formation. For example, cholesterol has been shown to interact with caveolin-1 and is enriched in caveolae and could therefore play an important role in

the formation and stability of caveolin-1 oligomers (45). However, there is no conclusive evidence to support a role of cholesterol in caveolin-1 oligomer formation. The oligomeric state of caveolin-1 and what drives the formation of these complexes is still very much under investigation in the scientific community.

The misregulation and mutation of the caveolin-1 protein has been implicated in a large number of diseases such as heart disease and breast cancer (46, 47). However, the direct effect of caveolin-1 in disease states is not clearly understood. For example, the loss of caveolin-1 expression has been shown to lead to an increase in tumor proliferation and metastasis in several types of cancer (48). Uniquely, in prostate cancer it has been found that caveolin-1 is over-expressed and that the silencing of the caveolin-1 gene actually has positive effect in slowing prostate cancer progression (49). Therefore, the role of caveolin-1 in cancer progression seems to be cell type specific. A point mutation in the caveolin-1 C-terminal domain (Proline 132 to Leucine) has also been identified in patients with breast cancer and is thought to cause an increase in metastasis (50). However, while it was initially reported that 16% of patients possess the P132L mutation, recent studies have called the prevalence of P132L into question (51, 52). The ambiguity of the role of caveolin-1 in breast cancer is an example of the lack of understanding of how caveolin-1 functions *in vivo* and the true effects of its misregulation. To fully understand and appreciate how caveolin-1 participates in cellular disease it is necessary to have a detailed understanding of the protein on a molecular level.

Caveolin-1 Structure

The first structural characterization of caveolin-1 was based on primary sequence analysis (53). It was found that caveolin-1 contains a large hydrophobic domain (33 amino acids), that is too long to span the bilayer once, but is too short to span the bilayer twice (Figure 1-5). The lack of soluble residues means that any loop/turn would have to reside in the membrane. To establish which side of the plasma membrane the N- and C-termini reside, glycosylation, biotinylation and immunofluorescence studies were employed (43, 54, 55). Based on these studies caveolin-1 is predicted to have an unusual topology with the protein forming a turn within the hydrophobic core of the membrane that results in both the N- and C- termini facing the cytosol with no portion of the polypeptide entering the extracellular space (43). However, this would place unsatisfied hydrogen bonds within the water depleted membrane. But recent molecular simulations studies along with fluorescence experiments agree with the placement of the turn within the membrane (56).

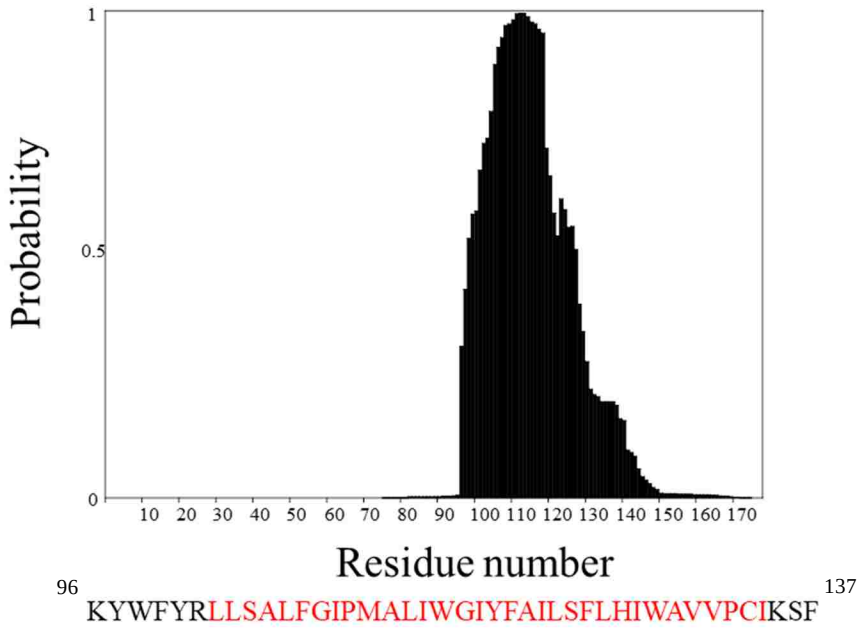

Figure 1-5. Hydropathy plot of caveolin-1. Residues in red are the hydrophobic domain.

Caveolin-1 is traditionally represented by four domains that are based on primary sequence analysis: the N-terminal domain (residues 1-81), the scaffolding domain (residues 82-101), the intra-membrane domain (residues 102-134), and the C-terminal domain (residues 135-178) (53) (Figure 1-6). Initially, structural studies were carried out on individual caveolin-1 domains. The limitation to use only short peptides was largely due to the difficulty of purification and solubility of full length caveolin-1.

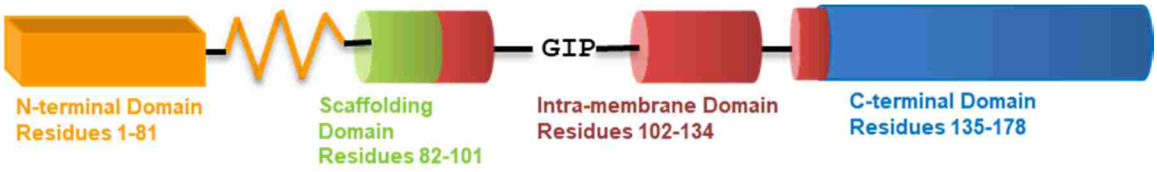

Figure 1-6. Cartoon illustrating the domains of caveolin-1. The residues within each domain are indicated. The proposed break region is indicated by "GIP".

A caveolin construct containing only the N-terminal domain (residues 1-81) has been shown to be unstructured in an aqueous environment (57). This domain is the most variable between the isoforms of the caveolin family and it has been shown that the removal of the first 61 amino acids has no effect on the trafficking of caveolin-1 or the formation of caveolae (58). However, it has been implicated in several interactions of the caveolin-1 protein such as cholesterol recruitment (59). Additionally, the N-terminal domain has been shown to be phosphorylated which may be critical for caveolin-1 function (60). There are two forms of caveolin-1 that are found *in vivo*, caveolin-1α and caveolin-1β. The two forms are identical with the exception that caveolin-1β is lacking the first 31 amino acid residues and begins at methionine 32 (61).

The next domain has been designated the scaffolding domain (residues 82-101). The scaffolding domain appears to be important for binding signaling molecules such as endothelial nitric oxide synthase, along with oligomerization and cholesterol binding (35). Initially, based on primary sequence analysis it was predicted that the scaffolding domain was a short amphipathic helix which rested on the surface of the membrane (53). The scaffolding domain was found to be unstructured in DPC micelles using NMR spectroscopy. The addition of a small portion of the intramembrane domain increased the

helical character of the scaffolding domain (62). However, another study utilizing solid state NMR spectroscopy showed that in the presence of cholesterol a similar construct contained beta sheet characteristic (63). The final characterization of the scaffolding domain showed that in the presence of the full intramembrane domain a portion of the scaffolding domain contained both unstructured and helical residues (residues 82-86 are unstructured and residues 87-101 are helical). Importantly, the helix continues from the scaffolding domain into the intramembrane domain (56). The contrast in these studies could be attributed to the presence of cholesterol in the Hoop et. al. experiments however; it is difficult to make absolute assumptions without the full protein being present (63).

The intramembrane domain has been postulated to be critical for the formation of caveolae and is the most conserved region between all of the caveolin-1 isoforms (Figure 1-2). Initially, based on primary sequence analysis, the intramembrane domain was predicted to contain two helices separated by a short four residue break (residues 108-111) (53). Recent structural studies using NMR have examined the secondary structure of the intramembrane domain and revealed that this domain contains a helix-break-helix motif which is consistent with the proposed U-shaped topology of caveolin-1 (64). The break region was also confirmed utilizing site directed mutagenesis although it was shown to include only three residues 108, 109 and 110. This break is hypothesized to be the location of the intramembrane turn (64). The insertion of the two helices into the bilayer can be thought of as a "wedge" which will asymmetrically separate lipid molecules in the bilayer causing the curvature found in caveolae (Figure 1-7).

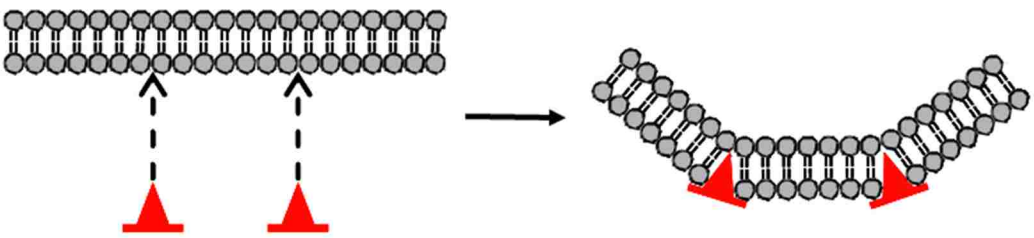

Figure 1-7. Cartoon representation of caveolin-1 insertions into the bilayer.

The C-terminal domain has been the most under-studied domain of the caveolin-1 protein. The previous structural studies were performed on truncated constructs that do not contain the C-terminal domain. The C-terminal domain is predicted to be an amphipathic helix that rests on the surface of the membrane (53). The location of the C-terminal helix at the membrane surface is supported by the presence of three cysteine residues within the C-terminal domain which have been shown to be palmitoylated *in vivo* (31). Additionally the C-terminal domain has been implicated in several functions of caveolin-1. The C-terminal domain has been shown to be important for caveolin-1 trafficking to the membrane and formation of the large oligomeric complexes that are thought to stabilize caveolae(58, 65, 66). Additionally, many caveolin-1 binding partners such as endothelial nitric oxide synthase, connexin, and Retrovirus NSP4, also interact directly with the C-terminal domain making it an important binding region within caveolin-1 (37, 67, 68). Recent studies have identified a frameshift mutation within the C-terminal domain that is found in patients with familial pulmonary arterial hypertension and a patient with idiopathic pulmonary hypertension (69, 70). It is clear that the C-terminal domain is intimately involved in caveolin-1 function and needs to be structurally characterized to fully elucidate its role.

The structure of caveolin-1 is an on-going and important question that needs to be answered to fully understand how this protein functions within the cell. One of the goals of the following chapters is to present new work that has contributed to the structural determination of caveolin-1.

Biophysical Characterization of Membrane proteins

About 30% of proteins encoded in the genome are membrane proteins (71). However, the majority of solved protein structures consist of soluble proteins (72). The lack of structural data is because of the unique challenges that membrane proteins present not only for structure determination but also for functional characterization. Membrane protein expression and purification has been a major challenge in the structural characterization of membrane proteins because of the large amounts of protein that are needed to utilize conventional techniques such as X-ray crystallography. The low protein production is due to the toxicity of membrane proteins when they are over-expressed in expression systems such as *E. coli* and the relative low level of native expression in mammalian cells (73). Therefore, the majority of membrane protein structures that have been solved are extremely stable helical bundles or beta-barrels which can be expressed and purified at high levels (74). While these proteins have advanced several structural techniques, less stable membrane proteins that have unique motifs have not been explored. Chapter 8 in this dissertation presents work on the purification of highly insoluble membrane proteins for structural determination.

Another major challenge in the biophysical characterization of membrane proteins is the need for a suitable membrane mimetic to solubilize the protein. The presence of

these mimetics can cause significant challenges when utilizing traditional techniques because the mimetic alters the size of the protein-lipid complex and also most lipids/detergents are not compatible with these techniques. For example, X-ray crystallography has gained popularity as the gold standard of structural determination. There is a significant challenge when trying to apply X-ray crystallography to membrane proteins because most lipids and detergents will affect crystal formation (75). It is however essential to keep these molecules around in order to prevent the membrane proteins from aggregating or falling out of solution. Additionally, the crystalline lattice that is formed by some detergents may make it impossible to glean intermediate or fluid information about the protein structure that may be present in the fluid membrane. The presence of lipids has also been shown to have a major effect on membrane protein structure and proteins can have different specificity for lipid environments (76). There are three main membrane mimetics that are commonly used in membrane protein characterization: micelles, bicelles and vesicles (Figure 1-8). Each of these mimetics contains their own advantages, but not all are compatible with all techniques.

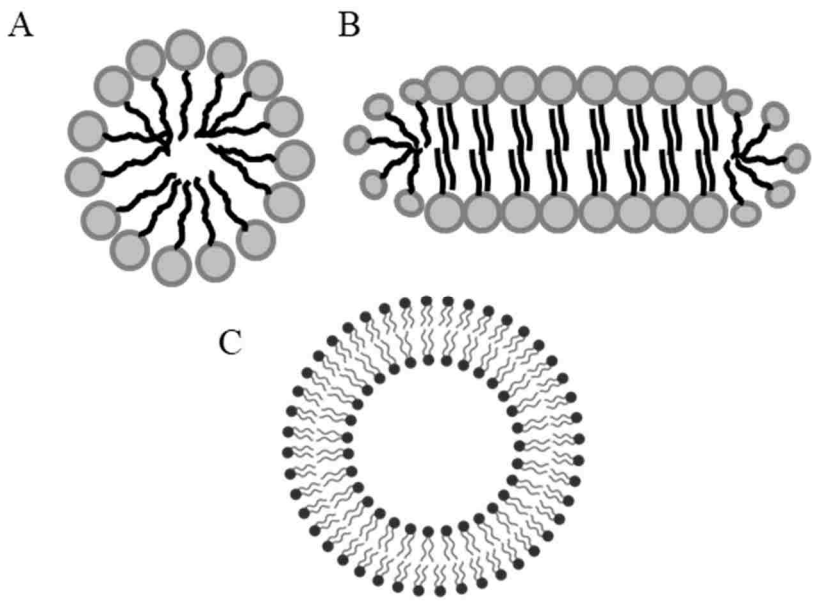

Figure 1-8 Illustrations of A) Micelle, B) bicelle, and C) vesicle

Micelles

Micelles are detergent aggregates which contain a water depleted core and a polar surface. Most often, they are represented as spherical aggregates however studies have shown that the shape of the aggregates depends greatly on the characteristics of the detergent (77). Micelles are small and dynamic with a constant flux between aggregate and monomer. The critical micelle concentration (CMC) is the minimum amount of detergent required to form aggregates. Micelles are an attractive membrane mimetic and have been utilized in membrane protein structure determination by solution state NMR and also to lesser extent X-ray crystallography (77, 78). It has been shown that most membrane proteins can maintain their secondary structure in micelles and also that there are very few changes between structures determined in bilayer mimetics and micelles (79). However, micelles have the disadvantage that they are not a true bilayer and cannot

handle the introduction of physiological levels of molecules such as cholesterol (which can be important in the case of raft associated proteins). Additionally, micelles are small and highly curved which can introduce artifacts in membrane protein structure determination (80).

Bicelles

Bicelles are discoidal lipid/detergent aggregates that have been shown to have several advantages over micelles and are still compatible with several biophysical techniques such as NMR spectroscopy (81). Bicelles are formed by mixing a long chain phospholipid with a short chain phospholipid or detergent molecules. One common system is bicelles composed of DMPC (long chain) and DHPC (short chain). The long chain phospholipid forms a long planar region and the short chain molecules form a rim that protects the hydrophobic core of the long chain lipid form the solution (82, 83). Bicelles have an advantage because the short chain detergent molecules are in flux which makes these structures dynamic (84). The size and other properties of bicelles are governed by the molar ratio of the long chain lipid to the short chain detergent designated as q. It is possible to tune the size of the planar region by adjusting the molar ratio to give a larger q. Additionally, it has been shown that bicelles can be formed with lipid molecules of various chain lengths making the overall thickness tunable. This tunability allows for characterization of membrane proteins in a true bilayer environment under more native like conditions. However, it is not possible to determine membrane protein orientation in bicelles, and at lower q values (between 0.1-0.3) the planar region becomes very small and there is significant mixing with the rim region (forming a mixed micelle

rather than a true bilayer). The incorporation of large amounts of cholesterol into bicelles can also be challenging with the upper limit being ~5%. Additionally bicelles have been used extensively in solid state NMR, though some techniques require large amounts of protein which can be difficult to achieve (85).

Vesicles

Vesicles are hollow aggregates of bilayer forming amphipathic molecules. Vesicles that are formed from phospholipids are referred to as liposomes. When phospholipids are exposed to an aqueous environment they will spontaneously form vesicles. Liposomes can contain one layer (uni-lamellar) or multiple layers multi-lamellar). Liposomes are often characterized by size which can be controlled based on preparation. Unilammelar liposomes can be formed in three sizes small (SUV), medium (MUV) and large (LUV). Often SUVs are unstable and will fuse over time to form LUVs. Liposomes are widely used as drug delivery tools because of their biocompatibility (86). Vesicles have several advantages when compared to both bicelles and micelles. Because liposomes contain an aqueous interior it is possible to determine the orientation of a protein in the bilayer. Additionally, vesicles allow high levels of incorporation of cholesterol which can be used to determine how cholesterol affects a proteins behavior. However, vesicles cannot be utilized in the structural techniques such as NMR spectroscopy and X-ray crystallography.

Biophysical techniques]

Circular dichroism spectroscopy

The most common technique to determine the major secondary structure components of a membrane protein is circular dichroism spectroscopy (CD). Based on the differences in how molecules absorb right and left handed polarized light, it is possible to assign the overall secondary structure. A α-helical protein shows a signature of a maximum at 190 nm and two distinct minima at 208 and 222 nm. A beta sheet shows a minimum at 217 nm. A random coiled structure shows a minimum at 204 nm (Figure 1-9) (87). Additionally, using CD it is possible to determine how changes in the protein environment (pH, concentration, or temperature) affect the secondary structure. While CD can give an overall picture of the secondary structure of a membrane protein, it cannot give residue specific structural information. It is possible to use fitting algorithms to determine the percentage of each type of structure, however there can be significant bias if there is a large helical content in the protein which can dominate the spectra. It can be difficult to acquire quantitative data from a CD spectrum because there can be increases in peak intensity based on concentration and also background from helical character. It is known that if a protein contains even a small amount of helical character, the spectrum will be overpowered by that signal (88). The lack of resolution means that there is a need for an additional technique to give more atomistic information. However, CD is a powerful tool to quickly determine if a protein is folded or to examine how environmental elements affect protein structure.

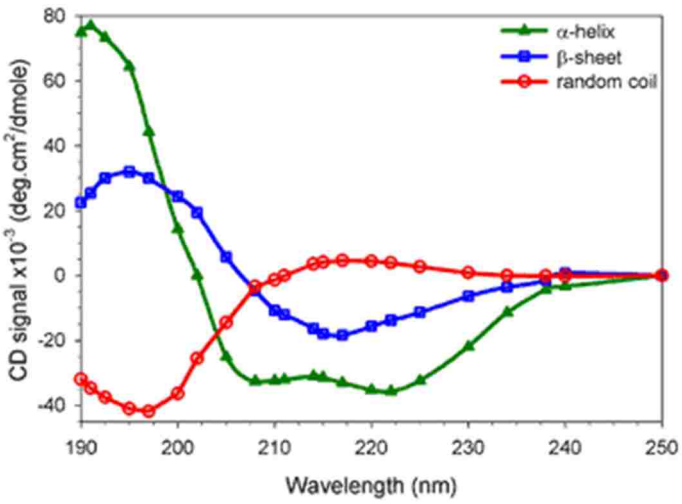

Figure 1-9. Representative spectra for the three major secondary structures of proteins (87).

NMR Spectroscopy

Nuclear magnetic resonance spectroscopy has emerged as a powerful tool to elucidate protein structure. It is especially attractive for the structural determination of membrane proteins because of its compatibility with many detergent systems. therefore membrane protein structure can be determined in solution (89). Nuclear magnetic resonance has the advantage that it can give residue specific structural information based on chemical shift. Using isotopically labeled proteins it is possible to elucidate the secondary and tertiary structure of the protein. Protein NMR relies on samples that are enriched in isotopically labeled atoms such as ^{15}N and ^{13}C. There have been several advancements in the expression and purification of isotopically labeled protein samples that are suitable for NMR experiments (90).

Structural determination utilizing solution state NMR requires several consecutive experiments that are compiled to elucidate the overall secondary structure. The initial experiment is called heteronuclear single quantum correlation (HSQC). The chemical shifts in a two dimensional NMR spectrum (HSQC) arises from the transfer of magnetism from the backbone nitrogen and amide proton. This is often the first experiment to determine the optimal detergent system for further NMR experiments. A well dispersed spectrum indicates that all of the amino acids are experiencing a unique environment and therefore the protein is well structured under the current conditions. It can also be utilized for monitoring structural changes introduced by the addition of point mutations.

After a high quality HSQC is obtained, three dimensional NMR experiments (HNCA, HNCACB, and HNCO), can be performed to give the chemical shifts of the Cα carbon, Cβ carbon and carbonyl carbon. However, when utilizing NMR for membrane protein structure determination, there is a significant amount of spectral overlap. The high degree of overlap can make peak assignment challenging. It is therefore necessary to utilize specific amino acid labeling to help identify peaks within the NMR spectra. In this technique only a single amino acid in the protein sequence (for example alanine) is isotopically labeled. Specific amino acid labeling can aid significantly in assigning backbone chemical shifts. After all the chemical shifts have been assigned it is possible to predict the secondary structure of the protein backbone.

Homo-FRET

A common biophysical technique to determine protein-protein interactions is Förster resonance energy transfer (FRET). This technique utilizes two fluorophores that have overlapping excitation and emission spectra. When one fluorophore is excited (designated as the donor), energy is transferred to the second fluorophore (designated as the acceptor). This energy transfer can only occur when the donor labeled molecule and the acceptor labeled molecule are in close proximity (91) . While FRET experiments can give valuable information about what proteins belong to a complex, it lacks the ability to distinguish oligomeric states between the same molecules. For example, if the same protein forms a homo-oligomeric complex, FRET will be observed. However, there is no way to glean the number of monomers that are contained within the complex.

Homo-FRET is a process in which a single fluorophore transfers emission energy with itself upon excitation. Therefore, homo-FRET is most pronounced in fluorophores with a small Stokes shift. Advantageously, homo-FRET can be used to determine the oligomeric state of membrane proteins by measuring changes in steady-state anisotropy as a function of the degree in which the population of subunits are labeled with a fluorophore (92). If the identical fluorophores are part of an oligomeric complex, they will reside in close proximity to each other, and thus be able to participate in energy transfer. However, during the energy transfer process, polarization is lost, and the degree of polarization loss can be used to determine the order (e.g. dimers *vs*. trimers) of the complex (93). Practically, various degrees of subunit labeling can be achieved by mixing, in appropriate ratios, solutions of labeled and unlabeled membrane protein, and plotting the anisotropy as a function of fractional labeling. Normally, homo-FRET is

measured by photobleaching of the fluorophore (to generate the dark sample) and measuring the change in the anisotropy at different ratios of non-photobleached fluorophore (considered the light sample) (92, 94). Chapter 6, discusses the efforts to utilize point mutations that render a “dark” fluorophore that is compatible with homo-FRET.

All of these techniques are powerful tools for the biophysical characterization of membrane proteins. However, because caveolin-1 is a unique protein, there is added complexity when utilizing each technique. Therefore, not only is the use of these techniques being discussed in this dissertation but also several novel approaches to these techniques are presented.

Chapter2. Structural characterization of Caveolin-1(62-136).

Abstract

Previous structural studies of caveolin-1 have been conducted on each domain separately. While these studies have given important initial insights, because of the unique topology of caveolin-1 it is necessary to analyze the domains in the context of one another. Additionally, caveolin-1 has been implicated in several biological functions but without structural context it is not possible to determine mechanistically how the protein affects cellular biology. To begin to garner a more complete structural picture of caveolin-1 a construct containing residues 62-136 was analyzed in LMPG micelles utilizing NMR spectroscopy. This construct contains the intact scaffolding and intramembrane domains as well as a portion of the N-terminal domain which has not been previously characterized in the context of the other two domains. This study revealed that caveolin-1 contains a helix-break helix motif with Helix-1 containing residues 89-107 and Helix-2 containing residues 111-128. The remaining residues were found to be unstructured. This is the first study to indicate that the N-terminal domain is unstructured in the presence of the scaffolding and intramembrane domain. Additionally, the study shows that the addition of N-terminal residues, does not affect the length of Helix-1.

Introduction.

Previous studies conducted on the intramembrane domain identified three key residues (108, 109, and 110) that are proposed to be the location of the helix break (turn) that facilitates return of the C-terminus to the cytoplasmic face of the plasma membrane. This study was the first reported evidence of the Helix-break-Helix motif (64). However, this study examined only the transmembrane domain and a portion of the scaffolding domain (residues 96-136). Interestingly, the first helix was shown to start at the beginning of the construct indicating that a construct with additional N-terminal residues may show a continuation of the helix. To explore further where the first transmembrane helix begins, the truncated construct was expanded to include residues 82-136 which encompasses the scaffolding domain. Through secondary structure analysis it was revealed that the first helix actually begins at A87 (56). This indicates that the previously termed "scaffolding domain" is actually part of helix-1 and there is no break in the helix to separate these regions as was proposed by previous models (53).

While both of these previous studies gave vital information on the scaffolding and intramembrane domains, they lacked any portion of the N-terminal domain. The N-terminal domain has been shown to be the most variable among the three isoforms of caveolin (See Figure 1-3). Caveolin-1 has the longest N-terminal region followed by caveolin-2 and -3 respectively. Studies examining the role of the different caveolin-1 domains have shown that a deletion construct lacking the first 61 amino acids, has been shown to be functional (58). However, while the N-terminal domain does not play a role in the formation of caveolae, it has been shown to perform several other roles such as cholesterol binding and also several sites of phosphorylation have been identified.

To elucidate the effect of N-terminal residues on the previously reported helix-break-helix motif, an additional 20 amino acids were appended to the previously studied construct caveolin-1 (82-136). This construct, caveolin-1(62-136), contains the intact scaffolding and transmembrane domains and the portion of the N-terminal domain that has been shown to be important for the formation of caveolae. Using NMR spectroscopy the secondary structure of caveolin-1(62-136) was determined. Three dimensional NMR experiments and specific labeling protocols were performed to assist in the secondary structure assignment of this region.

Materials and Methods

Expression of isotopically labeled samples for NMR spectroscopy

Caveolin-1(62-136)_M111L_C133S (caveolin-1(62-136)) was expressed as a TrpLE fusion as described previously (see Appendix 2-1) (95). Methionine 111 was mutated to leucine to prevent off target cleavage. The mutation of this position is a conservative mutation as position 111 is a leucine in both caveolin-2 and caveolin-3. Cysteine 133 was mutated to serine to prevent non-biologically relevant disulfide bonding. This mutation has been shown to have no effect on the protein function *in vivo* (31). Briefly, caveolin-1(62-136) was cloned into pet24a and transformed into BL-21(DE3) cells. A 5 mL overnight culture was used to inoculate 1L of M9 minimal media that was enriched with ^{15}N nitrogen to yield an isotopically labeled sample for NMR (see Appendix 2-2). Cultures were grown for 18 hours at 37°C and harvested at 5780 x*g* for 30 minutes. Cell pellets were them washed with 200 mL of 0.9% (w/v) saline and stored at -80C until purification. Similarly, doubly (^{15}N and ^{13}C) and triply (^{15}N, ^{13}C and ^{2}H) labeled samples were generated utilizing the optimized protocol of Marley *et. al.*(96). Briefly, 1L LB cultures were grown to an optimal OD_{600} of 0.8 and harvested at 5000 x*g* for 30 min at 25°C. Cells were washed by resuspension in minimal media containing no ^{13}C or ^{15}N and pelleted again at 5000 x*g* for 30 minutes at 25°C. The pellets were resuspended in minimal media containing ^{13}C and ^{15}N and grown for 2 hours at 37C. Protein expression was induced by the addition of 1 mM IPTG and the culture was grown for another 8 hours. In the case of the triply labeled samples, the procedure was the same except that the water in the media was supplemented by D_2O. Specific labeled samples

were generated utilizing M9 minimal media supplemented with ^{15}N amino acid of interest (see Appendix 2-3).

Purification

All isotopically labeled samples were purified utilizing the previously reported method by Diefenderfer et. al. (95). Briefly, cell pellets were resuspended in 200 mL of 20% sucrose solution and lysed by sonication for 15 minutes. Inclusion bodies were isolated by centrifugation for 2 hours at 27,000 x*g* at 15°C. Pellets were washed with a solution containing 1% triton X-100 to remove any membrane components and sonicated for 15 minutes. The solution was centrifuged for 1 hour at 27,000 x*g* at 15°C. Pellets were resuspended with 80 mL of 1 M Tris pH 8.0 and sonicated for 10 minutes. After sonication, 180 mL of isopropyl alcohol was added and the solution was centrifuged at 27,500 x*g* for 2 hours. The supernatant was removed and the inclusion body pellet was resuspended in 30 mL of 88% formic acid. The TrpLE protein was cleaved by addition of 0.2 g of cyanogen bromide and reacted for 18 hours. The fusion was separated from caveolin-1 utilizing reverse phase HPLC.

Protein reconstitution

Based on previous data, LMPG was chosen as the detergent for these studies. Please note that extensive detergent screening was performed on this construct with only LMPG yielding high quality NMR spectra. In addition, LMPG is a detergent that is widely used for membrane protein NMR studies (97, 98, 99, 100). Approximately 1 mM of lyophilized protein was reconstituted into 600 μL of 100 mM LMPG, 20 mM Pi pH

7.0, 100 mM NaCl and 10% D_2O. Samples were vortexed and heated to homogeneity and filtered through a 0.2 uM spin filter.

NMR Spectroscopy

TROSY-HSQC spectrum were acquired for caveolin-1(62-136) on a 600 MHz Bruker Advance II spectrometer equipped with a cryoprobe using 256 (^{15}N dimension) x 2048 (^{1}H dimension) complex points and 64 scans. Additional 3-dimensional experiments (HNCA, HNCACB, HNCO and HN(CO)CA) were also acquired to aid in the backbone assignment. All NMR data was processed utilizing NMRpipe. Dihedral angles were obtained utilizing the processing program TALOS+.

Chemical shift indexing (CSI) plot

The CSI plot is generated by subtracting the reference Cα chemical shift from the Cα that was recorded from the spectrum. If the resulting value is positive it demonstrates α-helical structure, if the value is negative it demonstrates β-sheet (101). Importantly, when identifying secondary structure, a stretch of either positive or negative values is needed.

Results and Discussion

Secondary Structure assignment of Caveolin-1(62-136)

Figure 2-1 shows the assigned 2-dimensional ^{1}H-^{15}N TROSY-HSQC spectrum of caveolin-1(62-136). From the TROSY-HSQC it can be seen that the NMR spectrum of caveolin-1(62-136) has a significant amount of spectral dispersion indicating that the protein is well behaved under the experimental conditions. Once a high quality HSQC spectrum is obtained, giving the nitrogen and amide proton chemical shift, it is necessary to determine which amino acid corresponds to which peak. Three-dimensional experiments can give the chemical shifts for the Cα carbon (HNCA), C-beta carbon (HNCACB), and carbonyl carbon (HNCO and HN(CO)CA).

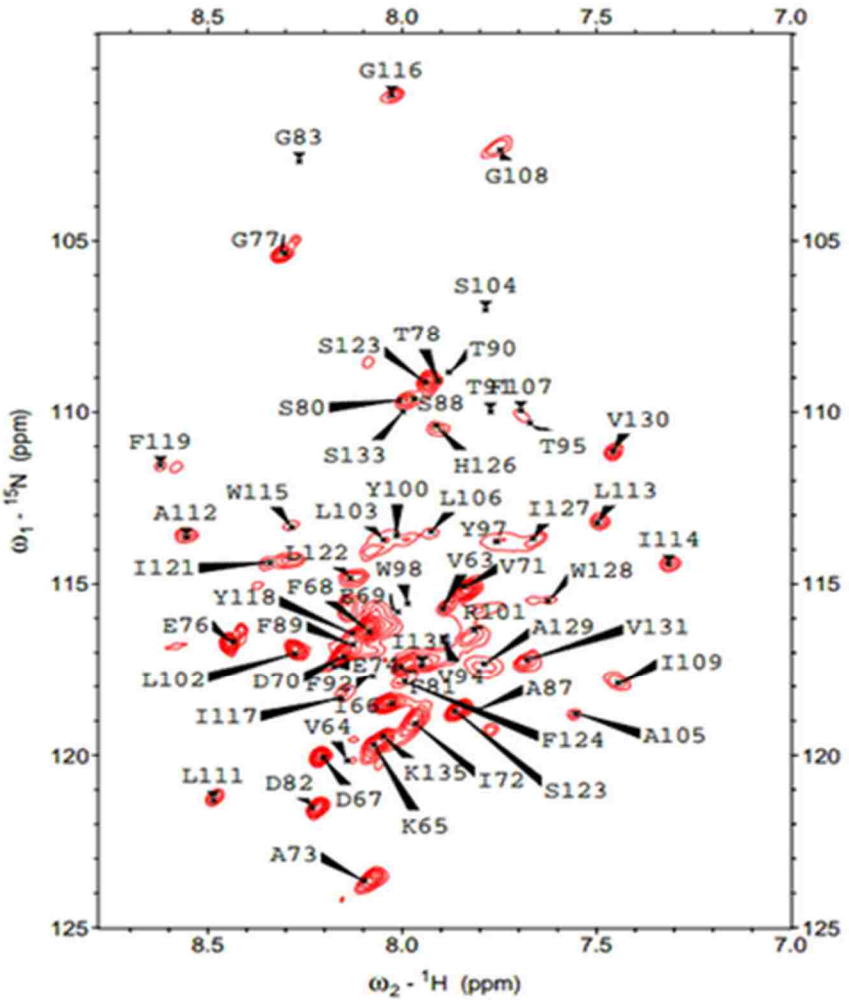

Figure 2-1. Assigned TROSY-HSQC of caveolin-1 (62-136).

Specific amino acid labeling

Because caveolin-1 is a membrane protein, there is also a significant amount of spectral overlap that can make assigning the HSQC difficult. To aid in the assignment specific amino acid labeling can be employed to help elucidate which amino acids correspond to a particular peak. There are several considerations when choosing which amino acid to specifically label in order to yield the most effective data. First, the amino

acid should be prevalent in the sequence and also well dispersed. Examining the sequence of caveolin-1(62-136) (see Appendix 2-1), there are several prevalent residues that are well dispersed throughout the sequence. For example, there are six valine residues that are located throughout the protein sequence. Once the specific labeled spectrum is acquired, it can be overlaid with the WT spectrum to identify which peaks correspond (in this case) to valine (Figure 2-2).

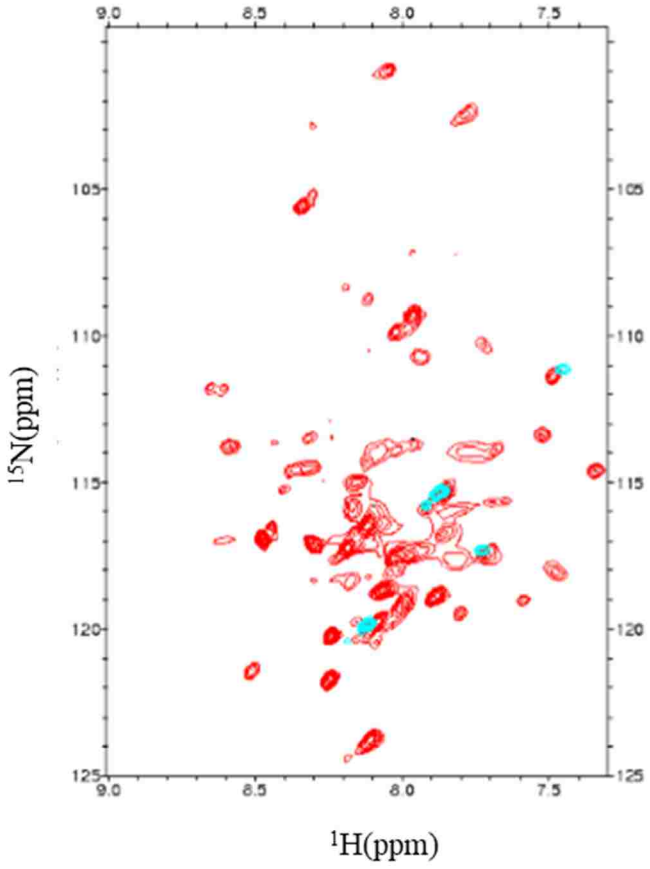

Figure 2-2. Overlay of caveolin-1(62-136) (red) and specifically labeled valine caveolin-1(62-136) (cyan).

The second consideration when selecting which amino acid to specifically label is the degree of scrambling. Because several amino acids are used as the template for other amino acids during protein expression (i.e. glycine and phenylalanine) they are not ideal choices for specific labeling (90). For example, there are 8 phenylalanine residues in caveolin-1(62-136) and therefore only 8 peaks should be on the HSQC. However, the phenylalanine spectrum is showing more than 8 peaks indicating that there is some degree of off target isotopic labeling (Figure 2-3). However, it is still possible to utilize the data obtained by comparing with the other spectrum obtained but caution should be used.

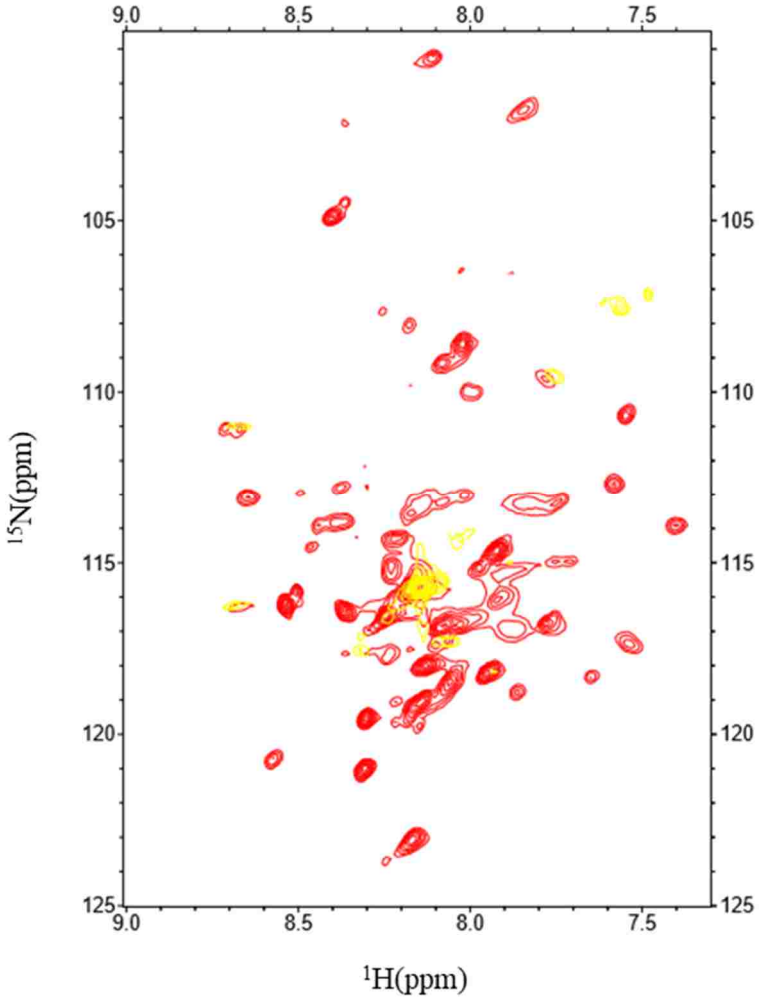

Figure 2-3. Overlay of caveolin-1(62-136) (red) and specifically labeled phenylalanine (yellow).

Chemical shift index plot

The HNCA is the most sensitive of the three dimensional experiments and is often the first performed (101). Because the nitrogen is coupled to the Cα carbon on the same amino acid and also the α carbon on the previous amino acid, a strong and weak peak are observed. The strong peak is associated with the Cα that is directly bonded to the

nitrogen and the weak peak is associated with the previous Cα carbon (Cα-1). This allows for assignment of the protein backbone in a stepwise fashion. Additionally, the Cα chemical shifts can give information about the secondary structure of the protein. Figure 2-4 shows the chemical shift indexing plot of caveolin-1(62-136). As can be seen within the CSI plot of 62-136, there are two distinct helices that contain a break at residues G108, I109, and P110. Interestingly, the N-terminal residues appear to be showing some beta sheet characteristic (stretch of negative values). However, because the CSI plot relies only on the C-α chemical shift, it is necessary to refine the structural prediction by adding more restraints.

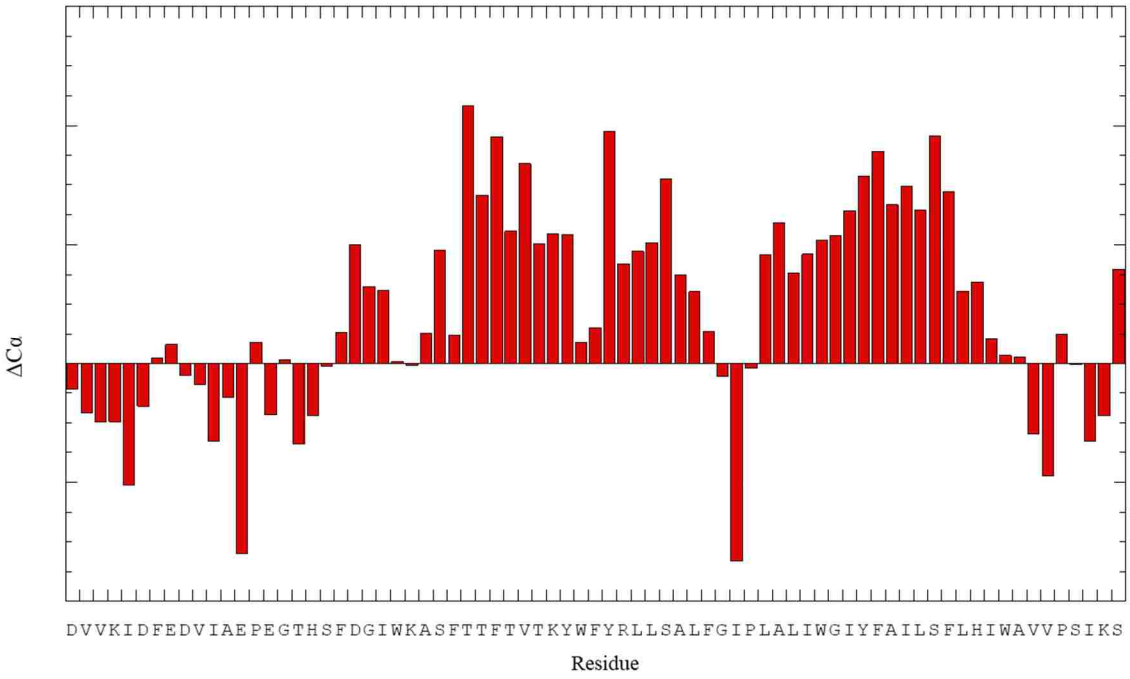

Figure 2-4. The Chemical shift indexing plot of caveolin-1(62-136)

While the HNCA contains a large amount of preliminary information, it can often be difficult to assign a full spectrum using only the Cα chemical shift. This is due in large

part to significant overlap and peak ambiguity. The HN(CA)CB gives the Cβ chemical shift. The HNCO will give the CO chemical shift. The combination of all of these experiments along with the specific amino acid labeling allow for complete backbone assignment of the protein. The chemical shifts obtained can then be utilized to predict the overall secondary structure.

Talos+ prediction for caveolin-1(62-136)

To determine the secondary structure of caveolin-1(62-136) the chemical shifts for the HN, N, Cα, Cβ and CO chemical shifts can be entered into TALOS+. Table 2-1 shows the TALOS+ output file. This file indicates the assigned Φ and Ψ angles based on the restraints that are entered from the backbone assignments. Φ angles around -60 and Ψ angles around -40 indicate an α-helix. Clearly, from this data, caveolin-1(62-136) shows a helix-break-helix motif with Helix-1 containing residues 87-107 followed by a three residue break and Helix-2 containing residues 111-128. Residues 62-86 are shown to be dynamic. When comparing the Talos+ prediction with the CSI plot, there are several residues in the N-terminal region with negative ΔCα values which could indicate the presence of β structure. However the N-terminal region is dynamic based on the Φ and Ψ angles predicted by Talos+. Additionally, there is a short segment of helical residues within the N-terminal domain (residues 78-81). This single helix turn was previously predicted and is thought to aid in membrane attachment (53).

Residue	Φ angles	Ψ angles	Structure Prediction	Residue	Φ angles	Ψ angles	Structure Prediction
D	----------	---------	None	Y	-62.196	-41.304	α-helix
V	-117.321	140.184	Dynamic	R	-62.356	-42.091	α-helix
V	-98.852	140.681	Dynamic	L	-62.048	-44.97	α-helix
K	-86.934	135.048	Dynamic	L	-60.966	-43.951	α-helix
I	-115.187	133.807	Dynamic	S	-64.009	-38.429	α-helix
D	-87.828	118.907	Dynamic	A	-64.347	-42.146	α-helix
F	-117.577	140.82	Dynamic	L	-64.116	-42.612	α-helix
E	-98.677	137.93	Dynamic	F	-87.852	0.537	α-helix
D	-93.109	-15.174	Dynamic	G	90.559	2.564	unstructured
V	-117.85	127.953	Dynamic	I	-86.158	129.854	unstructured
I	-95.148	-16.137	Dynamic	P	-59.382	140.555	unstructured
A	-94.14	161.392	Dynamic	L	-54.127	-38.561	α-helix
E	-83.383	136.48	Dynamic	A	-60.213	-39.198	α-helix
P	-69.411	148.881	Dynamic	L	-65.687	-41.329	α-helix
E	-83.036	131.988	Dynamic	I	-63.827	-42.572	α-helix
G	77.638	10.305	Dynamic	W	-67.21	-37.725	α-helix
T	-60.375	-40.752	α-helix	G	-72.463	-40.14	α-helix
H	-62.201	-43.477	α-helix	I	-67.228	-40.026	α-helix
S	-69.838	-30.784	α-helix	Y	-64.836	-40.901	α-helix
F	-67.965	-35.879	α-helix	F	-65.118	-38.802	α-helix
D	-79.402	-10.415	Dynamic	A	-66.815	-39.364	α-helix
G	83.88	16.12	Dynamic	I	-65.104	-45.313	α-helix
I	-67.556	-22.703	Dynamic	L	-65.843	-42.467	α-helix
W	-82.324	-21.343	Dynamic	S	-68.467	-38.701	α-helix
K	-76.72	-23.606	Dynamic	F	-63.778	-37.488	α-helix
A	-67.641	-36.472	α-helix	L	-60.795	-46.389	α-helix
S	-67.436	-36.365	α-helix	H	-64.893	-41.228	α-helix
F	-64.512	-45.214	α-helix	I	-67.803	27.275	α-helix
T	-65.138	-36.406	α-helix	W	-88.141	-18.04	Dynamic
T	-62.98	-40.967	α-helix	A	-89.369	-9.301	Dynamic
F	-76.844	-27.585	α-helix	V	-106.302	2.888	Dynamic
T	-62.563	-41.032	α-helix	V	-84.904	130.917	Dynamic
V	-63.123	-40.627	α-helix	P	-63.012	145.178	Dynamic
T	-66.431	-39.997	α-helix	S	-87.195	-4.42	Dynamic
K	-62.344	-39.45	α-helix	I	-112.535	-2.614	Dynamic
Y	-66.196	-39.699	α-helix	K	-84.364	116.019	Dynamic
W	-62.902	-39.367	α-helix	S	----------	----------	None
F	-62.483	-44.139	α-helix				

Table 2-1. Talos+ data for caveolin-1 (62-163).

Based on the Talos+ data a preliminary model of the secondary structure of caveolin-1(62-136) can be determined (Figure 2-5). From the data presented caveolin-1 contains a helix-break-helix motif which is in agreement with previous structural characterization. Interestingly the addition of N-terminal residues has no effect on the location of the start of Helix-1. By determining the secondary structure of caveolin-1 (62-136), a greater understanding the complete structure of caveolin-1is achievable.

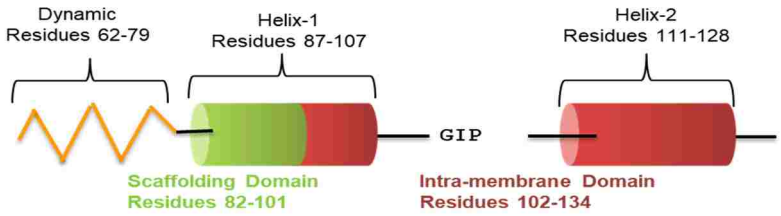

Figure 2-5. Cartoon model of the secondary structure of caveolin-1(63-136).

Conclusions

Using solution state NMR spectroscopy the secondary structure of caveolin-1(62-136) was assigned and it was determined that the protein contains a dynamic N-terminal domain and that the scaffolding and intramembrane domains form a helix-break-helix motif. Interestingly, there is a short stretch of helical amino acids in the N-terminal domain (about four residues) which can indicate that there is a single helix turn. This finding is in agreement with previous structure predictions that predicted the N-terminal domain contains a short helix that is important for membrane attachment. This is the first characterization of the functional portion of the N-terminal domain in the context of the scaffolding and intramembrane domain. The presence of the short helix turn highlights that working with larger protein constructs (that contain several protein domains) is vital as the previous circular dichroism spectroscopy showed that the N-terminal domain alone is unstructured(57). This also highlights the need to use structural techniques that can give structural assignments with greater resolution so that small structural nuances can be determined.

The determination of the secondary structure of caveolin-1 is not only vital for understanding the protein function it also introduces a new class of structural proteins whose function is to shape the membrane. The unique helix-break-helix motif is the key to understanding how caveolin-1 works to shape the membrane and form caveolae. Additionally, the secondary structure can also help to understand how the protein interacts with its proposed binding partners.

Appendix 2.1- Sequence for NMR studies

Caveolin-1(61-136)_M111L_C133S	DVVKIDFEDVIAEPEGTHSFDGIWKASFTTFTVTKYWFY RLLSALFGIP**L**ALIWGIYFAILSFLHIWAVVP**S**IKS

Appendix 2-2. Recipe for auto-induction media

MDG starter
10 μL 1 M $MgSO_4$
1 μL 1000X trace metals
50 μL 25% aspartate
100 μL 50XM
40 μL 40% glucose
4.8 mL sterile water
5 μL 1000X kanamycin

N-5052
14.196 grams Na_2HPO_4
13.609 grams KH_2HPO_4
1.42 grams Na_2SO_4
1956 mL water
5.45 grams $^{15}NH_4Cl$
4 mL 1 M $MgSO_4$
400 μL 1000X trace metals
40 mL 50x5052

Appendix 2-3. Recipe for specific amino acid labeling media

1L of M9 media
778mL of H2O 200mL of 5X M9 salts Na2HPO4 : 33.9g KH2PO4 : 15g … NaCl : 2.5g … NH4Cl : 5.0g 2mL of 1M MgSO4 20mL of 20% Glucose 0.1mL of 1M CaCl2 Weigh out 500mg of 19 amino acids and add into 1L M9 media Microwave 1-2mins to aid dissolution Cool and pH to 7 Add 100mg of 15N amino acid Sterile filter Pour into sterile 6L flask

Growth conditions
Start growth at 37°C (1mL of MDAG starter into 1L of M9 media) Shake at 225rpm Induce with IPTG when O.D. is between 0.6 and 0.7 (usually takes 4-5hr) 6hr growth after inducing

Chapter 3: Structural characterization of the caveolin-1 C-terminal domain

Abstract

The structural characterization of caveolin-1 has been focused on short non-functional peptides. While these studied have given invaluable insight into caveolin-1, there is a need to study not only a longer construct which contains all the caveolin-1 domains but also a construct that has been shown to be functional. Caveolin-1 residues 62-178 contain the functional portion of the N-terminal domain and the intact scaffolding, intramembrane and C-terminal domains. Importantly this construct has been shown to be functional *in vivo*. Additionally, the intact C-terminal domain has not been previously characterized, but has been shown to be vital for the biological function of caveolin-1. Complete backbone assignments of caveolin-1(62-178) were made, and it was determined that residues 62-80 were dynamic, residues 89-107, 111-128, and 132-175 were helical, and residues 81-88, 108-110, and 129-131 represent unstructured breaks between the helices. When this construct was compared to one lacking the C-terminal domain (residues 62-136), it was observed that its presence produced modest but significant chemical shift perturbations in the regions 80-103 and 129-136.

Introduction

Typically, caveolin-1 is divided into four domains: the N-terminal domain (residues 1-81), the scaffolding domain (residues 82-101), the intramembrane domain (102-134), and the C-terminal domain (residues 135-178) (figure 1-3). The N-terminal domain has been identified as a key binding domain within caveolin-1 interacting with other molecules and also cholesterol (59, 102). The intramembrane domain is postulated to be the critical structural domain of caveolin-1. It has been shown that the intramembrane domain contains a helix-break-helix motif and that the break is the location of the intramembrane turn which gives caveolae its shape (64). Arguably the most characterized domain within caveolin-1 is the scaffolding domain. The scaffolding domain peptide has been identified as the major binding and oligomerization domain within caveolin-1 (66). The scaffolding domain is postulated to interact with several signaling molecules such as SRC kinase and endothelial nitric synthase (103, 104). Additionally, the scaffolding domain contains a cholesterol recognition amino acid consensus (CRAC) motif, however, the role of this motif in cholesterol recognition is unclear (45).

Surprisingly, very little is known about the C-terminal domain. The initial characterization of the C-terminal domain was based on primary sequence analysis which predicted that it formed an amphipathic helix which rests on the surface of the membrane (9, 53). The location of the C-terminal domain at the membrane surface is supported by the presence of three cysteine residues in the C-terminal domain that have been shown to be palmitoylated *in vivo*, and that the C-terminal domain is important for membrane attachment (31, 65).

However, there have been no experimental studies to validate these conclusions despite the fact that biological studies have demonstrated that the C-terminal domain is vital for the overall function of caveolin-1. The C-terminal domain plays important roles in the movement of the protein from the Golgi apparatus to the plasma membrane and in membrane attachment (58, 65). *In vivo*, caveolin-1 is isolated as a high molecular weight oligomeric complex. The initial oligomerization of caveolin-1 has been attributed to the scaffolding domain (residues 82-101), but the formation of networks of oligomers has been shown to be governed by the C-terminal domain (66). This implies that the C-terminal domain is required for the formation of the hallmark striated coat that is formed at the membrane surface to help stabilize caveolae (33). Additionally, many caveolin-1 binding partners such as endothelial nitric oxide synthase, connexin, and Retrovirus NSP4, interact directly with the C-terminal domain making it an important binding region within caveolin-1 (37, 67, 68). Clearly, the C-terminal domain plays a plethora of important biological roles. To begin to understand the structural context of the C-terminal domain in caveolin-1, the secondary structure of a construct of caveolin-1 containing residues 62-178 which includes the C-terminal domain was determined using NMR spectroscopy. This construct is functional as it has been shown to have a behavior *in vivo* that is indistinguishable from that of the wild-type protein (58).

Materials and Methods

Design of Caveolin-1 constructs

Caveolin-1 residues 62-178 (Caveolin-1(62-178)) was expressed as a TrpLE fusion in *E. coli* (see appendix 3-1). Methionine 111, which is not strictly conserved with respect to the other caveolin isoforms, was mutated to leucine to facilitate cyanogen bromide cleavage. Caveolin-1 has three sites of cysteine palmitoylation (133, 143, 156). However *in vivo* studies have clearly shown that removal of palmitoylation by mutation of cysteine residues 133, 143, and 156 to serine, does not affect the correct trafficking of the protein to caveolae (31).

NMR sample preparation

Uniformly ^{15}N-labeled caveolin-1(62-178) was prepared as described previously by Diefenderfer *et al* and Studier *et al* (95, 105). ^{2}H, ^{15}N, and ^{13}C labeled samples were prepared as described in Marley *et al* (96) (described in detail in Chapter 2). To aid in the assignment of the Caveolin-1(62-178) spectra, specific amino acid labeling was employed (I, V, F, S, A, L, Y) using previously described methods (64, 106). Caveolin-1(62-178) NMR samples were prepared by dissolving 6.5 mg, of lyophilized protein into 600 μL of buffer containing 100 mM lyso-myristoylphosphatidylglycerol, 20 mM phosphate pH 7.0, 100 mM sodium chloride and 10% (v/v) D_2O to yield a 1 mM sample. Samples were then filtered through a 0.2 mM regenerated cellulose spin filter.

NMR experiments

TROSY-based pulse programs were utilized for NMR experiments (107, 108). The ^{1}H-^{15}N HSQC, HNCA, HNCACB, HNCACO, and HNCO experiments were acquired on a 600 MHz Bruker Avance II NMR spectrometer equipped with a cryoprobe. Additional HNCA and ^{1}H-^{15}N HSQC experiments performed on caveolin-1(62-178) were acquired on an 850 MHz Bruker Avance III NMR spectrometer equipped with a room temperature probe. The spectra were processed using NMRpipe and Sparky (109, 110). The assigned chemical shifts were then processed using TALOS+ (111).

Chemical shift perturbation

The chemical shift perturbation plot was prepared using the method of Ziarek *et al*, using the average amide chemical shift differences from caveolin-1(62-178) and an equivalent data set from a construct containing residues 62-136(112).

Equation 3.1

$$\Delta\delta = \sqrt{\left[(\omega HN)^2 + \left(0.1(\omega N)^2\right)\right]}$$

Chemical shift index plot

The chemical shift index plot was generated by subtracting the reference Cα chemical shift from the observed Cα chemical shift for each residue (101). If the ΔCα is $\pm$ 0.7 from the reference Cα, the residue cannot be assigned a consensus secondary structure and is labeled as ambiguous or coil. A stretch of positive ΔCα values is indicative of α-helical secondary structure.

Circular Dichroism spectroscopy

Circular dichroism experiments were performed using a JASCO circular dichroism spectrophotometer (Easton, MD). The experiments were carried out at 37°C in a 0.1 mm cuvette. The blank and protein spectra were collected from 260 to 190 nm using a bandwidth of 1 nm, a step size of 0.5 nm and 16 accumulations.

Results and Discussion

Circular dichroism spectroscopy of caveolin-1(62-178)

To determine the overall secondary structure of caveolin-1(62-178) circular dichroism was performed. From the spectrum it is clear that caveolin-1(62-178) has significant helical character based on the minima at 208 nm and 222 nm and the maximum at 190 nm (Figure 3-1). This agrees well with previous data that the scaffolding and intramembrane domains are mostly helical with only small non-helical regions. This also gives insight that the C-terminal domain is also helical. This result agrees with previous primary sequence analysis that predicted the C-terminal domain is an amphipathic helix (53).

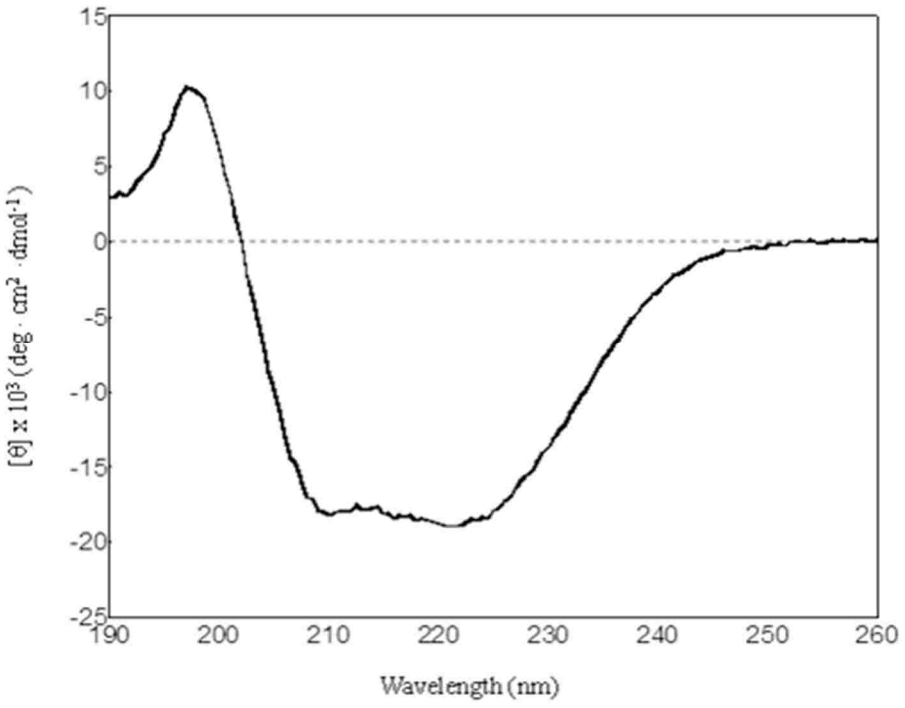

Figure 3-1. CD spectrum of caveolin-1(62-178) (113).

Secondary structure assignment of caveolin-1(62-178)

To begin to form a better understanding of the secondary structure of caveolin-1(62-178), chemical shifts were obtained for the HN, N, Cα, Cβ and CO using NMR spectroscopy. Utilizing the chemical shifts from all of the experiments it is possible to make complete backbone assignments of caveolin-1 (62-178) in lyso-myristoylphosphatidylglycerol (LMPG) micelles (Figure 3-2). From the spectrum, it can be seen that there is significant overlap between the peaks. This can make assigning chemical shifts challenging and therefore specific amino acid labeling can be employed to help identify which peaks in the HSQC correspond to particular residues by overlaying with the wild type spectrum.

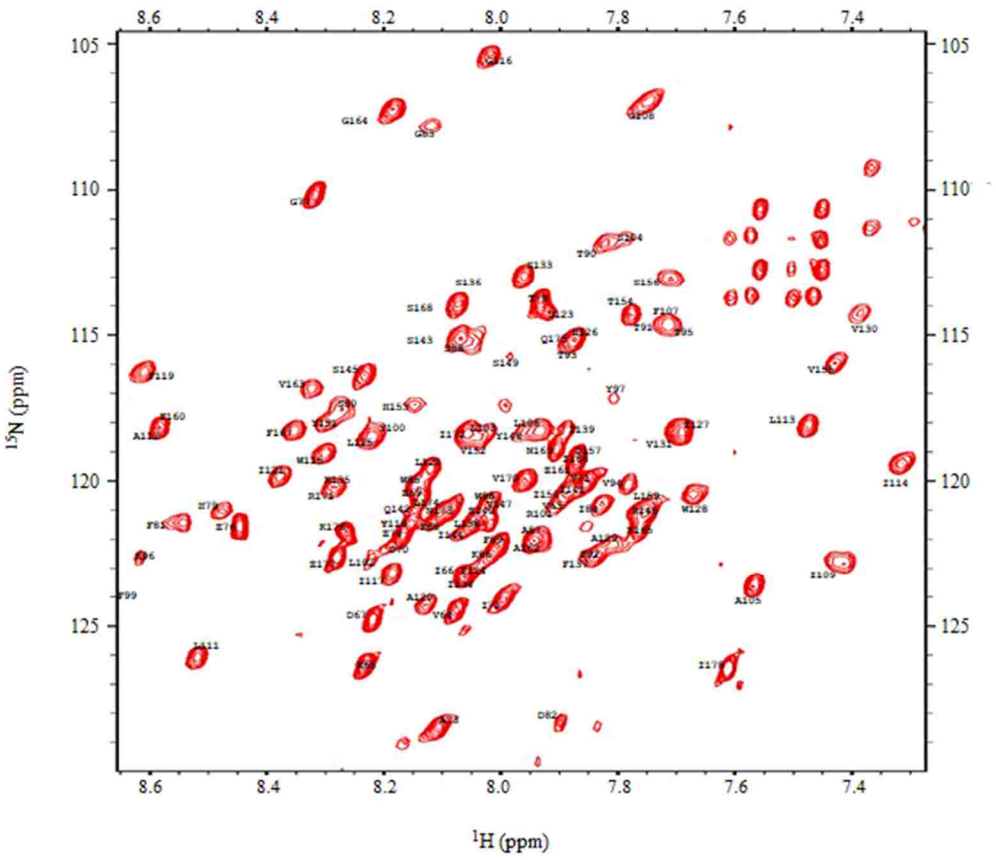

Figure 3-2. Assigned ^{1}H-^{15}N TROSY-HSQC spectrum of caveolin-1(62-178). The spectrum was acquired with 256 complex points in t1 (^{15}N) and 2048 complex points in t2 (^{1}H) (113).

Chemical shift index plot

With the chemical shifts obtained from the HNCA it is possible to create a chemical shift indexing plot (CSI). This plot is generated by subtracting the reference Cα chemical shift from the experimentally determined Cα. A long stretch of positive ΔCα indicates helical structure, while a long stretch of negative ΔCα indicates β-strand. The CSI plot of caveolin-1(62-178) shows three long stretches of positive ΔCα values (Figure

3-3). Importantly, the C-terminal domain shows significant helical character. Differences in Cα chemical shifts that fall below standard error cannot be assigned a secondary structure and are labeled as ambiguous (seen in red in Figure 3-3). Because of this ambiguity it is necessary to refine the structural prediction to include more parameters than just the Cα chemical shift.

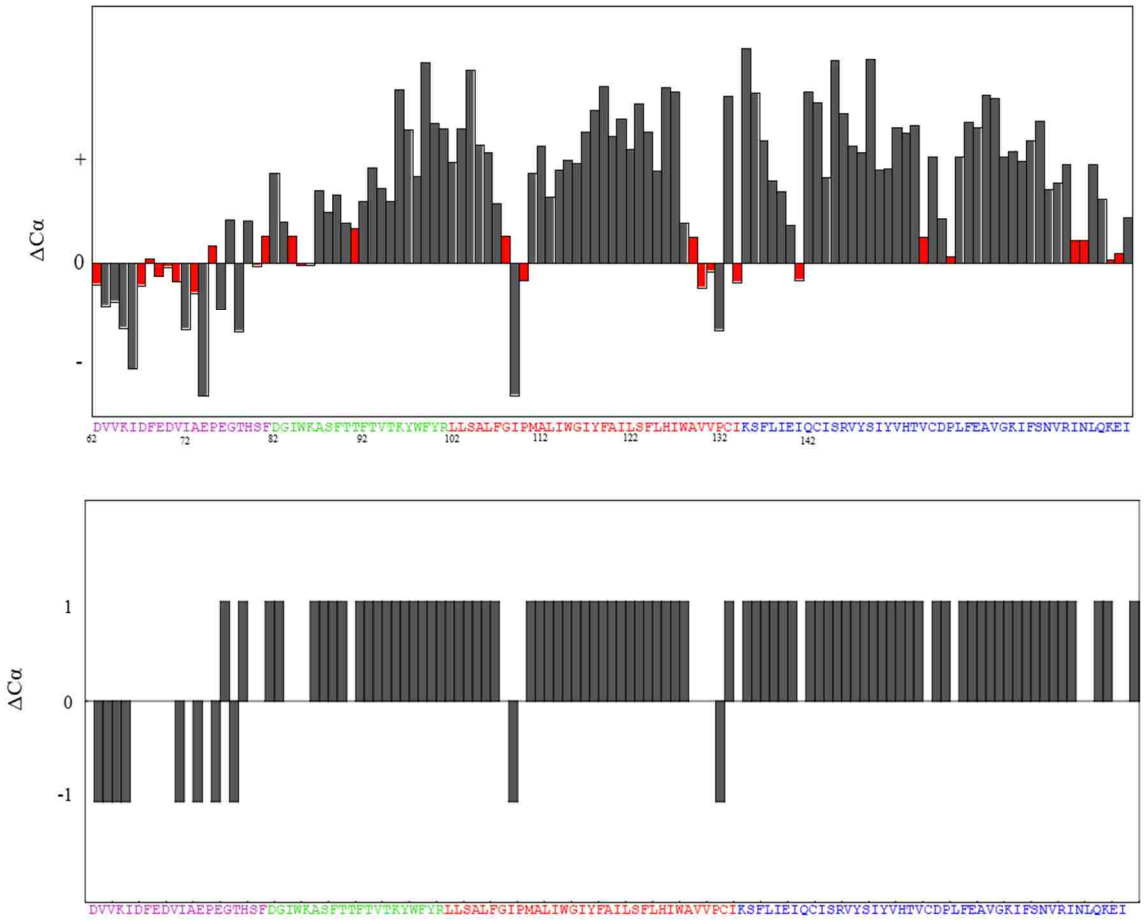

Figure 3-3. Chemical shift index plot of caveolin-1(62-178). A) Plot of the difference between the observed Cα and the reference Cα. Red indicates differences that are predicted as a coil. B) Normalized plot of the chemical shift difference. If the ΔCα is greater than 0.7 ppm it is denoted as +1, if it is less than 0.7 ppm it is denoted as -1. If the ΔCα falls within + 0.7 it is denoted as 0 (113).

Talos+ prediction for caveolin-1(62-178)

To further refine the structural prediction the chemical shifts for the H, N, Cα, Cβ and CO can be entered into a program called Talos+(111). This program utilizes a data base of possible Ψ and Φ angles compiled from the Protein Data Bank (PDB) to predict secondary structure. Based on the Talos+ data for cavoelin-1 (62-178), residues 62-80 are dynamic, and residues 81-88 are unstructured. The first major helix (Helix-1) begins at residue 89 and ends at residue 107. Helix-1 is immediately followed by a three residue break (residues 108-110), and helical character is restored for the second helix (Helix-2) from residues 111-128. Following the second helix there is another break (residues 129-131), and the third helix (Helix-3) begins at residue 132 and continues throughout the entire C-terminus until residue 175, just three residues from the end of the protein (Table 3-1).

Residue	PHI	PSI	Prediction	Residue	PHI	PSI	Prediction	Residue	PHI	PSI	Prediction
D	9999	9999	None	R	-61.62	-40.988	α-helical	E	-60.362	-39.526	α-helical
V	-117.321	140.184	Dynamic	L	-62.945	-45.523	α-helical	I	-68.431	-40.674	α-helical
V	-98.852	140.681	Dynamic	L	-61.803	-43.21	α-helical	Q	-61.136	-39.474	α-helical
K	-86.934	135.048	Dynamic	S	-62.99	-39.766	α-helical	S	-62.432	-43.565	α-helical
I	-115.187	133.807	Dynamic	A	-63.742	-40.386	α-helical	I	-65.465	-41.017	α-helical
D	-87.828	118.907	Dynamic	L	-67.175	-34.864	α-helical	S	-64.929	-37.017	α-helical
F	-117.577	140.82	Dynamic	F	-86.489	-1.962	α-helical	R	-67.177	-40.212	α-helical
E	-98.677	137.93	Dynamic	G	90.214	9.977	unstructure	V	-61.347	-42.183	α-helical
D	-93.109	-15.174	Dynamic	I	-89.661	125.897	unstructure	Y	-63.416	-41.266	α-helical
V	-117.85	127.953	Dynamic	P	-58.943	142.1	unstructure	S	-60.548	-45.107	α-helical
I	-95.148	-16.137	Dynamic	L	-54.638	-40.897	α-helical	I	-67.659	-37.573	α-helical
A	-94.14	161.392	Dynamic	A	-60.066	-41.349	α-helical	Y	-76.52	-26.175	α-helical
E	-83.383	136.48	Dynamic	L	-65.017	-41.983	α-helical	V	-64.181	-42.309	α-helical
P	-69.411	148.881	Dynamic	I	-63.991	-44.258	α-helical	H	-61.073	-39.411	α-helical
E	-83.036	131.988	Dynamic	W	-63.474	-42.16	α-helical	T	-69.467	-40.842	α-helical
G	77.638	10.305	Dynamic	G	-63.02	-42.879	α-helical	V	-64.894	-42.646	α-helical
T	-60.375	-40.752	α-helical	I	-67.192	-41.003	α-helical	S	-68.881	-35.395	α-helical
H	-62.201	-43.477	α-helical	Y	-60.738	-47.006	α-helical	D	-64.083	-29.33	α-helical
S	-69.838	-30.784	α-helical	F	-61.871	-38.994	α-helical	P	-61.307	-31.309	α-helical
F	-67.965	-35.879	α-helical	A	-68.165	-37.271	α-helical	L	-65.061	-33.635	α-helical
D	-79.402	-10.415	Dynamic	I	-68.3	-40.731	α-helical	F	-66.847	-38.394	α-helical
G	83.88	16.12	Dynamic	L	-60.708	-40.015	α-helical	E	-63.494	-39.21	α-helical
I	-66.724	-30.6	Dynamic	S	-66.899	-37.863	α-helical	A	-62.584	-42.532	α-helical
W	-82.081	-12.267	Dynamic	F	-65.25	-37.881	α-helical	V	-66.754	-45.248	α-helical
K	-74.811	-23.705	Dynamic	L	-68.56	-29.35	α-helical	G	-62.369	-41.34	α-helical
A	-68.808	-34.485	Dynamic	H	-66.141	-31.693	α-helical	K	-61.988	-44.874	α-helical
S	-69.594	-37.612	Dynamic	I	-68.037	-31.438	α-helical	I	-63.213	-40.285	α-helical
F	-63.791	-44.832	α-helical	W	-78.083	-21.061	unstructure	F	-65.829	-39.891	α-helical
T	-65.071	-42.496	α-helical	A	-73.668	-24.403	unstructure	S	-69.557	-39.306	α-helical
T	-64.177	-37.429	α-helical	V	-106.043	-4.654	unstructure	N	-63.707	-44.413	α-helical
F	-64.524	-42.047	α-helical	V	-86.852	122.377	unstructure	V	-65.121	-45.18	α-helical
T	-63.011	-39.14	α-helical	P	-58.481	-28.698	α-helical	R	-63.348	-35.143	α-helical
V	-63.326	-43.505	α-helical	S	-63.951	-28.902	α-helical	I	-63.805	-41.515	α-helical
T	-69.525	-27.472	α-helical	I	-74.2	-26.635	α-helical	N	-60.76	-39.417	α-helical
K	-95.073	-0.768	α-helical	K	-69.701	-28.726	α-helical	L	-63.957	-34.102	α-helical
Y	-56.442	-41.535	α-helical	S	-62.877	-41.358	α-helical	Q	-76.931	-23.509	α-helical
W	-65.703	-19.831	α-helical	F	-62.39	-45.533	α-helical	K	-93.168	0.649	unstructure
F	-88.905	-37.898	α-helical	L	-65.326	-39.301	α-helical	E	-78.731	131.915	unstructure
Y	-64.418	-42.732	α-helical	I	-64.97	-45.485	α-helical	I	9999	9999	None

Table 3-1. Talos+ data showing PHI and PSI angles and structural prediction for caveolin-1(62-178).

Caveolin-1 residues (62-178) adopts a helix-break-helix-break-helix motif, with the previously uncharacterized C-terminal domain forming a long amphipathic helix (Figure 3-4) This data agrees well with the CSI plot but has the added resolution of relying on five chemical shift parameters rather than one. One important note is that both Helix-2 and Helix-3 start with proline residues (P110 and P132). It has been shown previously that having a proline at the start of a helix is a common feature in many helical proteins, and that the presence of a proline residue at the start of a helix may be energetically favorable (114).

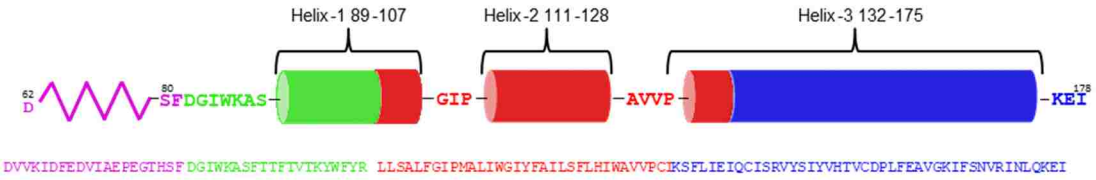

Figure 3-4. Cartoon representation of TALOS+ data for caveolin-1(62-178). Zigzag line denotes dynamic structure. Purple, N-terminal domain; green, scaffolding domain; red, intramembrane domain; blue, C-terminal domain (113).

Chemical shift perturbation plot

Finally, there has been some indication that the scaffolding domain and the C-terminal domain play similar roles in caveolin-1 function. The C-terminal domain plays an important role in membrane attachment, and in the formation of the homo-typic network of oligomers that help to shape caveolae (65, 66). Caveolin-1 is thought to oligomerize *in vivo* and to form high order complexes. The initial oligomerization has been isolated to the scaffolding domain (82-101) but the formation of networks of oligomers has been shown to be isolated to the C-terminal domain (66). This implies that

the C-terminal domain is required for the formation of the striated coat that is formed at the membrane surface to help stabilize caveolae (33). The C-terminal region is also required for the movement of the protein from the Golgi apparatus to the plasma membrane (58). Many caveolin-1 binding partners such as endothelial nitric oxide synthase, connexin, and Retrovirus NSP4, also interact directly with the C-terminal domain making it an important binding region within caveolin-1 (37, 67, 68). Because of the overlap in function between these two domains, it has been proposed that these domains may be spatially close. To examine this hypothesis, a chemical shift perturbation plot was made (Figure 3-5). This plot is generated by examining the difference between the amide chemical shifts for two separate constructs. In this case, caveolin-1(62-178) was compared to caveolin-1(62-136), which is the same construct except it is lacking the C-terminal domain. The largest chemical shift perturbation can be seen in the scaffolding domain indicating that the C-terminal domain is in close proximity to the scaffolding domain. There is also a significant perturbation at the C-terminal residues of caveolin-1(62-136), but this is expected because of the addition of the C-terminal domain in caveolin-1(62-178).

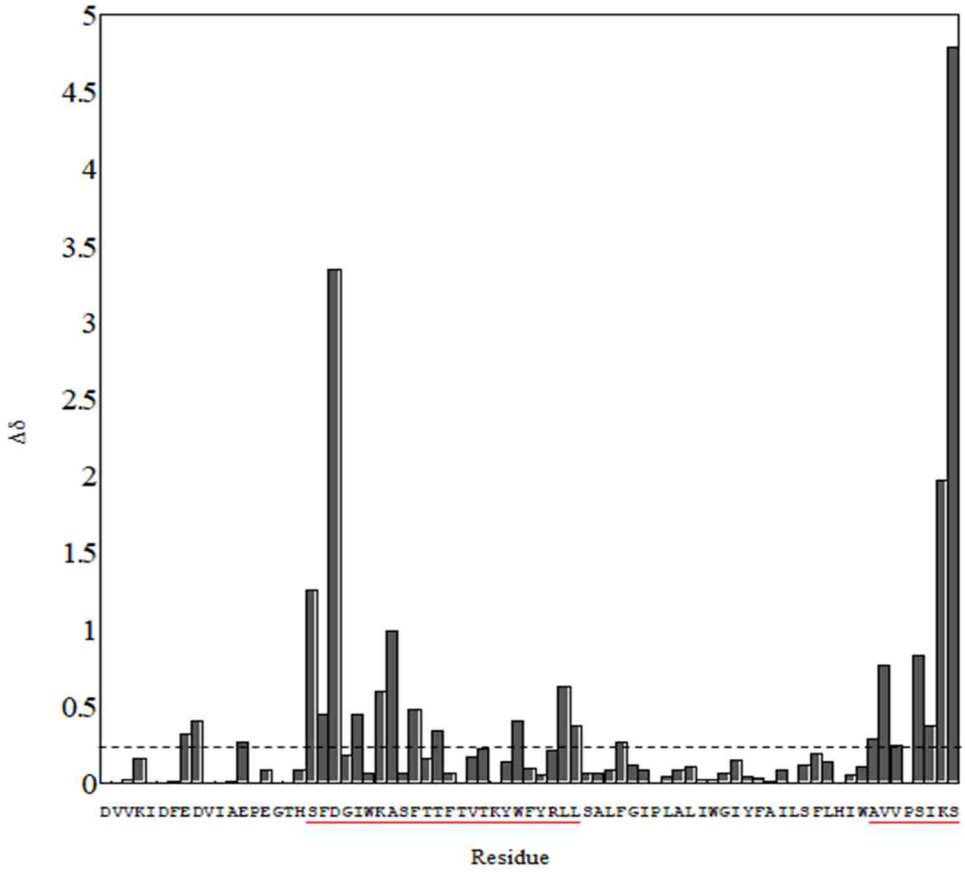

Figure 3-5. Chemical shift perturbation plot comparing caveolin-1(62-136) and caveolin-1(62-178). Dashed line indicates the threshold for significance. Residues that experience significant perturbation are underlined in red (113).

Analysis of the two critical break regions in caveolin-1(62-178)

Interestingly, the caveolin-1 structure appears to be governed by two break regions (break 1 residues 108-110 and break 2 residues 129-131). Break 1 has been previously reported to have three critical residues (Glycine, isoleucine and proline). Previous reports have identified that it is critical to have a small amino acid (glycine or alanine) followed by a β-branched amino acid (valine or isoleucine) and ending with a

proline (64). When examining break 2 there is a similar trend in the sequence with (alanine, valine, valine, proline) . Here again there is a small amino acid side chain followed by a β-branched side chain, and ending with a proline; however there is an additional β-branched amino acid within the second break implying that the second break needs to be longer then the first. Another difference is that proline 132 (end of break two) is predicted to be at the start of Helix-3 as opposed to P110 (end of break 1) which is not predicted to be helical. Previous studies have shown that proline residues are favorable to initiate helices, so the presence of proline residues at the start of Helix-2 and Helix-3 is significant (114). The presence of the same characteristic amino acid sequence draws similarities between break 1 and break 2. This also has functional implications. Break 1 is thought to occur in the membrane and help to give caveolin-1 its horseshoe like shape that helps to curve the membrane and form caveolae. The presence of proline 110 has been shown to be critical for the horseshoe topology of caveolin-1 that places both the N- and C-termini on the cytoplasmic side of the membrane (115). Here break 2 allows for the transition of the protein from an intramembrane helix to an interfacial helix that interacts intimately with the membrane at the head group region. Proline 132 (located at the start of Helix-3) has also been implicated as an important residue in breast cancer and its mutation has been shown to cause structural changes that disrupt trafficking (44, 116, 117) (Figure 3-6). This highlights that the presence of the two proline residues at the end of each break is critical for the proper structure and function of caveolin-1.

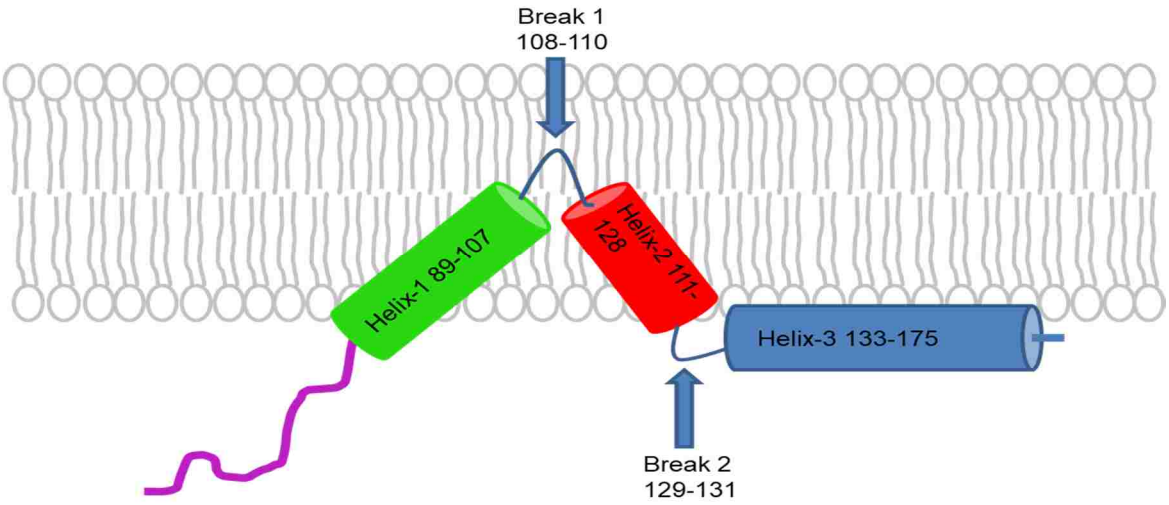

Figure 3-6. Cartoon representation of the hypothesized topology of caveolin-1. The three helices are highlighted along with the two break regions.

Conclusions

The determination of the secondary structure of caveolin-1(62-178) represents a critical step forward in the understanding of caveolin-1 structure. Using a functional construct, this is the first report of specific secondary structural data on the C-terminal domain of caveolin-1 and suggests that it is an amphipathic helix. Additionally, this is the first structural data on an elongated construct of caveolin-1 (the longest that has been structurally characterized) to produce a clearer picture of the secondary structure of caveolin-1 as a whole. The identification of two critical break regions allows for a deeper understanding of how caveolin-1 is structured in the membrane. Break-1 is the location of the intramembrane turn which allows for the C-terminus to return to the cytoplasmic side of the membrane. Break-2 allows for the transition of Helix-2, which is located in the membrane to Helix-3 which is resting on the membrane surface. The determination of the structure of the C-terminal domain also has important implications in disease states because the C-terminal domain has been shown to interact with several of the caveolin-1 binding partners. The disruption of the C-terminal helix has been implicated in pulmonary arterial hypertension, by interfering with the binding of eNOS with caveolin-1 (42). Therefore, the structural characterization of the C-terminal domain is a vital step in understanding the biological function of caveolin-1.

Appendix 3.1-Protein sequence for NMR studies

Caveolin-1(62-178) _M11L_C133S_C143S_ C156S	DVVKIDFEDVIAEPEGTHSFDGIWKASFTTFTVTKYWFYRL LSALFGIP**L**ALIWGIYFAILSFLHIWAVVP**S**IKSFLIEIQ**S** ISRVYSIYVHTV**S**DPLFEAVGKIFSNVRINLQKEI

Chapter 4. Alanine and phenylalanine scanning of caveolin-1(82-136).

Abstract

The previous chapters described the determination that the caveolin-1 intramembrane domain contains a helix-break-helix motif. Because of this unique motif it can be postulated that specific residues may be important for the motif stability. Additionally, it has not been established if these two helices interact with one another to garner additional stability. Sequence alignment of the three caveolin-1 isoforms revealed strictly conserved residues (residues that are the same in all three isoforms) in the scaffolding and intramembrane domains. To probe the importance of individual residues to the structure of caveolin-1, alanine and phenylalanine scanning was performed on all strictly conserved residues in the scaffolding and intramembrane domains of caveolin-1 (82-136). Nuclear magnetic resonance studies revealed that mutations to residues Y100, P110, A112, G116, S123, H126, and P132 are “not tolerated”, while mutations to S88, F92, K96, Y97, L103, F119, A120, I127, and W128 are “tolerated”. Based on these findings, a preliminary model of helix interaction can be presented. Additionally, this is the first identification of a conserved face within Helix-2 that may be important for the structure or function of caveolin-1.

Introduction

The relationship between protein structure and function has been emerging for several decades. The idea that the protein sequence can predict the overall fold of the protein is an attractive hypothesis when trying to assign *de novo* protein structure. In fact in many cases the mutation of one amino acid can have significant effects on the protein structure and lead to disease states. For example, in the caveolin family of proteins, Proline 132 has been identified to be critical for the proper structure of caveolin-1. Mutation to leucine causes a change in cellular trafficking and has been implicated in breast cancer (44, 50). Utilizing NMR spectroscopy it has been shown that the mutation of proline 132 to leucine causes an extension of Helix-2 and removes the second break which separates Helix-2 and Helix-3. Additionally, caveolin-1 P132L has been shown to behave as a dimer in vitro in contrast to the wild-type protein that has been shown to be monomeric (44). Importantly, Proline 132 is highly conserved between the three caveolin-1 isoforms. In caveolin-3, the analogous proline residue (P104) has been linked to misregulation of caveolin-3 and muscular dystrophy (118). This shows that single point mutations can have a dramatic effect on caveolin-1 structure and function.

Because of the unique fold of caveolin-1 it can be hypothesized that the two helices in the membrane may interact or that residues within the helices are critical for the fold. As discussed in Chapter 1, the three caveolin isoforms have a significant amount of sequence similarity (see Figure 1-3). In particular the scaffolding and intramembrane domains are highly conserved between the three isoforms. The high degree of conservation is an important observation because the scaffolding and intramembrane domains are part of the helix-break-helix motif that is thought to help

shape caveolae in the cellular membrane. While the break region (G108, I109 and P110) have been probed for their structural importance the role of the remaining residues with the helices has not been established (64). How these residues interact within a structural context can have a drastic effect on how the tertiary structure of this protein is viewed.

To determine amino acids that are critical for protein stability and structure, a common technique used is alanine scanning mutagenesis (119). Alanine is used because it is not bulky; it is chemically inert and can adopt the secondary structure preferences of most other amino acids. In addition, phenylalanine scanning mutagenesis probes the importance of steric bulk within a helix because phenylalanine has a large side chain. In this study, strictly conserved residues within the scaffolding and intra-membrane domains of caveolin-1 were mutated individually to both alanine and phenylalanine, and subjected to NMR experiments to determine the effect that each mutation has on the spectrum (^{1}H-^{15}N HSQC). These studies revealed that residues Y100, P110, A112, G116, S123, H126 and P132 may be critical for the structure of the protein, while alanine and phenylalanine mutations to residues S88, F92, K96, Y97, L103, F119, A120, I127 and W128 are unlikely to be critical for the structure.

Materials and Methods

Protein preparation

A caveolin construct that contains the scaffolding domain and the intra-membrane domain (residues 82-136) was chosen for this study (see Appendix 4-4). Uniformly ^{15}N-labeled caveolin-1 (82-136) wild-type and mutant constructs were prepared as described previously by Diefenderfer *et al*. (95). Methionine 111, which is not strictly conserved, was mutated to leucine to facilitate cyanogen bromide cleavage. The cysteine at position 133 was also mutated to serine to prevent non-biologically relevant disulfide bonding. Previous studies have shown that the mutation of cysteine 133 to serine does not affect the trafficking of caveolin-1 to the membrane (31). For this chapter, the notation "wild-type caveolin-1" refers to caveolin-1(82-136) M111L C133S. Primers were designed utilizing the wed-based PrimerX (see Appendix 4-5). Mutations were introduced using the Quikchange site-directed mutagenesis kit (Aligent Technologies, Santa Clara, CA) (see Appendix 4-1). All mutations were confirmed by DNA sequencing analysis. Constructs were transformed into Bl-21(DE3) cells for protein expression (see Appendix 4-2 and 4-3).

NMR sample preparation

NMR samples were prepared by dissolving lyophilized protein to 1 mM in 600 μL of a buffer containing the following components: 100 mM LMPG (lysomyristoyl-phosphatidylglycerol), 20 mM phosphate pH 7.0, 100 mM NaCl, and 10% D_2O. The sample was vigorously mixed and heated until a clear homogenous solution was

obtained. Finally, the sample was filtered through a 0.2 μm regenerated cellulose spin filter (Grace Davison Discovery Science, Deerfield, IL).

NMR experiments

NMR experiments were performed at 37°C using a 600 MHz Bruker Avance II spectrometer equipped with a cryoprobe. TROSY-based ^{1}H-^{15}N HSQC experiments were utilized for all mutations (107, 108). All NMR spectra were processed using NMRpipe and Sparky (109, 110).

Results and Discussion

Identification of strictly conserved residues in the three caveolin isoforms

Sequence alignment of the three caveolin isoforms shows that there are nineteen strictly conserved residues: D82, W85, S88, F92, K96, Y97, Y100, L103, P110, A112, G116, F119, A120, S123, H126, I127, W128, P132 and K135 (Figure 4-1). Alanine and phenylalanine scanning mutagenesis was carried out and $^{1}H,^{15}N$ HSQC spectra were generated for each residue, with the exception of D82, W85 and K135 because of their proximity to the ends of the construct, to elucidate their importance for protein structure. If the residue is critical, the ^{1}H, ^{15}N HSQC spectrum will show a global disruption when compared to the wild-type spectrum and the mutation can be classified as "not tolerated". The evaluation of a global structural change was defined as a loss in peak dispersion and/or a decrease in the number of peaks observed and/or chemical shift changes of a majority of the residues. If a residue is not critical, then the spectrum will overlay very well with the wild-type spectrum (less than 10% chemical shift changes) and the mutation can be classified as "tolerated".

Figure 4-1. Sequence alignment of the three caveolin isoforms. The strictly conserved residues are highlighted in red. The three terminal conserved residues are highlighted in grey.

NMR analysis of strictly conserved residues in the scaffolding and intramembrane domains of caveolin-1

Table 4-1 presents the findings of our NMR analysis. Of the sixteen strictly conserved residues, nine (S88, F92, K96, Y97, L103, F119, A120, I127, W128) were found to show no significant changes when compared to the wild-type spectrum and were thus labeled as "tolerated" (see Figures 4-2, 4-3, 4-4 and 4-5). The seven remaining conserved residues (Y100, P110, A112, G116, S123, H126 and P132) show significant changes when compared to the wild-type TROSY-HSQC spectrum and were thus labeled as "not tolerated" (see Figures 4-2, 4-3, 4-4 and 4-5). It is important to note that these spectral changes could represent changes other than structural ones such as aggregation and/or specific detergent effects. However, because it is not possible to perform NMR studies in other detergents, these studies cannot elucidate these detergent effects.

Residue	Alanine	Phenylalanine
S88	Tolerated	Tolerated
F92	Tolerated	----------
K96	Tolerated	Tolerated
Y97	Tolerated	Tolerated
Y100	Not tolerated	Not tolerated
L103	Tolerated	Tolerated
P110	Not tolerated	Not tolerated
A112	----------	Not tolerated
G116	Not tolerated	Not tolerated
F119	Tolerated	----------
A120	----------	Not tolerated
S123	Not tolerated	Not tolerated
H126	Not tolerated	Not tolerated
I127	Tolerated	Tolerated
W128	Tolerated	Tolerated
P132	Not tolerated	Tolerated

Table 4-1. Results of alanine and phenylalanine scanning of the strictly conserved residues within caveolin-1(82-136)

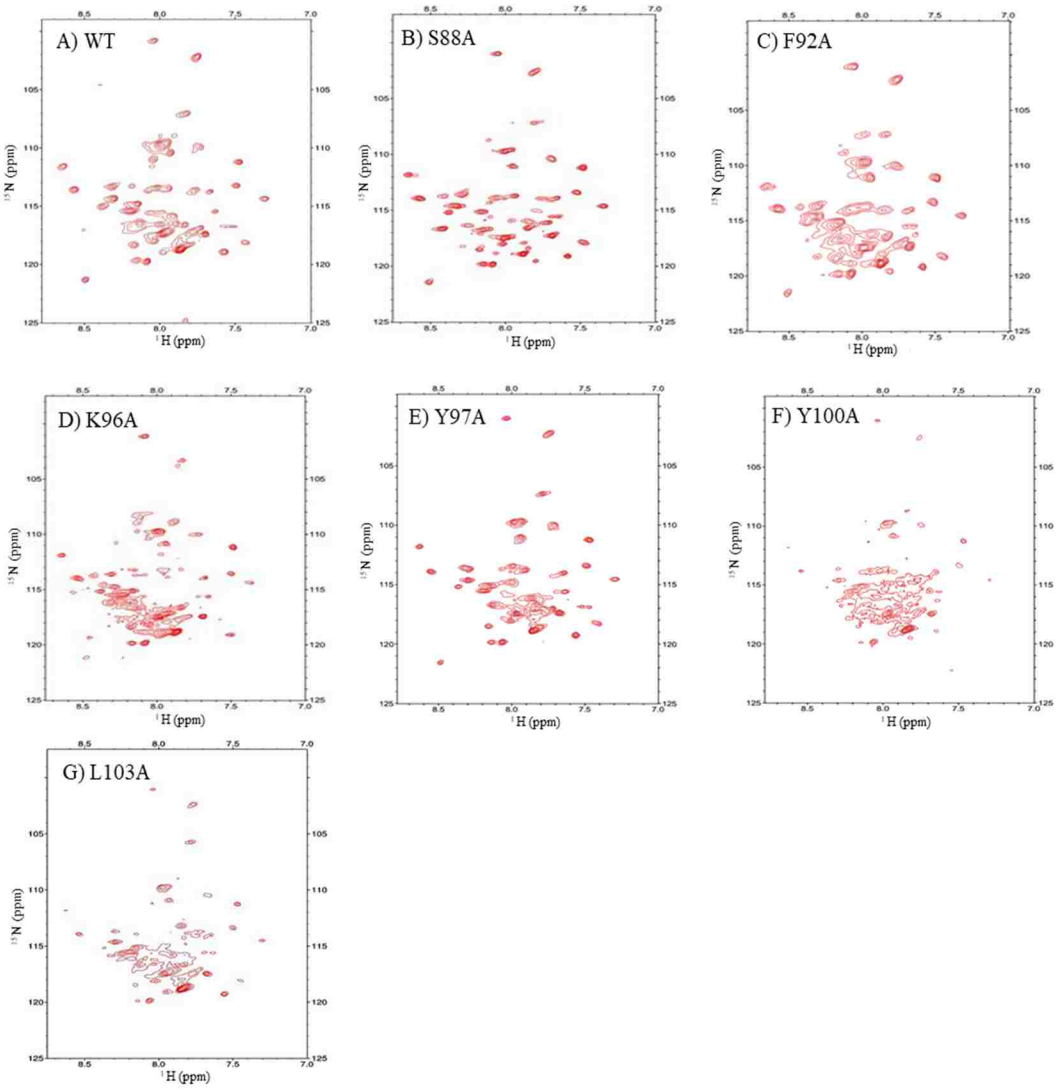

Figure 4-2.TROSY-HSQC spectra of Helix-1 alanine mutants. Wild-type is included in the first panel as a comparison. F) Y100A which shows significant disruption compared to the wild-type.

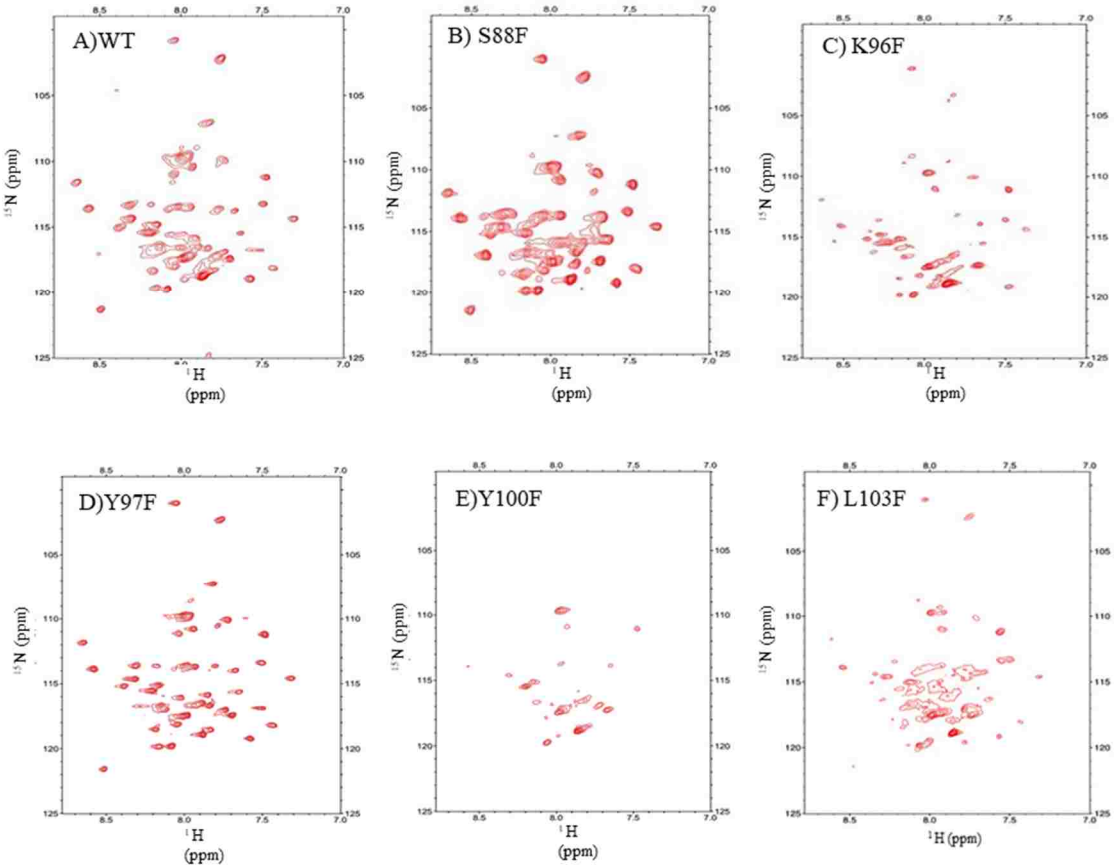

Figure 4-3. TROSY-HSQC spectra of Helix-1 phenylalanine mutants. Wild type is included in the first panel for comparison. E) Y100F which shows significant disruption compared to the wild-type.

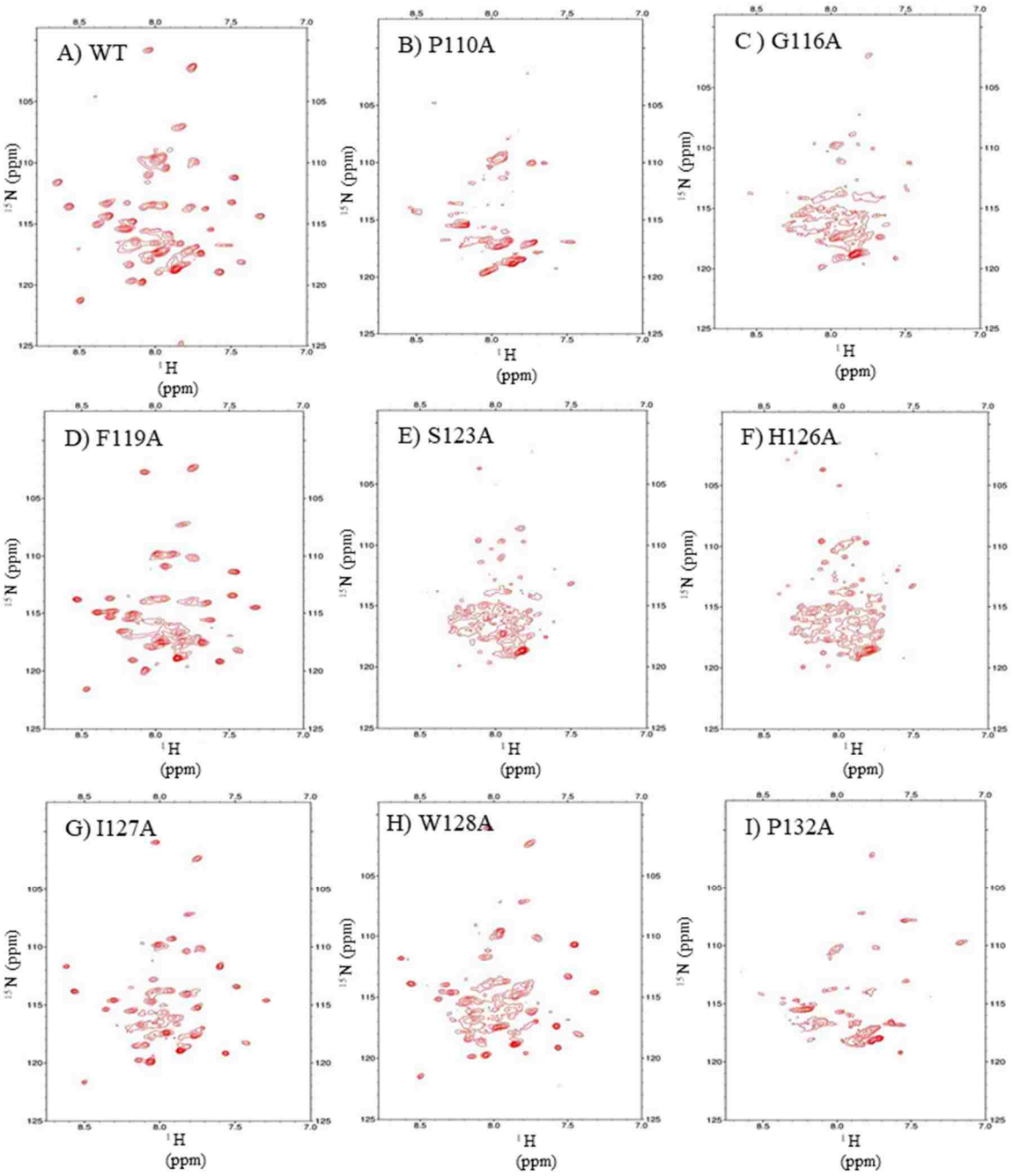

Figure 4-4. TROSY-HSCQ spectra of Helix-2 alanine mutants. Wild-type is included in the top panel for reference.

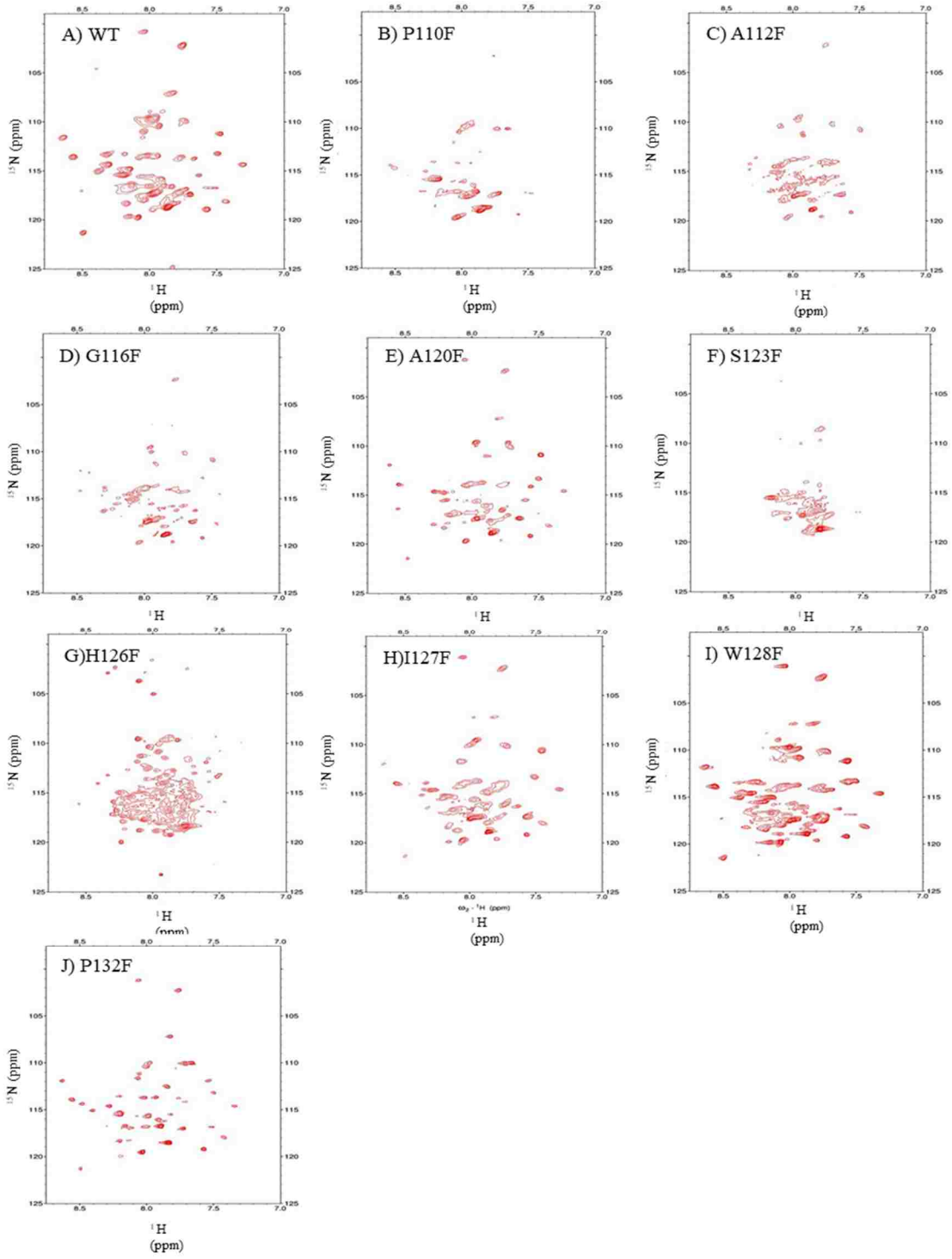

Figure 4-5. TROSY-HSQC spectra of Helix-2 phenylalanine mutants. Wild-type is included in the top panel for comparison.

In contrast to Helix-2, nearly all conserved residues within Helix-1 are "tolerated". The only residue that is critical is Y100 (figure 4-2F and figure 4-3E). When Y100 is mutated to alanine there is a disruption that could be attributed to the loss in steric bulk. However, phenylalanine is also "not tolerated". This leads to the hypothesis that the hydroxyl group on the tyrosine side chain is needed to stabilize the caveolin structure through a hydrogen bonding interaction.

Most of the remaining conserved residues within Helix-1, (F92 and Y97) including S88 which directly precedes the start of the helix, reside within the more soluble scaffolding domain (Figure 4-2B, D, G and Figure 4-3B, D, F). This domain is implicated in binding signaling proteins (e. g. endothelial nitric oxide synthase), and the current study supports the postulation that this region may be more important for binding than structure. For example, previous studies have shown that when F92 is mutated to alanine, caveolin-1 no longer binds to endothelial nitric oxide synthase, but the current study shows that this mutation was "tolerated" (120). Therefore the scaffolding domain may be permissive towards mutations structurally but not functionally. The remaining residue, L103, is the only conserved residue within Helix-1 to reside in the intra-membrane domain and mutations at this position are "tolerated". This suggests that Helix-1 is permissive to mutations structurally; however overall this may have larger implications functionally.

The only other residue to show disruption when mutated to phenylalanine is K96 (Figure 4-3C). However, when K96 is mutated to alanine there are no significant changes to the overall structure. This indicates that there could be steric effects at position 96 that cannot tolerate the bulk of phenylalanine. However, because alanine is

"tolerated" at this position, K96 is not considered critical for the overall structure of caveolin-1(82-136) (Figure 4-2C).

Studies have shown that P110 is a critical residue that is found in the break region and is proposed to participate in the formation of the putative intramembrane turn that is the cause of the N- and C- termini lying on the same side of the plasma membrane. Recent results from the Glover lab also support that proline is needed at position 110 to stabilize the caveolin-1 structure based on mutations to alanine, and glycine (64). Additionally, circular dichroism and fluorescence spectroscopy studies have identified that the mutation of proline 110 has dramatic effects on the structure and topology of caveolin-1(121). The results of the current study are in agreement with the previous studies indicating that mutations at proline 110 are "not tolerated" (Figure4-4B and Figure 4-5B).

Analysis of the conserved face in Helix-2

The remaining conserved residues (A112, G116, F119, A120, S123, and I127), with the exception of W128 and P132, are contained within Helix-2. To analyze these residues, the angular position was tabulated with respect to A112 (the first conserved residue in Helix-2). Figure 4-6A shows this data. Interestingly, mutations to the conserved residues that are within 40 degrees of A112 are all "not tolerated" with the exception of F119 (Figure 4-6B). Mutations to A120 and I127 which lie outside of that range are "tolerated" (Figure 4-4G and Figure 4-5E and H). This is indicative of a conserved face within Helix-2 that may be important for interactions with Helix-1 or other structural contacts.

A

Residue	Θ	Θ*
M111	-100	-100
A112	0	0
L113	100	+100
I114	200	+160
W115	300	+60
G116	400	+40
I117	500	-140
Y118	600	-120
F119	700	-20
A120	800	+80
I121	900	+180
L122	1000	-80
S123	1100	+20
F124	1200	+120
L125	1300	-140
H126	1400	-40
I127	1500	+60
W128	1600	+160

Θ*: Angle with respect to A112

B

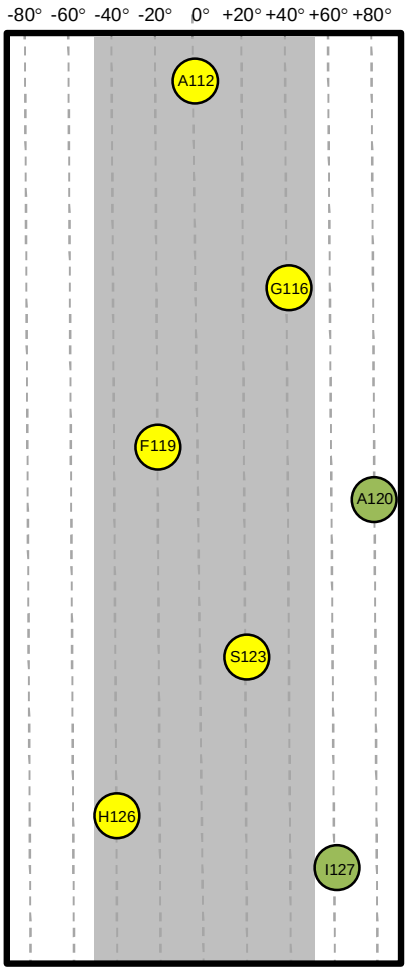

Figure 4-6. A) Conserved residue positioning in Helix-2. (A112 is referenced as 0°). B) Graphical representation of conserved residue positioning in Helix-2. Residues within the face are highlighted in yellow, those outside in green.

A112 is the first conserved residue in Helix-2 (Figure 4-6B). When a phenylalanine residue is placed at position 112 it introduces steric bulk that is not tolerated (Figure 4-5C). This suggests that this position is geometrically restricted and is

the first indication of a size limitation within the conserved face. This could be due to intra-helix steric clashing as the i+3 position contains a large bulky residue (W115).

The next residue within the conserved face of Helix-2 is G116. Interestingly, both mutations to alanine and phenylalanine are "not tolerated" (figure 4-4C and Figure 4-5D). This structural disruption is not due to glycine's high degree of conformational freedom as the Ψ and Φ angles based on TALOS+ calculations show that position 116 is helical (113). The fact that an alanine residue, which is small and comparable to glycine in size, is not tolerated indicates that space requirements at position 116 are extremely tight; only hydrogen is tolerated. Additionally, for the G116A mutant it is unlikely that intra-helix steric clashing is at play due to the small size of the alanine side chain. This implicates position 116 as a key interaction point within the conserved face that stabilizes the caveolin-1 structure and could represent a contact point with Helix-1.

F119 is the only residue within the conserved face that "tolerated" mutation to alanine (Figure 4-4D). This indicates that the bulk of phenylalanine is tolerated but not required to stabilize the conserved face, because the small side chain of alanine does not disrupt the structure.

S123 shows disruption when mutated to both alanine and phenylalanine (Figure 4-4E and 4-5F). Serine has a small side chain that will not tolerate the introduction of a large phenylalanine residue, which is consistent with the trend of the conserved face to prefer smaller side chains. Along with the issue of steric bulk, hydrogen bonding could also be important at position 123 because alanine is also not tolerated. Serine and alanine are comparable in size but alanine lacks the hydroxyl functionality, which implies that the

hydrogen bonding interaction at position 123 maybe critical to stabilize the caveolin-1 structure.

The last structurally critical residue in Helix-2 is H126. Similar to S123, H126 could also participate in hydrogen bonding that is critical for the caveolin-1 structure. However, unlike S123, histidine has a large bulky side chain. The disruption to the structure when H126 is mutated to alanine could be due to the loss in residue size, but there is also disruption when H126 is mutated to phenylalanine (figure 4-4F and figure4-5G). This indicates that size is not the key factor in the interaction of H126, but more likely a hydrogen bonding interaction.

P132L has been a highly investigated mutation in caveolin-1 protein mainly because of its implications in cancer (122). Previous work has shown that when proline 132 is mutated to leucine the second helix is extended and the caveolin protein behaves as a dimer rather than a monomer in DPC micelles (44). The current study shows that phenylalanine is able to stabilize the structure but alanine is not because of the loss of steric bulk. The structural disruption by alanine at position 132 is not due to aggregation because gel filtration studies have shown that the mutated protein remains a dimer and does not behave as a high order oligomer (44). This means that the disruption in the NMR spectrum is likely due to a structural loss rather than aggregation.

Conclusions

Taken together, the mutagenesis data presented so far allows for the construction of a speculative model of caveolin structure. Previous studies have shown that the N- and C-termini lie on the same side of the plasma membrane, and that there is no portion of the protein that is accessible from the extracellular space (123, 124). In conjunction with the TALOS+ data previously presented, a model can be presented where the scaffolding and intra-membrane domains form two equal length helices that are separated by the putative turn. Clearly, with this model, residues in Helix-1 and Helix-2 that face each other and are close to the putative turn will be more space restricted. This is supported by residues A112 and G116, as both show intolerance to additional steric bulk. In contrast, residues that are further from the putative turn will have less space restriction. This is demonstrated by the bulk of phenylalanine at position 119 being tolerated. Also, moving further away from the putative turn, it appears that hydrogen bonding could dominate the stability as these studies revealed the need for hydroxyl functionalities at positions 100, 123 and 126.

Appendix 4-1. PCR conditions

PCR reactions with single primer
15.8 µL sterile water 0.5 µL vector DNA (50 ng/µL) 0.5 µL Forward primer (250 ng/µL) 2.5 µL 10X 9N° Ligase buffer 2.5 µL 10X PFU buffer 0.2 µL DMSO 1.0 µL DNTPS (25 mM) 1.0 µL PFU Turbo 1.0 µL 9N° ligase

PCR cycle for single primer		
Number of cycles	Temperature	Time
1	95°	30 seconds
30	95°C 55°C 68°C	30 seconds 1 minute 6 minutes
End	4°C	indefinite

Appendix 4-2. XL-1 blue transformation Protocol

1. Thaw one 100 µL aliquot of ultra-competent XL-1 blue cells on ice for 10 minutes
2. Place sterile 15 mL culture tube on ice for 10 minutes to pre-chill
3. Add 100 µL of cells to the pre-chilled culture tube
4. Add 1 µL of PCR reaction directly into cells
5. Leave on ice for 30 minutes
6. Heat shock at 42°C for 90 seconds
7. Leave on ice for 2 minutes
8. Add 900 µL of SOC
9. Incubate at 37°C with shaking (250 rpm) for 1-2 hours
10. Plate 400 µL of culture onto LB plate with kanamycin
11. Incubate overnight at 37°C
12. Pick single colony and grow in 5 mL LB broth with kanamycin

Appendix 4-3. Transformation protocol for BL-21(DE3) cells

1. Thaw one 50 µL aliquot of BL-21(DE3) cells on ice for 10 minutes
2. Place sterile 15 mL culture tube on ice for 10 minutes to pre-chill
3. Add 50 µL of cells to the pre-chilled culture tube
4. Add 1 µL of 20 ng/µL of purified DNA
5. Leave on ice for 30 minutes
6. Heat shock at 42°C for 90 seconds
7. Leave on ice for 2 minutes
8. Add 950 µL of SOC
9. Incubate at 37°C with shaking (250 rpm) for 1-2 hours
10. Plate various dilutions onto MDAG plate with kanamycin
11. Incubate overnight at 37°C
12. Pick single colony and grow in 5 mL MDG with kanamycin

Appendix 4-4. Primer sequences used

Primers for alanine mutants	
Construct	
S88A	GGT ATC TGG AAA GCG GCG TTC ACC TTC ACC
F92A	GAA AGC GTC TTT CAC CAC CGC GAC CGT TAC CAA ATA CTG G
Y97A	CTT CAC CGT TAC CAA AGC GTG GTT CTA CCG TCT GC
Y100A	CCA AAT ACT GGT TCG CGC GTC TGC TGT CTG CG
L103A	GTT CTA CCG TCT GGC GTC TGC GCT GTT C
S104A	GTT CTA CCG TCT GCT GGC GGC GCTTTC GGT ATC
G116A	GCG CTG ATC TGG GCG ATC TAC TTC GCG
F119A	GAT CTG GGG TAT CTA CGC GGC GAT CCT GTC TTT C
S123A	CTA CTT CGC GAT CCT GGC GTT CCT GCA CAT CTG G
H126A	GAT CCT GTC TTT CCT GGC GAT CTG GGC GGT TGT TC
I127A	CGA TCC TGT CTT TCC TGC ACG CGT GGG CGG TTG TTC CGT CTA TC
W128	CTG TCT TTC CTG CAC ATC GCG GCG GTT GTT CCG TCT ATC

Primers for phenylalanine mutants	
Construct	
S88F	GTA TCT GGA AAG CGT TTT TCA CCA CCT TCA C
Y97F	CTT CAC CGT TAC CAA ATT CTG GTT CTA CCG TCT G
Y100F	CAA ATA CTG GTT CTT CCG TCT GCT GTC TGC
L103F	GTT CTA CCG TCT GTT CTC TGC GCT GTT C
S104F	CTA CCG TCT GCT GTT CGC GCT GTT CGC GCT GTT CGG TAT C
A112F	GTT CGG TAT CCC GCT GTT CCT GAT CTG GGG TAT C
G116F	CTG GCG CTG ATC TGG TTC ATC TAC TTC GCG ATC C
A120F	GAT CTG GGG TAT CTA CTT CTT CAT CCT GTC TTT CCT GCA C
S123F	CTT CGC GAT CCT GTT CTT CCT GCA CAT CTG G
H126F	GAT CCT GTC TTT CCT GTT CAT CTG GGC GGT TGT TC
I127F	GTC TTT CCT GCA CTT CTG GGC GGT TG
W128F	CTT TCC TGC ACA TCT TCG CGG TTG TTC CGT C

Appendix 4-5 Protein sequences of alanine and phenylalanine mutants

Construct	Sequence of alanine mutants
S88A	DGIWKA**A**FTTFTVTKYWFYRLLSALFGIPLALIWGIYFAILSFLHIWAVVP SIKS
F92A	DGIWKASFTT**A**TVTKYWFYRLLSALFGIPLALIWGIYFAILSFLHIWAVVP SIKS
Y97A	DGIWKASFTTFTVTK**A**WFYRLLSALFGIPLALIWGIYFAILSFLHIWAVVP SIKS
Y100A	DGIWKASFTTFTVTKYWF**A**RLLSALFGIPLALIWGIYFAILSFLHIWAVVP SIKS
L103A	DGIWKASFTTFTVTKYWFYRL**A**SALFGIPLALIWGIYFAILSFLHIWAVVP SIKS
S104A	DGIWKASFTTFTVTKYWFYRLL**A**ALFGIPLALIWGIYFAILSFLHIWAVVP SIKS
P110A	DGIWKASFTTFTVTKYWFYRLLSALFGI**A**LALIWGIYFAILSFLHIWAVVP SIKS
G116A	DGIWKASFTTFTVTKYWFYRLLSALFGIPLALIW**A**IYFAILSFLHIWAVVP SIKS
F119A	DGIWKASFTTFTVTKYWFYRLLSALFGIPLALIWGIY**A**AILSFLHIWAVVP SIKS
S123A	DGIWKASFTTFTVTKYWFYRLLSALFGIPLALIWGIYFAIL**A**FLHIWAVVP SIKS
H126A	DGIWKASFTTFTVTKYWFYRLLSALFGIPLALIWGIYFAILSFL**A**IWAVVP SIKS
I127A	DGIWKASFTTFTVTKYWFYRLLSALFGIPLALIWGIYFAILSFLH**A**WAVVP SIKS
W128	DGIWKASFTTFTVTKYWFYRLLSALFGIPLALIWGIYFAILSFLHI**A**AVVP SIKS
P132A	DGIWKASFTTFTVTKYWFYRLLSALFGIPLALIWGIYFAILSFLHIWAVV**A** SIKS

Construct	Sequence of phenylalanine mutants
S88F	DGIWKA**F**FTTFTVTKYWFYRLLSALFGIPLALIWGIYFAILSFLHIWAVVPS IKS
Y97F	DGIWKASFTTFTVTK**F**WFYRLLSALFGIPLALIWGIYFAILSFLHIWAVVPS IKS
Y100F	DGIWKASFTTFTVTKYWF**F**RLLSALFGIPLALIWGIYFAILSFLHIWAVVPS IKS
L103F	DGIWKASFTTFTVTKYWFYRL**F**SALFGIPLALIWGIYFAILSFLHIWAVVPS IKS
S104F	DGIWKASFTTFTVTKYWFYRLL**F**ALFGIPLALIWGIYFAILSFLHIWAVVPS IKS
P110F	DGIWKASFTTFTVTKYWFYRLLSALFGI**F**LALIWGIYFAILSFLHIWAVVPS IKS
A112F	DGIWKASFTTFTVTKYWFYRLLSALFGIPL**F**LIWGIYFAILSFLHIWAVVPS IKS
G116F	DGIWKASFTTFTVTKYWFYRLLSALFGIPLALIW**F**IYFAILSFLHIWAVVPS IKS
A120F	DGIWKASFTTFTVTKYWFYRLLSALFGIPLALIWGIYF**F**ILSFLHIWAVVPS IKS
S123F	DGIWKASFTTFTVTKYWFYRLLSALFGIPLALIWGIYFAIL**F**FLHIWAVVPS IKS
H126F	DGIWKASFTTFTVTKYWFYRLLSALFGIPLALIWGIYFAILSFL**F**IWAVVPS IKS
I127F	DGIWKASFTTFTVTKYWFYRLLSALFGIPLALIWGIYFAILSFLH**F**WAVVPS IKS
W128F	DGIWKASFTTFTVTKYWFYRLLSALFGIPLALIWGIYFAILSFLHI**F**AVVPS IKS

Chapter 5. Functional assay of caveolin-1

Abstract

The major function of caveolin-1 is to form caveolae, highly curved invaginations in the cellular membrane, which can be difficult if not impossible to recapitulate *in vitro*. This is due to not only the high degree of complexity in the plasma membrane but also the lack of detailed mechanistic knowledge of how caveolae are formed. This can make it difficult to assess how mutations affect the overall function of caveolin-1 *in vitro*. In this chapter a novel *in vitro* functional assay for caveolin-1 is presented. This assay is based on the inhibition of endothelial nitric oxide synthase, a known binding partner of caveolin-1. The assay has been validated utilizing a known small molecule inhibitor of eNOS L-NAME and a caveolin-1 construct that has been shown to interfere with inhibition (caveolin-1 F92A). Additionally, the assay has been optimized for use with detergents which are necessary for caveolin-1 solubilization. Additionally, there has been some evidence that the presence of C-terminal tags affect the trafficking of caveolin-1. Utilizing the eNOS assay, the presence of C-terminal tags was shown to interfere with the function of caveolin-1, while N-terminal tags had no effect. Overall this assay will allow for point mutations in caveolin-1 to be evaluated not only in a structural context but also in the context of caveolin-1 function.

Introduction

To complement the alanine and phenylalanine scanning data presented in the previous chapter, a functional assay for caveolin-1 needs to be employed. One of the major challenges is that the only known function of caveolin-1 is the formation of caveolae. This can be difficult if not impossible to mimic *in vitro*, largely because the mechanism of caveolae formation is not known. The mechanism of caveolae formation goes to the core of membrane organization. It is not clear if lipid organization, cholesterol recruitment, or caveolin-1 oligomerization trigger the formation of these highly specialized domains (125). Additionally, the complexity of the plasma membrane makes it almost impossible to mimic the exact conditions that the caveolin-1 protein would experience in the cell. Studies have shown that over expression of caveolin-1 *in vivo*, which is often required to access protein function, can actually lead to disease like phenotypes (117). This complicates the use of *in vivo* assays to determine how mutations effect caveolae formation because it can be difficult to determine if the lack of formation of caveolae is from the mutation or simply overexpression. The fact that caveolin-1 has no enzymatic activity on its own, further complicates the *in vitro* analysis of caveolin-1 function. Therefore, it is necessary to form an indirect enzymatic assay with one of the caveolin-1 binding partners.

Caveolin-1 has been proposed as a binding partner to several signaling molecules. It was initially thought that these signaling molecules would recognize caveolin-1 for binding through a specific motif known as the caveolin-1 binding motif (CBM) (40). The CBM consists of an aromatic rich domain (ϕXϕXXXXϕ, ϕXXXXϕXXϕ or ϕXϕXXXXϕXXϕ, ϕ is an aromatic and X can be any amino acid) (40). However, a

recent computational study has shown that in many of the proposed binding partners the CBM is buried within the structure and therefore is not accessible for binding(41). The location of binding in caveolin-1 has also been questioned because all of these binding partners appear to bind to the scaffolding domain. This seems unlikely because the scaffolding domain is also described as the major oligomerization domain. If the scaffolding domain is involved in the formation of oligomers it seems implausible that it would also be available for binding to several different signaling molecules (35). Additionally, because several of these signaling molecules are soluble, it calls into question how the scaffolding domain can interact with both hydrophilic molecules and hydrophobic molecules such as cholesterol. This made it difficult to find a binding partner that has been well established for caveolin-1 that has enzymatic function.

Endothelial nitric oxide synthase is an enzymatic protein that controls the production of nitric oxide in endothelial cells (126). The regulation of nitric oxide has been shown to be important for protection against atherosclerosis which leads to artery hardening, platelet aggregation and also defects in vasodilation (127). The dysfunction of eNOS has been attributed to several cardiovascular diseases (128). Caveolin-1 has been shown to inhibit eNOS activity (129, 130, 131). This inhibition has been shown to be vital to maintaining endothelial health (42). Caveolin-1 does not completely stop the production of nitric oxide but rather helps to regulate the output. In the absence of caveolin-1 there is a buildup of nitric oxide within the cells that leads to severe endothelial health defects (132).

There are well established assays available to quantitate the amount of nitric oxide that is present in solution (133). Most of the assays rely on the reaction of nitrite with

2,3-diaminonaphthalene (DAN probe). Nitrite is generated from the decomposition of nitric oxide into both nitrite and nitrate. To reduce the nitrate to nitrite, nitrate reductase is used. While nitrate is partially reactive with the DAN probe, nitrite shows a significant increase in reactivity. When the DAN probe reacts with nitrite it creates the fluorescent compound 2, 3-naphthotriazole, and the fluorescence signal is enhanced by the addition of base. By evaluating the amount of nitrite produced when eNOS is incubated in the presence of caveolin-1 constructs, the functional consequences of mutations can be evaluated. These results can then be compared to the structural data presented in the previous chapter, to build an understanding of the structure/function relationship of caveolin-1

Material and methods

Construct design

Full length caveolin-1 (residues 1-178) was purchased from Genscript and cloned into the pGEX vector which encodes for an N-terminal GST fusion utilizing Nde1 and Xho1 restriction sites. The three C-terminal cysteine mutations were mutated to serine as previously described which has been shown to not affect caveolin-1 function. GST_caveolin-1_F92A was generated utilizing Agilent Quickchange site directed mutagenesis. Both constructs were expressed in BL-21(DE3) cells. Full length caveolin-1_Myc_H6 and caveolin-1_F92A_Myc_H6 were cloned into pET 24a and transformed into BL-21(DE3) cells. Purified eNOS was purchased from Cayman Chemical (Ann Arbor, Michigan). The caveolin-1 scaffolding domain peptide was purchased from Genscript (Piscataway, New Jersey) (see appendix 5-2 for sequences).

Protein expression

All constructs were expressed utilizing the auto-induction method described in Studier (105). For GST_caveolin-1 and GST caveolin-1_F92A 1L ZYM-5052 cultures were inoculated with 1 mL of a 5 mL overnight MDG starter and incubated for 12 hours with shaking (250 rpm) at 37°C (see appendix 5-1). Full length caveolin-1_Myc_H6 and Caveolin-1_F92A_Myc_H6 was expressed in a similar manner except that 1L ZYM-5052 cultures were incubated at 25°C for 24 hours. All cultures were harvested by centrifugation at 5,807 xg for 15 minutes at 4°C. Pellets were washed with 200 mL 0.9% (w/v) saline and centrifuged for 30 minutes at 5000 x*g* for 30 minutes. The supernatant was removed and pellets were stored at -80°C until purification.

Purification of GST_caveolin-1 and GST_caveolin-1_F92A

Cell pellets were resuspended in 40 ml of 1X TAE and treated with 1 mg/ml lysozyme for 15 minutes on ice with stirring. After lysozyme treatment BME was added to 20 mM. Cells were lysed using sonication for a total of 20 minutes (5 minutes on and 10 minutes off). The membranes were isolated by centrifugation at 50,000 x*g* for 2 hours and the supernatant was removed. Membrane pellets were resuspended in 40 ml of 1XPBS 0.5% Brij with 20 mM BME and stirred on ice for 15 minutes. Insoluble cellular components were removed by centrifugation for 2 hours at 50000 x*g* at 4°C. The supernatant was filtered through a 0.2 μm filter and incubated at 4°C overnight with 1 mL of GST resin. After overnight incubation with stirring, the solution was loaded into an empty Bio-rad column and the flow-through was collected. The column was washed with 10 column volumes of 0.1% brij in 1 X PBS. Protein was eluted from the column in 1 mL fractions with elution buffer (10 mM reduced glutathione, 50 mM tris pH 8.0 and 0.1% brij). The most concentrated fractions were pooled and concentrated to 100-200 μM utilizing an amicoron ultra concentrator.

Purification of caveolin-1_Myc_H6 and Caveolin-1_F92A_Myc-H6

Pellets were resuspended in 40 ml lysis buffer (50 mM Pi pH 8.0, 300 mM NaCl, 2% Empigen BB). Cells were lysed by sonication for 45 minutes and the temperature was maintained at <10°C. Lysate was cleared for 1 hour at 50000 xg and filtered through 0.2 μm filter. The lysate was loaded onto Ni-NTA column at a rate of 1 ml/min. The column was washed with five column volumes of wash buffer (20 mM imidazole, 50 mM phosphate pH 8.0, 300 mM NaCl, and 0.5% Empigen BB). Protein was eluted with

elution buffer (50 mM phosphate pH 8.0, 300 mM NaCl, 250 mM imidazole and 0.5% Empigen BB) and 1 mL fractions were collected. The concentrated fractions were pooled and concentrated to 200 μL and loaded onto a Sephacryl S300 HR column (GE healthcare, Pittsburg, PA) in gel filtration buffer (0.5% Empigen BB, 25 mM phosphate pH 8.0, 150 mM NaCl).

eNOS assay

To bench mark the assay 1 mM L-NAME was mixed with eNOS and reacted at room temperature for 15 minutes. 25 μL of reaction cofactor mix (50 mM Hepes pH 7.4, 50 μM arginine, 2 mM calcium chloride, 0.5 μM BH_4, 4 μM FAD, 4 μM FMN, 100μM calmodulin, 1 mM NADPH, 1 unit of nitrate reductase) was added and reacted for 45 minutes at room temperature. The reaction was quenched by the addition of 280 μL of DAN probe and reacted for 10 minutes. 76 μL of 3 M NaOH was added and the samples were diluted to 3 ml with water. The levels of nitrite were detected by excitation at 360 nm and emission at 410 nm. All other reactions were carried out in a similar fashion by mixing varying amounts of the protein constructs (GST_caveolin-1, GST_caveolin-1_F92A, caveolin-1_Myc_H6, caveolin-1_F92A_Myc_H6, and caveolin-1 82-101) with eNOS. In all cases, the buffer that the protein was dissolved in was used in a control reaction with eNOS to establish that the buffer did not have an effect on eNOS activity.

Results and Discussion

Previous studies on the interaction of caveolin-1 and eNOS used Glutathione S-transferase (GST) tagged caveolin-1 constructs of varying lengths (37). From this study it was shown that there was no effect on eNOS activity in the presence of GST alone and that a significant decrease in activity was only observed in the presence of full length caveolin-1, the scaffolding domain and the C-terminal domain. The N-terminal domain and intramembrane domain were shown to have no effect on eNOS activity (37). This is an important finding that indicates if mutations are made outside of the C-terminal and scaffolding domains any change in eNOS activity can be attributed to an overall global structural change in caveolin-1. In all cases, the maximum decrease in eNOS activity was approximately 50%. This is congruent with *in vivo* studies that show caveolin-1 attenuates the production of nitric oxide but does not abolish it.

Effect of detergents on eNOS activity

One of the challenges of investigating the interaction of caveolin-1 with eNOS is the presence of detergent. Caveolin-1 contains significant hydrophobic character which makes it necessary to have detergents present in order to keep caveolin-1 soluble. However, detergents are known to be denaturing and can affect enzyme activity. Therefore the detergent selected for the assay must have a relatively low CMC, which will allow for lower concentrations of detergent. Brij is an attractive choice because it has a low CMC and is also relatively inexpensive (see Appendix 5-2). Additionally, Brij is a relatively mild detergent, which should not disrupt the enzyme activity. There is no effect on eNOS activity at high concentrations of either Brij 35 or Brij 58 (Figure 5-1).

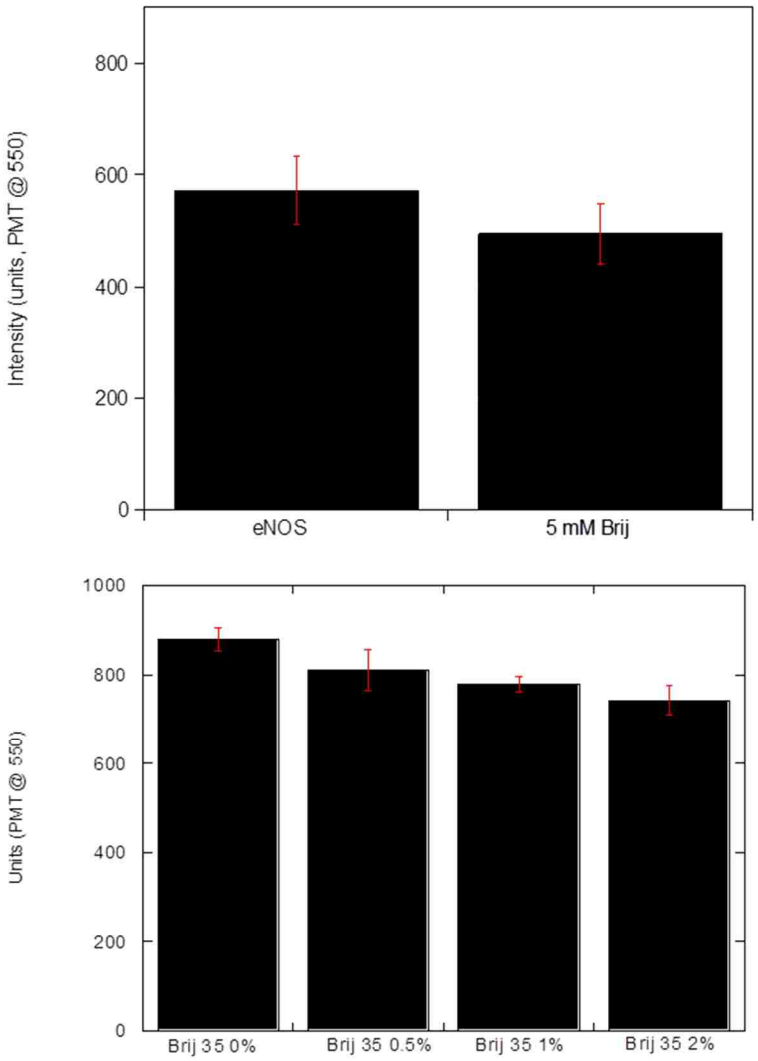

Figure 5-1. the results of eNOS activity in the presence of various amounts of Brij. The top panel shows reaction with 5 mM Brij 58 and the bottom panel shows reaction in the presence of 0%, 0.5%, 1% and 2% Brij 35

Validation of eNOS assay

To validate that the eNOS assay was working, initially eNOS was reacted with a known small molecule inhibitor N(G)-nitro-L-arginine methyl ester (L-NAME). L-NAME is an arginine derivative that binds to eNOS and prevents the generation of nitric oxide. It has been shown *in vivo* that when the caveolin-1 gene is silenced there is an increase in eNOS activity and therefore a build-up of nitric oxide leading to pulmonary defects. Treatment with L-NAME reverses the pulmonary defects and decreases nitric oxide levels in cells (134). When the assay is performed in the presence of 1 mM L-NAME there is a significant decrease in eNOS activity (Figure 5-2).

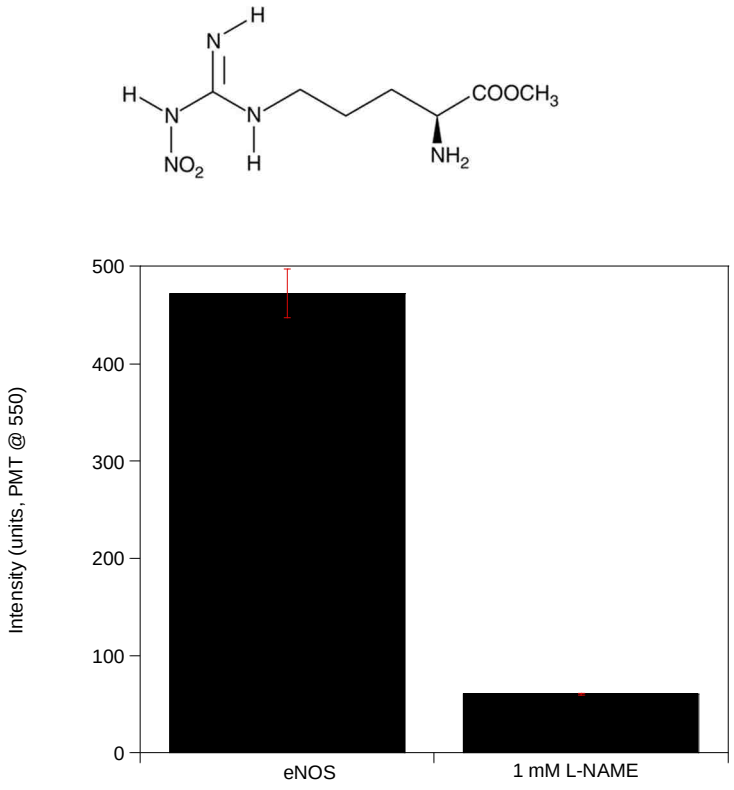

Figure 5-2. A) Structure of L-NAME. B) the results of the eNOS assay in the presence of 1 mM L-NAME.

It has been shown that the caveolin-1 scaffolding domain peptide (residues 82-101) inhibits eNOS (135, 136, 137). *In vivo* delivery of the caveolin-1 scaffolding domain in caveolin-1 deficient mice reduces the level nitric oxide and reverses endothelial dysfunction (103). Because of this well established interaction, eNOS was incubated with various concentrations of the purified scaffolding domain peptide to show a concentration dependence on inhibition (Figure 5-3). These two results prove eNOS enzyme is active in the context of the assay.

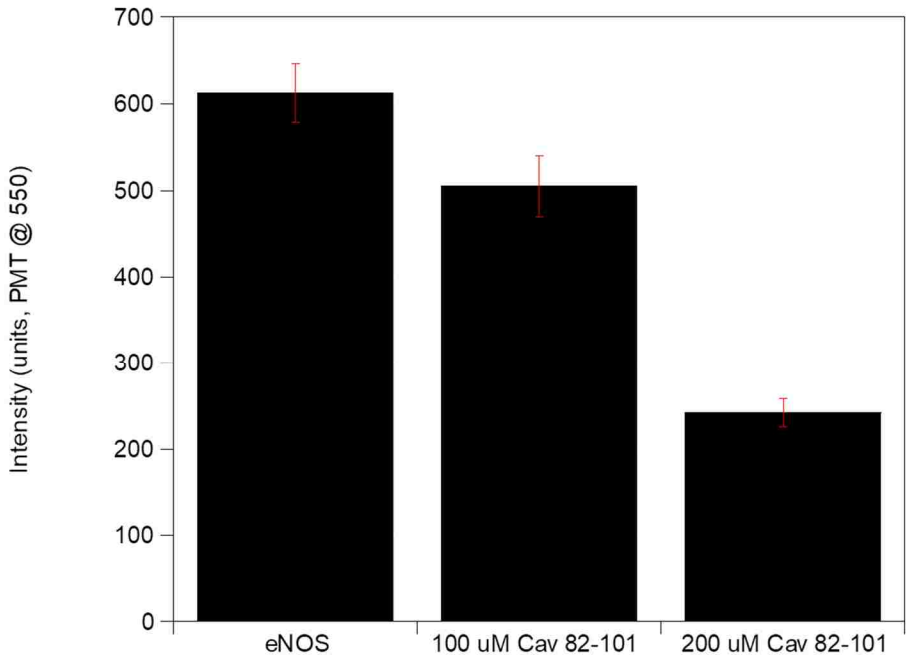

Figure 5-3. Results of eNOS assay with varying amounts of the caveonlin-1 scaffolding domain. Error bars based on the average of 5 trials.

eNOS reaction with caveolin-1 F92A

Alanine scanning mutagenesis of the caveolin-1 scaffolding domain revealed that residue 92 was critical for caveolin-1 inhibition of eNOS. When residue 92 (a phenylalanine in the WT protein) was mutated to alanine, there was no inhibition of eNOS activity and in some studies there was actually an increase in the overall levels of nitric oxide (138). Interestingly, based on the NMR data presented in chapter 4, there was no structural change when F92 was mutated to alanine. In agreement with these studies, it has been shown that caveolin-1 F92A still binds to eNOS but does not exhibit the inhibitory function of wild-type (135). In the context of the assay presented, the presence of the wild-type protein showed a decrease in eNOS activity while the presence of caveolin-1 F92A restored the eNOS activity (Figure 5-4). All of these studies together show the detection of nitric oxide levels in solution in the presence of caveolin-1 is a good method to probe the structural effects of mutations to caveolin-1 on its function.

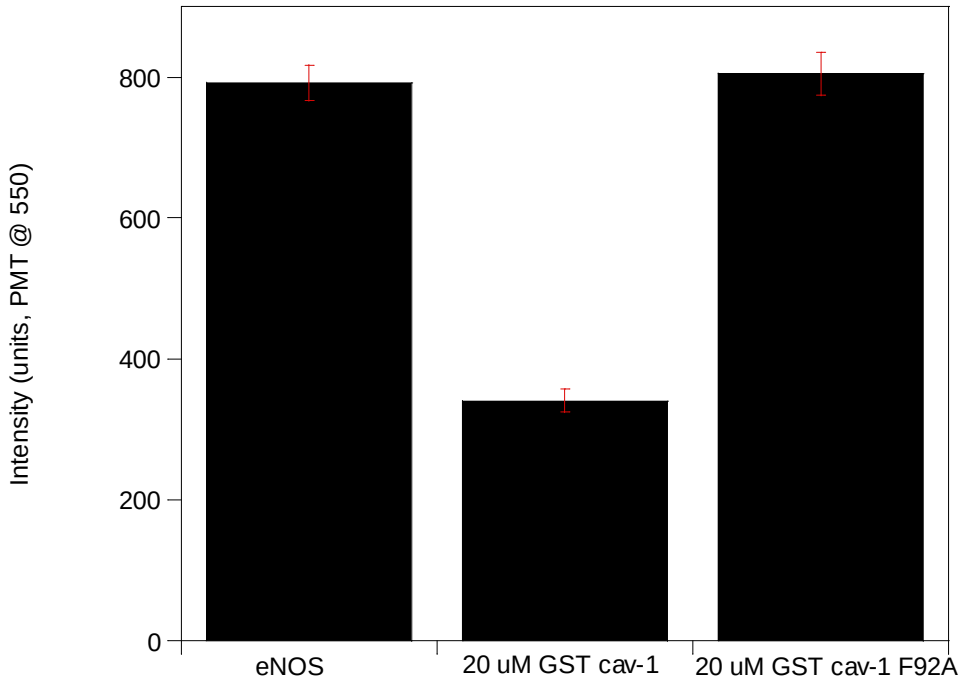

Figure 5-4. The results of the eNOS assay in the presence of N-terminal GST tagged caveolin-1comparing eNOS alone and in the presence of wild-type caveolin-1and F92A.

Effect of C-terminal tags on eNOS activity

The caveolin-1 C-terminal domain is the least characterized domain of the caveolin-1 protein. However, it appears to play a much larger role in the overall structure and function of the protein than previously thought. An *in vivo* study conducted on caveolin-1 constructs containing different C-terminal tags revealed that the presence of these tags cause significant deviation in behavior from the wild-type protein (139). The addition of bulky fluorescent tags (GFP and m-Cherry), caused larger aggregates of caveolin-1 to form when compared to the wild-type. The addition of a myc antibody tag showed the least amount of perturbation when compared to the wild-type (139). It is

important to note that in all three of the C-terminal tags, none of the over-expressed constructs interacted with endogenous caveolin-1 in cells (139). This shows that the presence of C-terminal tags causes a change in caveolin-1 trafficking and the cells do not recognize C-terminal tagged caveolin-1 in the same manner as the wild-type.

When the eNOS assay is performed in the presence of caveolin-1_myc_his (myc added as an antibody tag and the histidine tag for purification), the wild type protein behaves identically to the N-terminally tagged protein. However, when caveolin-1_myc_his_F92A is reacted with eNOS there is a loss of eNOS activity (Figure 5-5A and 5-5B). It has been shown that the caveolin-1 C-terminal domain can inhibit eNOS activity to the same extent as the scaffolding domain (37). This agrees that the presence of C-terminal tags has an effect on the overall structure and function of caveolin-1.

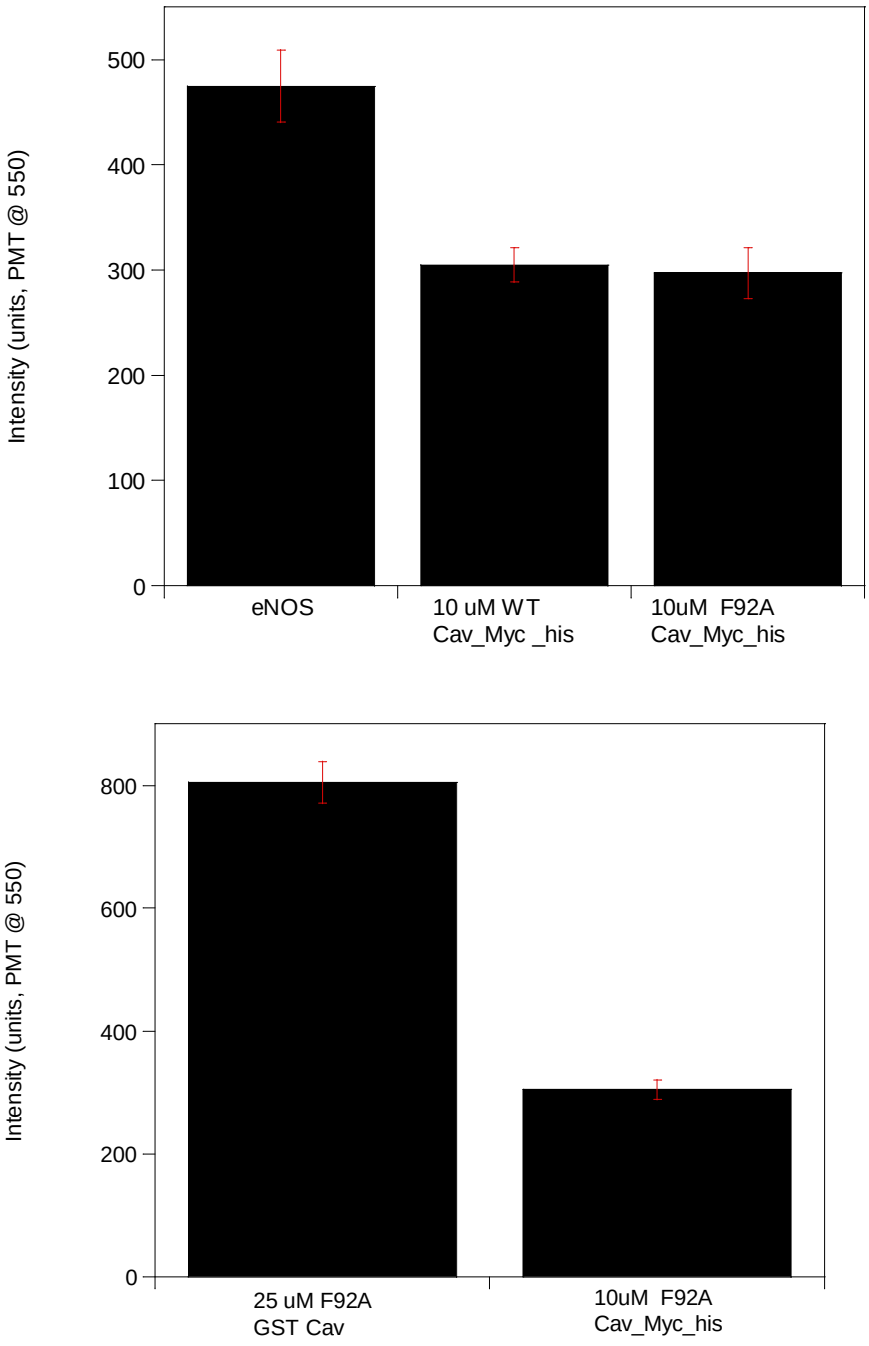

Figure 5-5. A) results of eNOS assay with C-terminal tagged cavolin-1 wild-type and F92A. B) Comparison of the results of the eNOS assay in the presence of N-terminal and C-terminal tagged caveolin-1_F92A. Error bars are based on the average of 5 trials.

Conclusions

The development of an *in vitro* functional assay is critical for understanding the effects of caveolin-1 mutations. Overall, these studies have shown that the interaction of eNOS with caveolin-1 can be used to probe structural changes of caveolin-1 *in vitro*. This can give a complementary data set for the alanine and phenylalanine scanning mutagenesis presented in chapter 4. Importantly, this assay can be utilized to determine long range structural effects caused by point mutations. Because it has been shown that the intramembrane domain alone does not inhibit eNOS, mutations made to this domain that show inhibition indicate a global structural change. Additionally, this assay can be utilized to investigate how the presence of fluorescent and antibody tags affect the structure and function of caveolin-1. Based on the data presented even the presence of a small antibody tag (in this case a myc tag) causes dramatic changes in caveolin-1 function. This indicates that the integrity of the C-terminal domain is essential for caveolin-1 biology. Having an *in vitro* assay that can rapidly detect changes in caveolin-1 function will have broad implications in the biophysical characterization of caveolin-1 and also add a complementary technique to further elucidate how structural changes affect caveolin-1 function.

Appendix 5-1. Recipe for auto-induction media

ZYM-5052
20 grams NZ Amine 10 grams yeast extract 1916 mL water 4 mL 1 M $MgSO_4$ 400 μL 1000X trace metals 40 mL 50x5052 40 mL 50xM

Appendix 5-2. Protein sequences for functional assay

Construct	Sequence
GST_caveolin-1_Myc	MPPYTVVYFPVRGRCAALRMLLADQGQSWKEEVVTVETWQEGSLKASCL YGQLPKFQDGDLTLYQSNTILRHLGRTLGLYGKDQQEAALVDMVNDGVE DLRCKYISLIYTNYEAGKDDYVKALPGQLKPFETLLSQNQGGKTFIVGD QISFADYNLLDLLLIHEVLAPGCLDAFPLLSAYVGRLSARPKLKAFLAS PEYVNLPINGNGKQMSGGKYVDSEGHLYTVPIREQGNIYKPNNKAMADE LSEKQVYDAHTKEIDLVNRDPKHLNDDVVKIDFEDVIAEPEGTHSFDGI WKASFTTFTVTKYWFYRLLSALFGIPMALIWGIYFAILSFLHIWAVVPC IKSFLIEIQCISRVYSIYVHTVCDPLFEAVGKIFSNVRINLQKEIEQKL ISEEDL
GST_caveolin-1_F92A_Myc	MPPYTVVYFPVRGRCAALRMLLADQGQSWKEEVVTVETWQEGSLKASCL YGQLPKFQDGDLTLYQSNTILRHLGRTLGLYGKDQQEAALVDMVNDGVE DLRCKYISLIYTNYEAGKDDYVKALPGQLKPFETLLSQNQGGKTFIVGD QISFADYNLLDLLLIHEVLAPGCLDAFPLLSAYVGRLSARPKLKAFLAS PEYVNLPINGNGKQMSGGKYVDSEGHLYTVPIREQGNIYKPNNKAMADE LSEKQVYDAHTKEIDLVNRDPKHLNDDVVKIDFEDVIAEPEGTHSFDGI WKASFTT**A**TVTKYWFYRLLSALFGIPMALIWGIYFAILSFLHIWAVVP CIKSFLIEIQCISRVYSIYVHTVCDPLFEAVGKIFSNVRINLQKEIEQK LISEEDL
Caveolin-1_Myc_H6	MSGGKYVDSEGHLYTVPIREQGNIYKPNNKAMADELSEKQVYDAHTKEI DLVNRDPKHLNDDVVKIDFEDVIAEPEGTHSFDGIWKASFTTFTVTKYW FYRLLSALFGIPMALIWGIYFAILSFLHIWAVVPCIKSFLIEIQCISRV YSIYVHTVCDPLFEAVGKIFSNVRINLQKEIEQKLISEEDLHHHHHH
Caveolin-1_F92A_Myc_H6	MSGGKYVDSEGHLYTVPIREQGNIYKPNNKAMADELSEKQVYDAHTKEI DLVNRDPKHLNDDVVKIDFEDVIAEPEGTHSFDGIWKASFTT**A**TVTKY WFYRLLSALFGIPMALIWGIYFAILSFLHIWAVVPCIKSFLIEIQCISR VYSIYVHTVCDPLFEAVGKIFSNVRINLQKEIEQKLISEEDLHHHHHH
Caveolin-1(82-101)	DGIWKASFTTFTVTKYWFYR

Appendix 5-3. Structure of Brij 35 and Brij 58

Brij 58

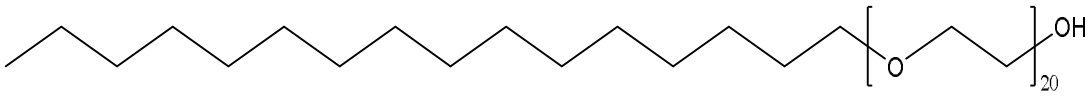

Brij 35

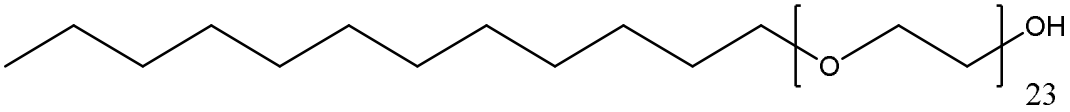

Chapter 6 Utilizing cysteine accessibility to determine membrane protein topology

Abstract

The caveolin-1 scaffolding domain is thought to play a critical role in membrane attachment and the formation of the oligomeric complex. However, the scaffolding domain is also reported as the major binding domain for almost all of the caveolin-1 binding partners as well as cholesterol. This is unusual because it indicates that the scaffolding domain interacts with both soluble and insoluble binding partners. Because of this it is unclear what environment the scaffolding domain exists in. To probe the position where the protein transitions from the aqueous environment to the plasma membrane, single cysteine mutations were made to residues 82-101 (the scaffolding domain). Several different maleimide probes were employed to determine the accessibility of the scaffolding domain. It was found that large thiol reactive groups (5 kDa PEG) were unable to interact with the caveolin-1 protein in membranes, even when reacted with an exposed residue. However, smaller thiol reactive probes (0.5 kDa and 1.2 kDa PEG) were able to efficiently react with the cysteine residues, though several considerations are discussed for utilizing these small PEGs. Data acquired for single cysteine mutations at the four tryptophan residues agreed with previously published fluorescence data and showed that W85 was the most exposed and W115 (thought to be buried in the membrane) was the least exposed. Overall, the determination of the topology of caveolin-1 is a complex problem, several considerations are presented.

Introduction

The major membrane interacting domains of caveolin-1 are the scaffolding and intramembrane domain. The intramembrane domain has been shown to be extremely hydrophobic and therefore is thought to be membrane embedded. However, the sequence of the scaffolding domain is much more variable and it is therefore not clear which parts of this domain are inserted in the membrane (if any). Structural studies of the scaffolding and intramembrane domain have shown that these two domains for the helix-break-helix motif that is thought to give caveolae its shape (56, 64, 113). However, the topology of the protein with respect to the membrane normal has not been determined. In particular, at what residue within the scaffolding domain the protein transitions from the cytosol to the plasma membrane has not been established.

The caveolin-1 scaffolding domain has been the most extensively studied domain within caveolin-1. This is attributed to the fact that the scaffolding domain has been shown to be critical for caveolin-1 function. It has been shown that the scaffolding domain interacts with several of caveolin-1 binding partners such as Src-like kinases, H-Ras, G-proteins and eNOS (39, 104, 140). As discussed in chapter 5, the scaffolding domain has been shown to inhibit eNOS activity both *in vivo* and *in vitro* (138). The scaffolding domain has also been shown to be important for membrane attachment. Removal of the scaffolding domain shows a disruption of trafficking of caveolin-1 to the membrane (58). Therefore, there is a loss of caveolae at the plasma membrane when the scaffolding domain is removed. The caveolin-1 scaffolding domain has been shown to contain a cholesterol recognition amino acid consensus (CRAC) motif (45). Because of the high levels of cholesterol within caveolae, it is thought that the scaffolding domain

recruits cholesterol at high levels to stabilize caveolae. Additionally, the scaffolding domain plays a critical role in the formation of caveolin-1 homo-oligomeric complexes (124).

Because of its many roles in caveolin-1 biology, several studies have tried to determine the orientation of the scaffolding domain within the membrane. These studies have revealed that the scaffolding domain reacts with the lipid bilayer and also is critical for the formation of the U-Shaped topology of caveolin-1 (141, 142). However, the previous studies were conducted on peptides of various lengths that did not contain the intact caveolin-1 protein. The presence of the other caveolin-1 domains may impact the orientation of the scaffolding domain in the membrane. As discussed in chapter 3, there is evidence that the C-terminal domain and the scaffolding domain may interact. Additionally, it has been shown that the presence of the intramembrane domain has an effect on the structure of the caveolin-1 scaffolding domain (56, 62). It is therefore necessary to determine the topology of the scaffolding domain in the context of the full length protein.

A common technique to determine the topology of a membrane protein is chemical accessibility assays (143). In these assays a reactive group is inserted into the protein sequence at various locations and accessibility is determined using either a membrane permeable or membrane impermeable probe. Therefore the exact residue where the protein transitions from the cytoplasm to the membrane is determined. Cysteine is often used to probe accessibility because it has a thiol group which has been shown to react *in vivo* with palmitic acid through a thioester bond (144). It is therefore a

non-perturbing insertion that can be reacted with a variety of probes that contain thiol reactive groups.

To investigate the topology of the caveolin-1 scaffolding domain in the context of the full length protein, 22 single cysteine mutations were made. The *E. coli* membranes were isolated and the cysteines were probed for accessibility utilizing several thiol reactive probes. By analyzing the protein in the *E. coli* membranes, only correctly folded protein that trafficked to the membrane is examined. Initially membranes were dissolved in q=0.5 bicelles and reacted with biotin maleimide. However, this method requires that the protein be purified because it is non-specific and all cysteine containing proteins will react. Therefore membranes were reacted with maleimide PEG derivatives, which do not require purification because reactivity with the probe is assessed by a molecular weight shift. Interestingly, the large PEG molecules showed no reactivity. However, smaller maleimide PEG derivatives showed significant reaction. By benchmarking the cysteine reactivity with the four tryptophan residues, whose location in the bilayer has been previously studied, several caveats to utilizing cysteine scanning to determine caveolin-1 topology were discovered.

Materials and Methods

Construct design and mutation

A full length caveolin-1 construct encompassing residues 1-178 was used as the template for the site directed mutagenesis and was designated as the "wild-type" construct (see Appendix 6-2). The three native cysteine residues were mutated to serine to avoid off target reaction with the thiol reactive probe and has previously stated the mutation of these cysteine residues has no effect on caveolin-1 function (31). Additionally a Myc tag was appended to the C-terminus to allow for antibody detection followed by a hexa-histidine tag. Single cysteine constructs were generated by Agilent Quickchange mutagenesis to generate at total of 23 constructs (cysteines at residues 82-101, W115, W128, and tyrosine 14). All constructs were cloned into pET 24a and transformed into BL-21(DE3) cells.

Protein expression

All constructs were expressed using auto-induction media as described by Studier (105). 1 L cultures were inoculated with 1 mL of a 5 mL overnight culture and grown for 24 hours at 25°C. Cells were harvested by centrifugation at 8300 x*g* for 15 minutes at 4°C. Pellets were washed with 200 mL of 0.9% (w/v) saline and collected by centrifugation at 5000 x*g* for 30 minutes at 4°C.

Membrane Isolation

1 L cell pellets were resuspended in 40 mL 1XTAE and reacted with 1 mg/mL lysozyme for 15 minutes on ice with stirring. Cells were lysed by sonication for 45

minutes with stirring on ice and the temperature was monitored to maintain <10°C. Unbroken cells and cellular debris were removed by centrifugation at 30,000 x*g* for 30 minutes at 4°C. The pellet was discarded and the membranes were extracted from the supernatant by centrifugation at 130,000 x*g* for 20 minutes at 4°C. Membrane pellets were washed with 30 mL of 1XPBS containing 100 μM TCEP and pelleted by centrifugation at 130,000 x*g* for 20 minutes at 4°C. Membranes were resuspended in 1X PBS, 100 μM TCEP with 30% sucrose and aliquoted for storage at -80°C until use in the assay.

Phosphate Assay

Lipid concentrations were determined by the method adapted from the protocol of Rouser *et. al*. (145) (see Appendix 6-1 for phosphate assay protocol). Initially 1 mL of membranes were pelleted and reacted with 5 μL of DNase for 1 hour at 37°C to remove any background phosphate. Membranes were pelleted at 50,000 x*g* for 2 hours at 4°C and resuspended in 1 mL of 1X TAE. The phosphate levels were normalized between all membrane samples by adjusting the final volume for resuspension after the final wash.

Bicelle preparation

A 2x DMPC/DHPC bicelle solution (q=0.5 and 3% (w/w)) containing 38% CHS and 19% sphingomyelin was prepared by drying down DMPC, CHS and sphingomyelin out of chloroform. Bicelles were rehydrated in 1XPBS and DHPC. 20 μL of 2 X bicelle

solutions was added to 20 μL of membranes and vortexed for 1 minute. Samples were cleared by centrifugation at 50,000 x*g* for 1 hour at 25°C.

Reaction with maleimide probe

20 μL of protein in bicelles were reacted with 2 mM maleimide PEG of varying lengths (0.5, 1.2 and 5 kDa) for 5 minutes at 37°C. Reactions were quenched by the addition of 5 mM β-Mercaptoethanol (BME). Samples were diluted to 100 μL with 1X PBS and 25 μL of 5X non-reducing SDS-page lading dye was added. Samples were vortexed and boiled for 2 minutes. A similar procedure was followed for the reaction with biotin maleimide.

Purification on Nickel magnetic agarose beads

After reaction with the biotin maleimide, 500 μL of lysis buffer (50 mM phosphate pH 8.0, 300 mM NaCl, 10 mM imidazole, 60 mM octyl-glucoside) was added to each sample. Samples were vortexed and 15 μL of Nickel-NTA magnetic agarose beads (Qiagen, Germantown, MD) were added and rotated overnight at room temperature. After overnight incubation, samples were placed on a magnetic stand and the supernatant was removed. The beads were washed twice with the lysis buffer containing 20 mM imidazole and 40 mM imidazole respectively. Samples were eluted from the beads with 25 μL of elution buffer (same as the lysis buffer with 250 mM imidazole added). SDS-page loading dye was added and samples were evaluated by western blot.

Western blot analysis of biotin maleimide

Biotin samples were run on a 0.75 mm 15% polyacrylamide gel and transferred to a PVDF membrane. Blots were co-blocked in 0.5% casin in TBST with 1:2800 avidin-AP. After imaging of the biotin, blots were stripped by washing with water then 100 mM NaOH and water again. After stripping blots were co-blocked in 0.5% powdered milk in TBST with 1:2800 myc-AP.

Western Blot analysis of the maleimide PEG reaction

All PEG samples were run on a 0.75 mm 15% polyacrylamide gel and transferred to a PVDF membrane. Blots were co-blocked with 0.5% (w/v) powdered milk and 1:2000 Anti-myc antibody for 1 hour. Blots were washed two times with 1X TBST. Blots were treated with 1:5000 anti-mouse antibody for 1 hour in 1X TBST.

Imaging

Anti-avidin and anti-myc blots were visualized utilizing BioRad ChemiDoc XRS+. Densitometry was performed utilizing Image Lab Software. Percent labeling was determined by the addition of the two protein bands which is equal to the total protein. Then the density of the PEGylated band was divided by the protein total. The percentages were normalized against the positive control (tyrosine 14) which is taken as 100% labeling.

Results and Discussion

Experimental design

To evaluate the accessibility of the caveolin-1 scaffolding domain 20 single cysteine constructs were generated. Additionally, a construct with Y14 mutated to cysteine was generated as a positive control. It has been shown that tyrosine 14 is phosphorylated *in vivo* and therefore it can be assumed that it is exposed to the aqueous environment and can represent 100% labeling (146). A cysteine-less construct (full length caveolin-1 with the three native cysteines mutated) was used as a negative control. Additionally mutations to W115 and W128 were generated for comparison to previously published tryptophan fluorescence experiments. With this method, the relative accessibility can be calculated based on the percent of biotin labeling compared to the total protein or the amount of PEGylated protein compared to the total protein.

Phosphate assay to normalize protein concentration

Because of variable expression between the different mutants, there is a need to standardize the concentrations. In general, the ratio of lipid to protein seems to be constant between the different constructs and therefore, the phosphate concentration can be used to normalize the amount of protein and lipid between the different constructs (Figure 6-1). This was true in the majority of the cysteine scanning mutants with the exception of four outliers that showed either significantly more protein (residues 99 and 100) or significantly less (residues 85 and 92). Even in the case of these extremes, the normalized intensity ratio did not exceed two-fold less protein or two-fold more protein.

Therefore, normalizing the phosphate levels in the *E. coli* membrane can be utilized, in the majority of cases to also normalize the protein concentration.

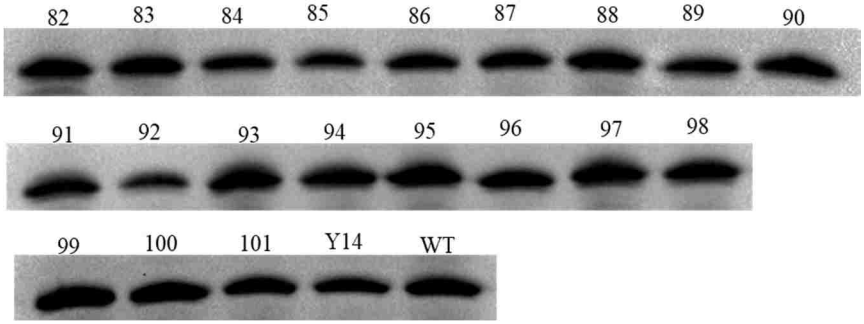

Figure 6-1. Anti-myc western blot showing that the protein levels can be normalized utilizing the phosphate assay. All intensities were within error with the exception of residues 99 and 100 which showed significantly higher intensities, and residues 85 and 92 which showed significantly lower intensities.

Purification on magnetic Ni- NTA beads

Because the E coli membranes likely contain native proteins that contain cysteine residues, it is necessary to purify the caveolin-1 constructs to avoid background contamination. By purifying the constructs after the reaction with the maleimide, the protein should be in its native conformation when it is reacted. However, because of the large number of samples, there needs to be a high throughput purification technique employed. Nickel affinity chromatography is a common technique that is used in protein purification. The advantage of a poly-histidine tag is that it is small and non- perturbing which means that in most cases it does not need to be cleaved. Ni-NTA magnetic beads allow for high through-put purification of poly-histidine tagged proteins. The use of Ni-NTA magnetic beads allowed for rapid purification of the cysteine containing constructs.

However, even with two washes at high imidazole concentrations (0, 25, 50, 75, 100, 125, 150 ,175 and 200 mM), there is still a significant amount of background (Figure 6-2). Additionally, at higher imidazole washes there is significant loss of the caveolin-1 band (marked as 25 kDa in Figure 6-2). This indicates that the reaction conditions are interfering with the nickel affinity reaction. Even at high imidazole washes (200 mM), there are still several impurities that are observed.

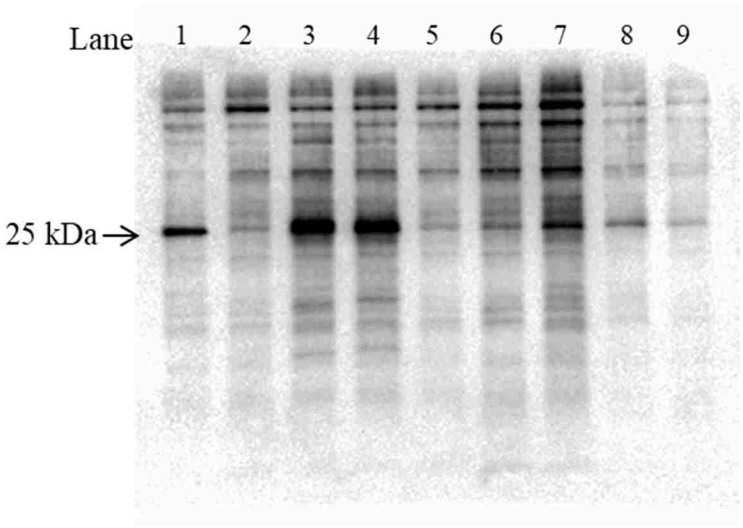

Figure 6-2. Representative biotin blot after imidazole washes of varying concentration. Y14C is used in this case as an example. Lane 1, 0 mM imidazole, Lane 2, 25 mM imidazole, Lane 3 50 mM imidazole, Lane 4, 75 mM imidazole, Lane 5, 100 mM imidazole, lane 6, 125 mM imidazole, lane 7 150 mM imidazole, lane 8, 175 mM imidazole, and lane 9, 200 mM imidazole.

Reaction with biotin maleimide

To assess the topology of the scaffolding domain of caveolin-1, the membrane fraction was isolated for all 22 cysteine containing constructs (20 constructs pertaining to

the scaffolding domain, Y14 as a positive control and wild-type as a negative control). The membrane fractions were then taken up into 2.3% q=0.5 bicelles that contained sphingomyelin and CHS which is a cholesterol derivative. Because the scaffolding domain is postulated to interact with cholesterol and the high levels of cholesterol that are found in caveolae, CHS is incorporated to 38%. After purification, there were significant differences in protein levels. For example, position 97 was not detected on either the biotin or myc_AP blot. Additionally, there is not a clear trend in accessibility (Figure 6-3). This highlights that the need to purify the protein adds significant error into the analysis.

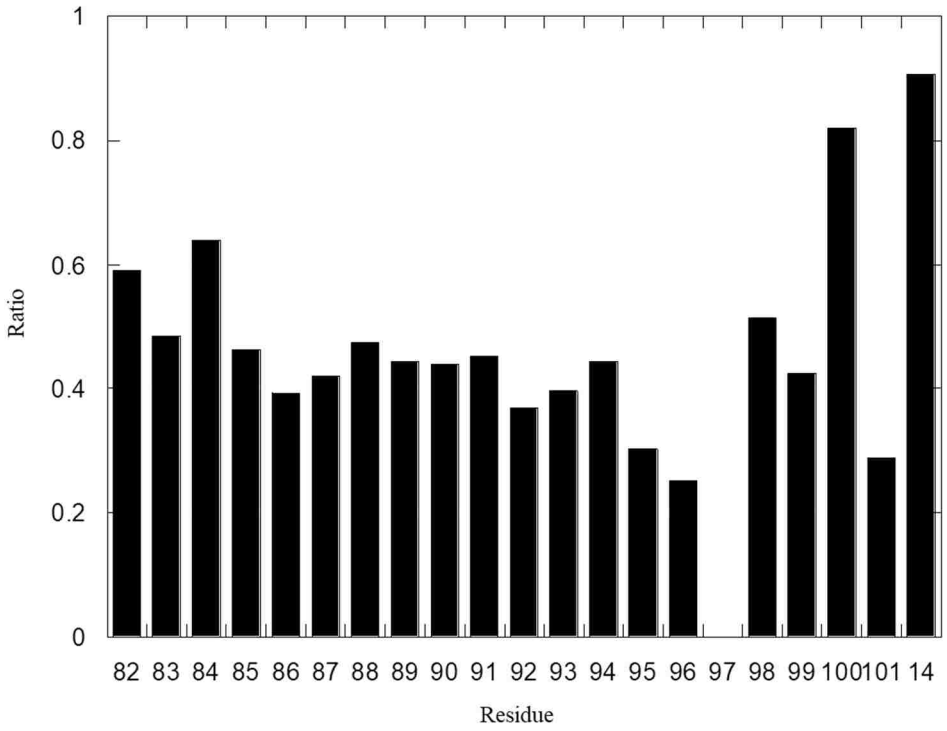

Figure 6-3. Relative labeling with biotin maleimide after nickel purification. 97 was not detected on either blot.

Reaction with maleimide PEG (5K)

The advantage of utilizing a maleimide PEG is that the protein does not have to be purified. Additionally, only one antibody is needed to probe the blots which can remove any error that is observed from stripping and re-probing. However, when the cysteine mutants in the scaffolding domain are reacted with the 5K maleimide PEG there was no significant molecular weight shift. This could indicate that the entire scaffolding domain is not exposed and is in fact buried in the plasma membrane. However, there is also no reaction with Y14C which is known to be exposed *in vivo* (Figure 6-4).

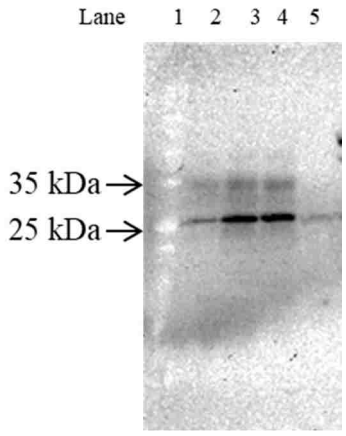

Figure 6-4. Representative western of Y14C and wild-type caveolin-1 reacted with 5 kDa maleimide PEG. Lane 1 molecular weight ladder, lane 2, Y14C reacted with 0.2 mM 5 kDa maleimide PEG, lane 3, Y14C reacted with 0.4 mM 5 kDa maleimide PEG, lane 4, Y14C reacted with 2 mM 5 kDa maleimide PEG, wild-type reacted with 2 mM 5 kDa maleimide PEG.

Additionally, when the 5 kDa maleimide PEG is reacted with a cysteine containing ubiquitin (which is a soluble protein) a molecular weight shift is seen but it is slowed significantly (reaction was only observed after 24 hours) (Figure 6-5). This indicated that the 5 kDa maleimide PEG has extremely slow kinetics and that the presence of the membrane may introduce steric bulk that will disrupt the reaction of the 5 kDa PEG with the protein.

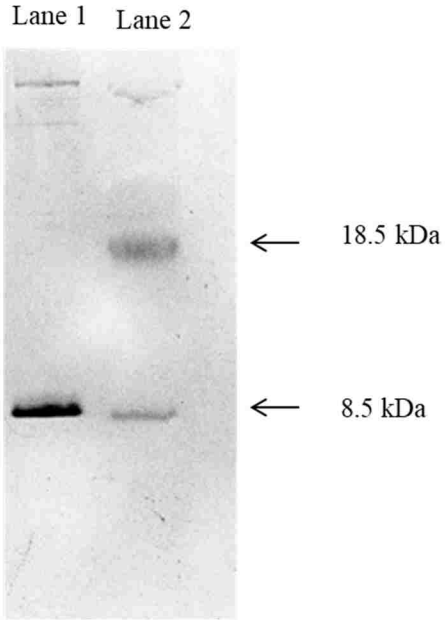

Figure 6-5. Reaction of ubiquitin_C2 with 5K maleimide PEG. Lane 1, no PEG added. Lane 2, after reaction with maleimide PEG for 24 hours.

Further, in the presence of 8M urea which is denaturing and should completely expose all the cysteine residues, there is still no significant molecular weight shift (Figure 6-6). All of this data supports that under the current reaction conditions the 5K maleimide PEG cannot react with the caveolin-1 scaffolding domain. This could be due

to steric effects from the presence of the membrane or this could indicate that the caveolin-1 scaffolding domain is not exposed when extracted from *E. coli* membranes.

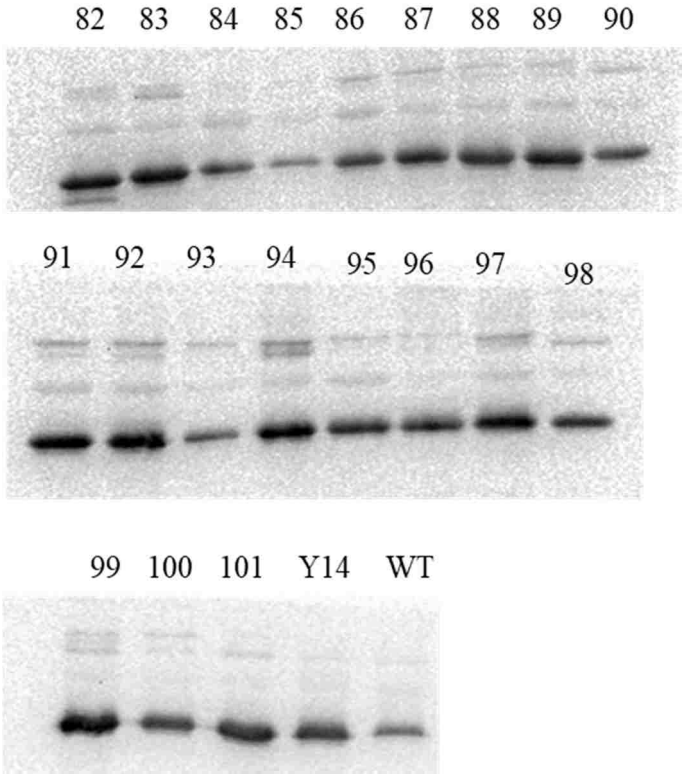

Figure 6-6. Representative western blot of the reaction of the cysteine mutants with 2 mM 5 kDa maleimide PEG in the presence of 8 M urea.

Reaction with smaller maleimide PEG derivatives

In order to confirm that the lack of reaction with the cysteine residues is due to the size of the 5K PEG and not because the protein is not exposed, smaller maleimide PEG derivatives were reacted with the constructs (Figure 6-7). Both the 0.5K PEG and 1.2K PEG showed a molecular weight shift when reacted with the cysteine residues in a subset of the scaffolding domain. However, it does not appear that there is a clear trend in the ratios of labeling. This could mean that the smaller maleimide PEG derivatives can (at

least to some degree) interact with cysteines in the membrane. While there is significant evidence that the 5K maleimide PEG does not pass through membranes, less is known about the permeability of the smaller PEG derivatives into the membrane.

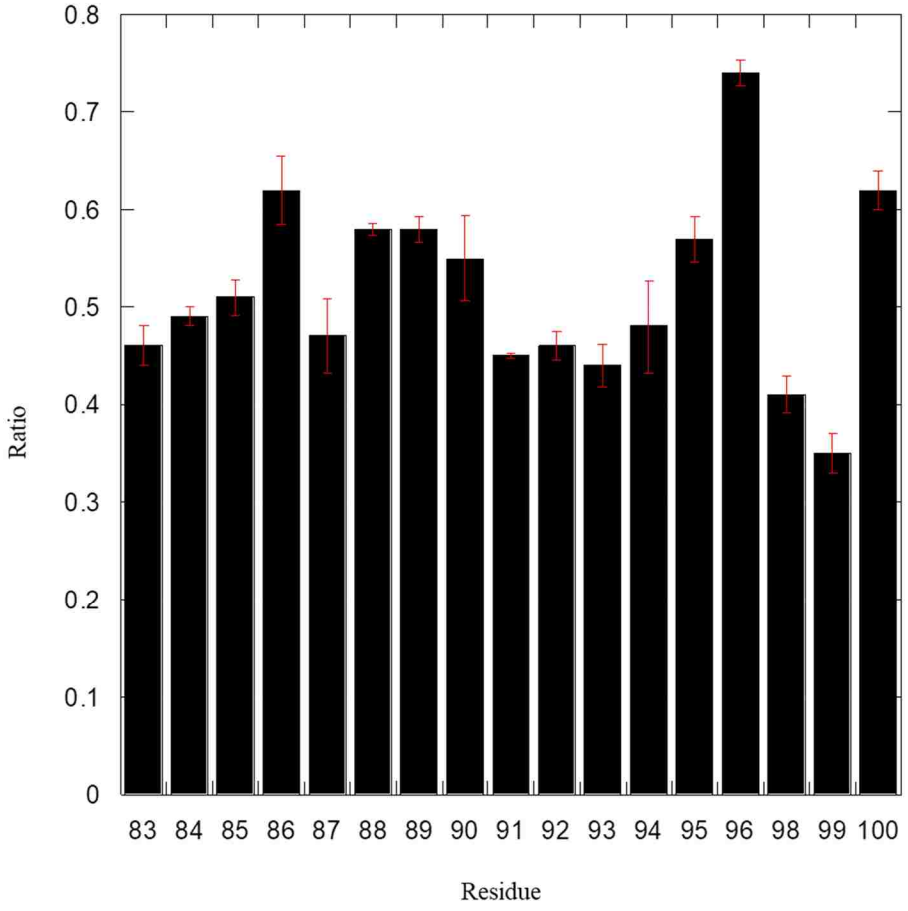

Figure 6-7. Relative PEGylation of the caveolin-1scaffolding domain when reacted with 1.2 kDa maleimide PEG. Error bars are based on three trials.

Utilizing tryptophan residues to benchmark 1.2 K maleimide PEG reaction in the bilayer

Caveolin-1 has four tryptophan residues within the scaffolding and intramembrane domains (W85, W98, W115, and W128). It has been shown previously

that the environment of the tryptophan residues (either exposed to the aqueous environment or buried in the membrane) can cause shifts in the fluorescence spectrum. Previous studies examining the exposure of the tryptophan residues of caveolin-1 in bicelles revealed that W85 and W128 were exposed, and W95 and W128 were buried in the membrane with W115 being the most buried (56). Because of these well-established exposures, it is possible to make cysteine mutations at the four tryptophan residues and react with the 1.2 kDa PEG and compare the results to the previously published data. Figure 6-8 shows the labeling ratios of the four tryptophan residues when they are mutated to cysteine and reacted with the 1.2 kDa PEG. As observed previously W 85 (which is the most exposed) shows the highest labeling ratio. However the remaining three tryptophan residues (W98, W1115 and W128) show similar labeling ratios. This indicates that the smaller PEG derivatives have some permeability into the membrane. The smaller PEG can therefore be used only to distinguish if a residue is exposed or buried and cannot establish subtle differences in residue depth within the bilayer.

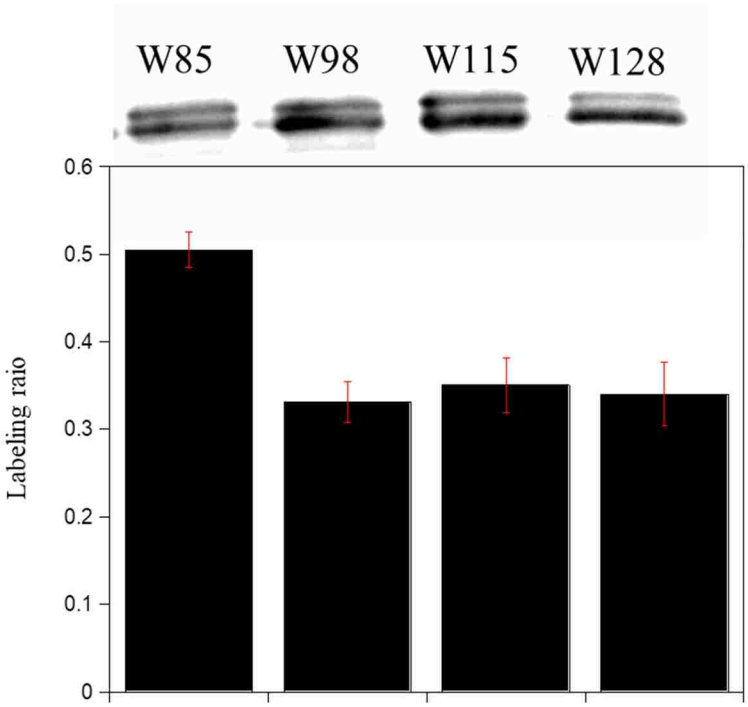

Figure 6-8. Representative western of the four tryptophan mutants replaced with cysteine and reacted with 1.2K maleimide PEG. The graph depicts the amount of labeling. The error bars are based on three trials.

Conclusion

Normally, the topology of a membrane spanning protein is easily determined by probing the accessibility of residues to a thiol reactive probe (143, 147). Residues that are exposed to the aqueous environment can be labeled, while residues that are located in the bilayer are shielded and no reaction is observed. Caveolin-1 presents a unique challenge because the protein does not actually span the bilayer. Instead, it is thought to remain mostly in the inner leaflet and contain an intramembrane turn. This presents unique challenges when attempting to determine the depth of the protein in the membrane as a large portion of the membrane domain (especially in the case of the scaffolding domain) may be interfacial. Additionally, while the intramembrane domain shows a distinct stretch of hydrophobic residues, the sequence of the scaffolding domain is much more variable and does not show a clear trend in hydrophobicity.

The reaction with biotin maleimide has several disadvantages, the first that the protein has to be purified. This can present technical challenges when examining a large sample set. Secondly, it requires a stripping step which can introduce error. One way to circumvent these challenges is to utilize maleimide PEG derivatives. Because this reaction will cause a molecular weight shift, there is no need to purify the protein and it only requires a single antibody for detection. Utilizing larger PEG derivatives will show the greatest molecular weight shift. However, the reaction of the 5 kDa maleimide PEG with a ubiquitin construct containing a single cysteine, which is a soluble protein, is slow and requires almost 24 hours achieve complete labeling. When the 5 kDa maleimide PEG is reacted with the cysteine mutations in the caveolin-1 scaffolding domain there is no significant reaction seen even after 24 hours or in the presence of denaturing agents

such as urea. Smaller maleimide PEG derivatives do show reaction; however there is no real trend in reactivity. This is most likely due to the ability of the smaller PEG maleimide to permeate the membrane (at least to a minor extent).

This chapter highlights the unique challenges that are presented when examining the topology of caveolin-1. While the maleimide probes are able to give a qualitative result of “exposed” or “not exposed”, they are not able to elucidate the subtle differences in exposure that are necessary to establish the interfacial characteristic of caveolin-1.

Appendix 6-1. Phosphate assay protocol

1. Dry down 5 to 10 µL of membranes into a film under N_2.
2. Add 330 µL of 70% percholric acid
3. Heat samples to 220-240°C for 45 minutes.
4. Prepare standards by adding the appropriate amount of potassium phosphate to 330 µL of 70% perchloric acid.
5. Allow lipid containing samples were cooled to room temperature and add 250 µL of ascorbic acid
6. Vortex to mix
7. Add 250 µL of 2.5% ammonium molybdate
8. Vortex to mix.
9. Bring samples and standards to a final volume of 2 mL with water.
10. Heat all samples and standards to 100°C for 10 minutes.
11. Cool to room temperature
12. Read the absorbance at 800 nm.

Appendix 6-2. Sequences of cysteine scanning constructs.

Construct	Sequence
D82C	MSGGKYVDSEGHLYTVPIREQGNIYKPNNKAMADELSEKQVYDAHTKEIDLVNRDPKHLND DVVKIDFEDVIAEPEGTHSF**C**GIWKASFTTFTVTKYWFYRLLSALFGIPMALIWGIYFAIL SFLHIWAVVPSIKSFLIEIQSISRVYSIYVHTVSDPLFEAVGKIFSNVRINLQKEIEQKLI SEEDLHHHHHH
G83C	MSGGKYVDSEGHLYTVPIREQGNIYKPNNKAMADELSEKQVYDAHTKEIDLVNRDPKHLND DVVKIDFEDVIAEPEGTHSFD**C**IWKASFTTFTVTKYWFYRLLSALFGIPMALIWGIYFAIL SFLHIWAVVPSIKSFLIEIQSISRVYSIYVHTVSDPLFEAVGKIFSNVRINLQKEIEQKLI SEEDLHHHHHH
I84C	MSGGKYVDSEGHLYTVPIREQGNIYKPNNKAMADELSEKQVYDAHTKEIDLVNRDPKHLND DVVKIDFEDVIAEPEGTHSFDG**C**WKASFTTFTVTKYWFYRLLSALFGIPMALIWGIYFAIL SFLHIWAVVPSIKSFLIEIQSISRVYSIYVHTVSDPLFEAVGKIFSNVRINLQKEIEQKLI SEEDLHHHHHH
W85C	MSGGKYVDSEGHLYTVPIREQGNIYKPNNKAMADELSEKQVYDAHTKEIDLVNRDPKHLND DVVKIDFEDVIAEPEGTHSFDGI**C**KASFTTFTVTKYWFYRLLSALFGIPMALIWGIYFAIL SFLHIWAVVPSIKSFLIEIQSISRVYSIYVHTVSDPLFEAVGKIFSNVRINLQKEIEQKLI SEEDLHHHHHH
K86C	MSGGKYVDSEGHLYTVPIREQGNIYKPNNKAMADELSEKQVYDAHTKEIDLVNRDPKHLND DVVKIDFEDVIAEPEGTHSFDGIW**C**ASFTTFTVTKYWFYRLLSALFGIPMALIWGIYFAIL SFLHIWAVVPSIKSFLIEIQSISRVYSIYVHTVSDPLFEAVGKIFSNVRINLQKEIEQKLI SEEDLHHHHHH
A87C	MSGGKYVDSEGHLYTVPIREQGNIYKPNNKAMADELSEKQVYDAHTKEIDLVNRDPKHLND DVVKIDFEDVIAEPEGTHSFDGIWK**C**SFTTFTVTKYWFYRLLSALFGIPMALIWGIYFAIL SFLHIWAVVPSIKSFLIEIQSISRVYSIYVHTVSDPLFEAVGKIFSNVRINLQKEIEQKLI SEEDLHHHHHH
S88C	MSGGKYVDSEGHLYTVPIREQGNIYKPNNKAMADELSEKQVYDAHTKEIDLVNRDPKHLND DVVKIDFEDVIAEPEGTHSFDGIWKA**C**FTTFTVTKYWFYRLLSALFGIPMALIWGIYFAIL SFLHIWAVVPSIKSFLIEIQSISRVYSIYVHTVSDPLFEAVGKIFSNVRINLQKEIEQKLI SEEDLHHHHHH
F89C	MSGGKYVDSEGHLYTVPIREQGNIYKPNNKAMADELSEKQVYDAHTKEIDLVNRDPKHLND DVVKIDFEDVIAEPEGTHSFDGIWKAS**C**TTFTVTKYWFYRLLSALFGIPMALIWGIYFAIL SFLHIWAVVPSIKSFLIEIQSISRVYSIYVHTVSDPLFEAVGKIFSNVRINLQKEIEQKLI SEEDLHHHHHH
T90C	MSGGKYVDSEGHLYTVPIREQGNIYKPNNKAMADELSEKQVYDAHTKEIDLVNRDPKHLND DVVKIDFEDVIAEPEGTHSFDGIWKASF**C**TFTVTKYWFYRLLSALFGIPMALIWGIYFAIL SFLHIWAVVPSIKSFLIEIQSISRVYSIYVHTVSDPLFEAVGKIFSNVRINLQKEIEQKLI SEEDLHHHHHH
T91C	MSGGKYVDSEGHLYTVPIREQGNIYKPNNKAMADELSEKQVYDAHTKEIDLVNRDPKHLND DVVKIDFEDVIAEPEGTHSFDGIWKASFT**C**FTVTKYWFYRLLSALFGIPMALIWGIYFAIL SFLHIWAVVPSIKSFLIEIQSISRVYSIYVHTVSDPLFEAVGKIFSNVRINLQKEIEQKLI SEEDLHHHHHH
F92C	MSGGKYVDSEGHLYTVPIREQGNIYKPNNKAMADELSEKQVYDAHTKEIDLVNRDPKHLND DVVKIDFEDVIAEPEGTHSFDGIWKASFTT**C**TVTKYWFYRLLSALFGIPMALIWGIYFAIL SFLHIWAVVPSIKSFLIEIQSISRVYSIYVHTVSDPLFEAVGKIFSNVRINLQKEIEQKLI SEEDLHHHHHH
T93C	MSGGKYVDSEGHLYTVPIREQGNIYKPNNKAMADELSEKQVYDAHTKEIDLVNRDPKHLND DVVKIDFEDVIAEPEGTHSFDGIWKASFTTF**C**VTKYWFYRLLSALFGIPMALIWGIYFAIL SFLHIWAVVPSIKSFLIEIQSISRVYSIYVHTVSDPLFEAVGKIFSNVRINLQKEIEQKLI SEEDLHHHHHH

V94C	MSGGKYVDSEGHLYTVPIREQGNIYKPNNKAMADELSEKQVYDAHTKEIDLVNRDPKHLND DVVKIDFEDVIAEPEGTHSFDGIWKASFTTFT**C**TKYWFYRLLSALFGIPMALIWGIYFAIL SFLHIWAVVPSIKSFLIEIQSISRVYSIYVHTVSDPLFEAVGKIFSNVRINLQKEIEQKLI SEEDLHHHHHH
T95C	MSGGKYVDSEGHLYTVPIREQGNIYKPNNKAMADELSEKQVYDAHTKEIDLVNRDPKHLND DVVKIDFEDVIAEPEGTHSFDGIWKASFTTFTV**C**KYWFYRLLSALFGIPMALIWGIYFAIL SFLHIWAVVPSIKSFLIEIQSISRVYSIYVHTVSDPLFEAVGKIFSNVRINLQKEIEQKLI SEEDLHHHHHH
K96C	MSGGKYVDSEGHLYTVPIREQGNIYKPNNKAMADELSEKQVYDAHTKEIDLVNRDPKHLND DVVKIDFEDVIAEPEGTHSFDGIWKASFTTFTVT**C**YWFYRLLSALFGIPMALIWGIYFAIL SFLHIWAVVPSIKSFLIEIQSISRVYSIYVHTVSDPLFEAVGKIFSNVRINLQKEIEQKLI SEEDLHHHHHH
Y97C	MSGGKYVDSEGHLYTVPIREQGNIYKPNNKAMADELSEKQVYDAHTKEIDLVNRDPKHLND DVVKIDFEDVIAEPEGTHSFDGIWKASFTTFTVTK**C**WFYRLLSALFGIPMALIWGIYFAIL SFLHIWAVVPSIKSFLIEIQSISRVYSIYVHTVSDPLFEAVGKIFSNVRINLQKEIEQKLI SEEDLHHHHHH
W98C	MSGGKYVDSEGHLYTVPIREQGNIYKPNNKAMADELSEKQVYDAHTKEIDLVNRDPKHLND DVVKIDFEDVIAEPEGTHSFDGIWKASFTTFTVTKY**C**FYRLLSALFGIPMALIWGIYFAIL SFLHIWAVVPSIKSFLIEIQSISRVYSIYVHTVSDPLFEAVGKIFSNVRINLQKEIEQKLI SEEDLHHHHHH
F99C	MSGGKYVDSEGHLYTVPIREQGNIYKPNNKAMADELSEKQVYDAHTKEIDLVNRDPKHLND DVVKIDFEDVIAEPEGTHSFDGIWKASFTTFTVTKYW**C**YRLLSALFGIPMALIWGIYFAIL SFLHIWAVVPSIKSFLIEIQSISRVYSIYVHTVSDPLFEAVGKIFSNVRINLQKEIEQKLI SEEDLHHHHHH
Y100C	MSGGKYVDSEGHLYTVPIREQGNIYKPNNKAMADELSEKQVYDAHTKEIDLVNRDPKHLND DVVKIDFEDVIAEPEGTHSFDGIWKASFTTFTVTKYWF**C**RLLSALFGIPMALIWGIYFAIL SFLHIWAVVPSIKSFLIEIQSISRVYSIYVHTVSDPLFEAVGKIFSNVRINLQKEIEQKLI SEEDLHHHHHH
R101C	MSGGKYVDSEGHLYTVPIREQGNIYKPNNKAMADELSEKQVYDAHTKEIDLVNRDPKHLND DVVKIDFEDVIAEPEGTHSFDGIWKASFTTFTVTKYWFY**C**LLSALFGIPMALIWGIYFAIL SFLHIWAVVPSIKSFLIEIQSISRVYSIYVHTVSDPLFEAVGKIFSNVRINLQKEIEQKLI SEEDLHHHHHH
Y14C	MSGGKYVDSEGHL**C**TVPIREQGNIYKPNNKAMADELSEKQVYDAHTKEIDLVNRDPKHLND DVVKIDFEDVIAEPEGTHSFDGIWKASFTTFTVTKYWFYRLLSALFGIPMALIWGIYFAIL SFLHIWAVVPSIKSFLIEIQSISRVYSIYVHTVSDPLFEAVGKIFSNVRINLQKEIEQKLI SEEDLHHHHHH
WT	MSGGKYVDSEGHLYTVPIREQGNIYKPNNKAMADELSEKQVYDAHTKEIDLVNRDPKHLND DVVKIDFEDVIAEPEGTHSFDGIWKASFTTFTVTKYWFYRLLSALFGIPMALIWGIYFAIL SFLHIWAVVPSIKSFLIEIQSISRVYSIYVHTVSDPLFEAVGKIFSNVRINLQKEIEQKLI SEEDLHHHHHH
W115C	MSGGKYVDSEGHLYTVPIREQGNIYKPNNKAMADELSEKQVYDAHTKEIDLVNRDPKHLND DVVKIDFEDVIAEPEGTHSFDGIWKASFTTFTVTKYWFYRLLSALFGIPMALI**C**GIYFAIL SFLHIWAVVPSIKSFLIEIQSISRVYSIYVHTVSDPLFEAVGKIFSNVRINLQKEIEQKLI SEEDLHHHHHH
W128C	MSGGKYVDSEGHLYTVPIREQGNIYKPNNKAMADELSEKQVYDAHTKEIDLVNRDPKHLND DVVKIDFEDVIAEPEGTHSFDGIWKASFTTFTVTKYWFYRLLSALFGIPMALIWGIYFAIL SFLHI**C**AVVPSIKSFLIEIQSISRVYSIYVHTVSDPLFEAVGKIFSNVRINLQKEIEQKLI SEEDLHHHHHH

Appendix 6-3. Structure of Biotin maleimide

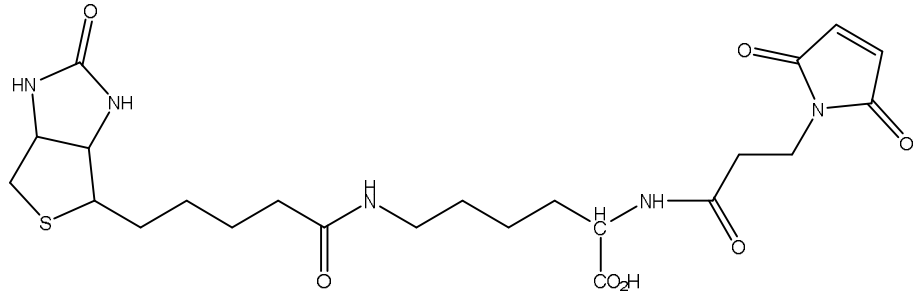

Nα-(3-Maleimidylpropionyl)Biocytin

Chapter 7 Utilizing Homo-FRET to determine the oligomerization of membrane proteins

Abstract

Understanding the oligomeric state of membrane proteins is vital to comprehending the overall organization of the membrane. For example, it has been postulated that high molecular weight complexes, of which caveolin-1 is a primary component, form a scaffold that directly supports the highly-curved structure of caveolae. However, it can be difficult to uncover the exact oligomeric state of membrane proteins because of the need for plasma membrane mimetics that encompass the complexity that the protein experiences *in vivo*. To begin to understand the oligomeric state of membrane proteins, we have developed a homo-FRET assay that utilizes liposomes, which can incorporate physiological levels of cholesterol. To benchmark our homo-FRET methodology, the oligomeric state of the transmembrane domain of Glycophorin A was examined which is known to form a stable dimer. Measurement of steady state fluorescence anisotropy as a function of fluorophore labeling revealed that Glycophorin A behaves as a dimer in our system, and the addition of a mutation known to disrupt the dimerization showed a significant shift to a more monomeric state. Preliminary data on caveolin-1 suggests that the presence of physiologically-relevant levels of cholesterol had no effect on the minimum oligomeric state or change in the amount of monomer in the system.

Introduction

The cellular membrane is a complex milieu of macromolecules of which membrane proteins constitute 50% by weight (148). In many cases, membrane proteins are members of multi-protein complexes where they engage in homo- and/or hetero-oligomerization (149, 150). However, these homo- and hetero-oligomeric interactions can be difficult to characterize due to the complexity of the oligomers and the lipid environment. Caveolae are an example of a domain that is unique to the bulk plasma membrane.

Caveolae have been shown to be enriched in cholesterol at levels approximately twice that of the bulk plasma membrane (21). Therefore, caveolae can be classified as a "raft-like" domain (151). It has been shown that the depletion of cholesterol causes a dramatic change in both the number of caveolae on the cell surface and their morphology (19). One of the major challenges when investigating how cholesterol effects membrane protein oligomerization is the inherent insolubility of cholesterol in most membrane mimetics. This is exacerbated by the need to incorporate large amounts (~38%) of cholesterol to accurately mimic the caveolae environment. Consequently, it is necessary to utilize and develop methodologies that can evaluate the oligomeric state of caveolin-1 under native-like conditions.

One example of a membrane protein that is localized to these "raft like" domains and interacts with cholesterol is caveolin-1. It has been postulated that there is a network of proteins (of which caveolin-1 is the most prevalent) that oligomerize at the caveolae surface that form a scaffold that helps to stabilize the highly curved nature of caveolae. However, the exact oligomeric state of caveolin-1 or the factors that contribute to the

formation of this network have not been established. Caveolin-1 was first isolated via detergent extraction of cell plasma membranes (32, 33). SDS-PAGE analysis of these detergent extracts revealed high molecular weight bands (200, 400, and 600 kD) that appeared to be predominantly the caveolin-1 protein, although these bands were found to be sensitive to the conditions in which the sample was loaded (43, 124). This observation established the postulation that caveolin-1 homo-oligomerizes. Later studies concluded that caveolin-1 forms high-order aggregates in a stepwise fashion, starting with 14-15 caveolin-1 monomers (identified as the 8S complex) which then combine to form larger oligomeric complexes (identified as 70S and 80S complexes) (7, 24, 65). However, all of these complexes have been shown to be highly sensitive to the sample conditions employed (i.e. detergent used), and therefore, it is unclear if these complexes fully recapitulate the caveolin-1-rich complexes observed *in vivo*. Because of the complex nature of caveolin-1 oligomerization, a new method to determine not only the size of the oligomeric complex, but also the effect of the environment (i.e. cholesterol) must be established.

In the current study, an *in vitro* homo-FRET methodology was developed to probe the oligomeric state of membrane proteins in liposomes (see Chapter 1 for homo-FRET introduction). First, the methodology was validated using the transmembrane domain of glycophorin A which is known to form a stable homodimer. It is also shown that this method is also able to determine changes in oligomeric state due to point mutations using known mutated constructs of glycophrin A that are shown to disrupt dimerization. This method was then used to determine the effect of physiologically relevant levels of cholesterol on the homo-oligomeric state of caveolin-1 in lipid vesicles.

Materials and Methods

Design of Construct.

M-Cherry_Caveolin1_MYC_His was expressed in Escherichia coli BL21(DE3) cells. The C-terminal MYC tag is known to preserve properties of native caveolin. (139) Caveolin-1 contains three native cysteine sites that are known to be palmitoylated *in vivo*. However, this palmitoylation has been previously shown to have no influence on the trafficking to the membrane or the formation of caveolae. (31) Therefore, the mutation of the three cysteine residues to serine has no effect on innate caveolin-1 function. The mCherry_Caveolin1_myc-H6_Y72F construct was generated by Quikchange mutagenesis and sequencing was confirmed. The mCherry_Glycophrin A_61-101_myc gene was purchased from genscript and cloned into pet24a. Two monomeric mutant constructs were generated by changing glycine 83 to an isoleucine and alanine which have been shown to disrupt dimerization. A "free" mCherry construct was generated by inserting a stop codon into a H6_mCherry_ caveolin-2 construct.

Cell Culture

An overnight culture was used to inoculate 1L of ZYM-5052 media. Cells were grown for 24 hours at 25°C. Cells were harvested at 8200 x*g* for 15 minutes. 1L cell pellets were washed with 200 mL of 0.9% saline and stored at -80C until ready for use. Protein pellets were thawed and resuspended in 40 mL of 1X TAE with 1 mg/ml of lysozyme and stirred on ice for 15 minutes. Cells were lysed by sonication using a Branson sonifier 450 (duty cycle 1, power 10) in 10 minute intervals for 30 minutes total (10 minutes on, 5 minutes off). The lysate was cleared for 30 minutes at 30,000 x*g*. The

supernatant was centrifuged at 130,000 x*g* for 15 minutes to pellet the membrane fraction. Membranes were resuspended in 2.5 mL of 1 X PBS with 30% (w/v) sucrose and stored at -20C for future analysis. H6_mCherry was prepared similarly, however 1L cell pellets were resuspended in 1 X PBS with 30% (w/v) sucrose containing 1 mg/ml lysozyme and lysed using sonication as described above. The lysate was cleared for 1 hour at 4C. The pellet was discarded and the supernatant stored at -20C.

Ni-NTA Purification

Caveolin-1 membranes were solubilized in 50 mM phosphate pH 8.0, 300 mM NaCl, 10 mM imidazole and 2% Empigen BB. Samples were cleared for 30 minutes at 20,000 x*g*. Samples were loaded onto a Ni-NTA column. The column was washed with 10 column volumes of 150 mM octylglucoside, 10 mM Tris pH 8.0 and 154 mM NaCl. Protein was eluted in 1 mL fractions with 150 mM octylglucoside, 10 mM Tris pH 8.0, 154 mM NaCl and 250 mM imidazole. The most concentrated samples were pooled and concentrated 10 fold.

Quantitation of light and dark constructs

After nickel purification, the amount of protein was determined using a micro BCA assay. The results from the BCA were confirmed by the examining the absorbance of the "light" sample at 587 nm. Once the concentration was accurately determined both the light and dark sample were diluted to 15 μM with 150 mM octylglucoside, 10 mM tris pH 8.0, and 154 mM salt.

Reconstitution of membrane proteins into vesicles

Vesicles were prepared following protocol outlined by Jiskoot *et al*. (152) Sets of seven phosphatidylcholine vesicles were made with increasing molar ratios of fluorescent label (0.1, 0.25, 0.4, 0.55, 0.7, 0.85, 1 molar ratio of fluorophore). Membrane fraction was solubilized using 150 mM octylglucoside, 0.9% NaCl, 10 mM Tris pH 7.4. Egg PC was solubilized in 150 μL of the same buffer for a final concentration of 10 mM. For cholesterol containing samples a mixture Egg PC and cholesterol were dried out of chloroform and resuspended in 150 μL of octylglucoside for a final concentration of 38% cholesterol. To ensure the incorporation of the lipids into the vesicles, lipids were quantified by phosphate assay as described by Rouser, et al. (145) and cholesterol content determined by Cayman Chemical Cholesterol Fluorometric Assay Kit according to manufacturer's instructions. It is important to note that in order to achieve cholesterol incorporation it is necessary to elevate the temperature to 40°C during vesicle preparation. Significantly less cholesterol is incorporated at lower temperatures.

Dilution was performed using Dionex P580 HPLC pump, by adding the appropriate amount of dilution buffer(154 mM NaCl, 10 mM Tris pH 7.4 with 250 mM sucrose) at a constant rate to achieve a final octylglucoside concentration of 15 mM (15 mL in the case of caveolin-1 samples and 3 mL for all other samples). Following dilution, samples were concentrated to <150 μL by ultrafiltration. Samples were subsequently washed by adding half of the initial volume of dilution buffer and concentrated to <150 μL and then dilution buffer was added for a final volume of 300 μL. Formation of vesicles was confirmed by Dynamic Light Scattering ALV/CGS-3 Compact Goniometer System.

Fluorescence Anisotropy.

Steady state anisotropy was measured using Horiba Scientific Fluorolog-3 at 25°C. Data was fit using correlation function for the determination of anisotropy in a population of oligomers, as outlined by Yeow *et al.*, (93) with Igor Pro 6.3a (equation 7-1).

Equation 7-1

$$r(f,N) = rm(x+(1-x)(1-f)^{(N-1)})$$

Results and Discussion

Creation of non-fluorescent mCherry

mCherry is an ideal fluorophore for homo-FRET because of its small Stokes shift (Forster distance of 5.10 nm) (153). However, for oligomeric analysis, one needs to vary the ratio of labeled to unlabeled subunits. *In vivo*, this is done by photobleaching the fluorophore to various extents to achieve the desired ratios (92, 154, 155). Unfortunately, this approach is not conducive to in vitro analysis, and certain fluorophores, such as mCherry, are highly resistant to photobleaching (156). In this study, the unlabeled sample was generated by making a point mutation to the mCherry protein. Mutation of tyrosine 72 to phenylalanine interferes with the generation of the chromophore, and hence renders mCherry non-fluorescent (Figure 7-1).

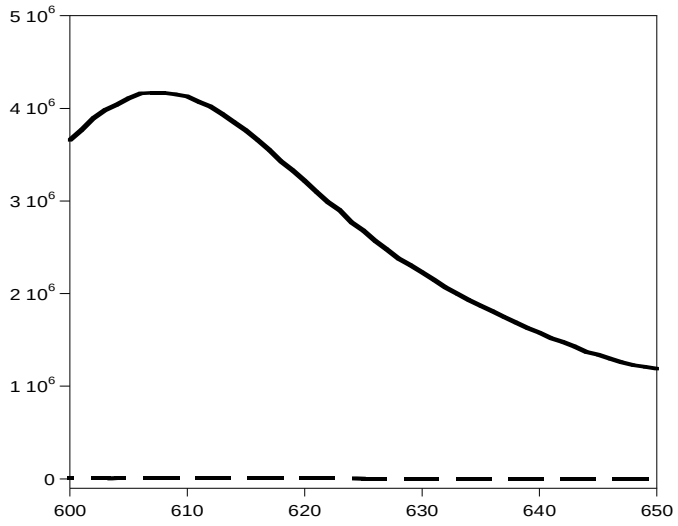

Figure 7-1. Comparison of the fluorescence intensity between wild-type H6_mCherry (light) and H6_mCherry_Y72F (dark). The dashed line represents the fluorescence of the dark at 587 nm and the solid black line represents the wild-type at the same wavelength.

However, to insure that this mutation is not altering the overall fold of the mCherry protein, circular dichroism analysis was undertaken. Figure 7-2 shows that both the wild-type and mutant mCherry have very similar far UV CD spectra which shows that the overall β-barrel fold of the protein remains intact. This indicates that the structural integrity of mCherry is not disrupted by the introduction of the point mutation. In addition, the CD spectra in Figure 7-2 is in agreement with previously published spectra of mCherry (157). Therefore, this methodology is suitable to obtain the various ratios of labeled to unlabeled protein needed for homo-FRET analysis.

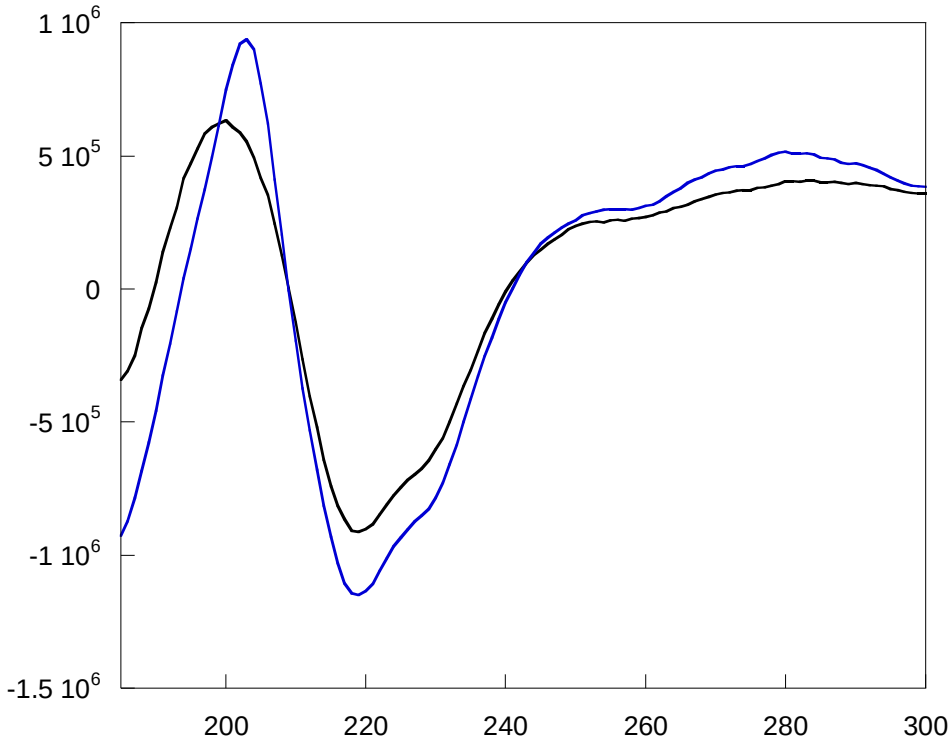

Figure 7-2. CD spectrum comparing H6-mCherry (black line) and H6_mCherry_Y72F (blue line). The signature minimum at 218 nm is indicative of a β-sheet structure.

Oligomeric behavior of mCherry itself in the absence and presence of liposomes

In the methodology described herein, the oligomeric state of a membrane protein is determined by creating a fusion construct with mCherry which serves as the homo-FRET reporter. However, before undertaking any inquisition into the oligomeric behavior, it is important to characterize first the behavior of mCherry itself in the presence and absence of liposomes. mCherry is a construct that has been engineered to have monomeric behavior, but it may behave differently in the presence of liposomes (158). First, a homo-FRET analysis was done of mCherry alone in buffer (Figure 7-3). When the data was fit to Equation 7-1, two quantities were determined, x which is the fraction of monomer and N which is the minimum oligomeric state.

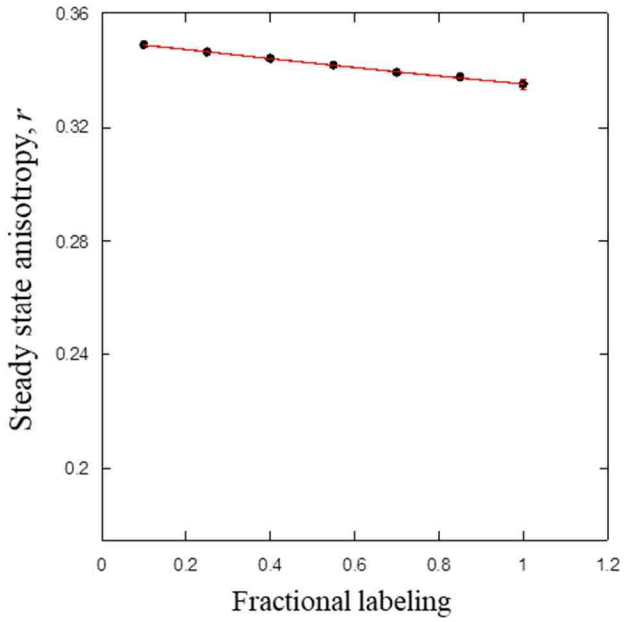

Figure 7-3. Anisotropy fit for H6_mCherry in buffer. Error bars are based on the average of three trials, however they are too small to be seen on the graph.

Clearly, the overwhelming majority of mCherry is monomeric as the fraction monomer, x, is 0.96 + 0.00087. The other 0.04 fraction has a minimum oligomeric state of 2.05 + 0.051. Therefore, although the engineered mCherry is largely monomeric there is a small oligomeric population (i.e. dimer). Therefore if results using an actual fusion protein construct show x values of 0.96 or higher, the determined N could be due to the mCherry itself and not the protein of interest. Therefore, conclusions should not be drawn from x values that are greater than 0.96. Next, a second homo-FRET analysis was done, this time in the presence of liposomes (Figure 7-4). Fortunately, no difference was observed when liposomes are added, x remains 0.96 + 0.0026 and N is 2.05 + 0.15. Therefore, the presence of a lipid bilayer does not influence the behavior of mCherry.

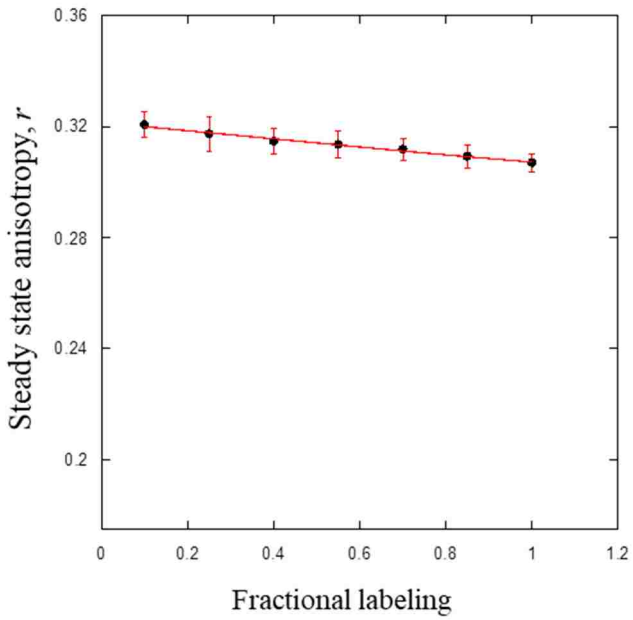

Figure 7-4. Steady state anisotropy fit for H6_mCherry in the presence of liposomes. Error bars are based on the average of three trials.

Validation of method with the transmembrane domain of Glycophorin A

The transmembrane domain of glycophorin A (GlyA) is a known stable homodimer, and has been extensively characterized (159, 160, 161). Additionally, the dimerization of Glycophorin A has been previously analyzed in vesicles prepared in several different ways and showed that there were no significant changes in the dimerization free energies (162). Therefore, it is an ideal membrane protein in which to benchmark this method.

To validate the homo-FRET method wild type GlyA was incorporated into liposomes and the steady state at varying molar ratios of "light" to dark was determined (Figure 7-5). The results were fit using equation7-1 and the minimum oligomeric state (N) was determined to be 2.02 $\pm$ 0.065 and the percent of monomer was determined to be 0.50 $\pm$ 0.009. This indicates that the major species is confirmed to be a dimer which is the expected oligomeric state of GlyA.

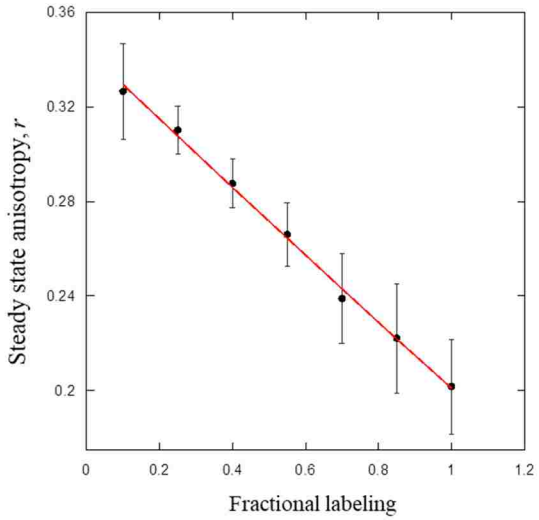

Figure 7-5 Anisotropy fit of wild type GlyA in the presence of liposomes. Error bars represent the average of three trials.

Detection of changes in oligomeric state due to point mutations

To evaluate if homo-FRET can determine changes in the oligomeric state based on the presence of point mutations, two separate monomeric GlyA constructs were designed (G83I and G83A). Glycine 83 has been identified as a critical residue to maintain the GlyA dimer. It is postulated to be part of the critical dimerization motif (GXXXG) (163). Through mutational scanning experiments it was shown that the introduction of any other amino acid at position 83, disrupts the dimerization but the alanine and isoleucine are particularly disruptive (164, 165, 166). Both G83A and G83I showed a change in percent of monomer when compared to the wild-type protein. However, there is also a change in the minimum oligomeric state when compared to the wild-type (Table7-1). This can be attributed to the presence of a high order inactive tetramer that has been previously reported in analytical ultra-centrifugation experiments of the monomer mutants in micelles (167). Additionally, all previous studies on these monomeric constructs have been performed either *in vivo* or on purified protein. It is unclear how utilizing the monomeric constructs extracted from membranes will affect the overall oligomeric state. But these results prove that utilizing homo-FRET, it is possible to evaluate changes in the oligomeric state from the introduction of point mutations. However, these results cannot be viewed in an absolute manner but rather used as a comparison with the wild-type.

Construct	N (minimum oligomeric state)	X (percent monomer)
WT _GLYA	2.02 ± 0.06	0.50 ± 0.009
G83A_GlyA	2.49 ± 0.23	0.73 ± 0.014
G83I_GlyA	2.35 ± 0.12	0.72 ± 0.001

Table 7-1. Comparison of the N and x values calculated for the wild-type_GlyA and the two mutant constructs.

Incorporation of cholesterol into liposomes

Because of the high percentage of cholesterol in caveolae, it was necessary to ensure that cholesterol was incorporated into the vesicles at relevant amounts. Vesicles were prepared according to Jiskoot *et al* with a projected concentration of cholesterol of 38% (152). To determine the percent of cholesterol incorporation, two assays were utilized: a cholesterol assay and a phosphate assay. In the lipid vesicle preparation the phosphate concentration was determined to be 5.8 mM + 0.72 while the cholesterol concentration was determined to be 3.75 mM + 0.45. Therefore the percentage of cholesterol was 39.3% + 4.2. Therefore, the cholesterol levels within the lipid vesicles is relevant to the levels of cholesterol in caveolae which have been shown to be between 35-38% (21).

Analysis of the oligomeric state of caveolin-1 in the presence of cholesterol

To evaluate the oligomeric state of caveolin-1 in the presence liposomes, varying ratios of light and dark mCherry_caveolin-1 were incorporated into liposomes. Previously, the oligomeric state of caveolin-1 was evaluated in micelles and bicelles using analytical ultracentrifugation. These studies revealed that the protein was monomeric (44). However, it is not possible to utilize liposomes in the AUC and therefore another technique such as homo-FRET must be utilized to compare how changing the bilayer mimetic affects the oligomeric behavior. When the anisotropy data for caveolin-1 was fit to equation 7-1, it was found that the majority of the protein is monomeric (Figure 7-6). However, the minimum oligomeric state was determined to be 4. This is the first *in vitro* analysis to show a high ordered species of caveolin-1. Importantly, there is no significant change in the oligomeric state of caveolin-1 in the presence of cholesterol. By utilizing homo-FRET not only can the oligomeric state of caveolin-1 be investigated but also changes in the environment and how the introduction of point mutations affect the overall oligomeric state can be probed. It should be noted that the homo-FRET studies of caveolin-1 are on-going and need further validation to determine the true oligomeric state. However, these are promising initial results.

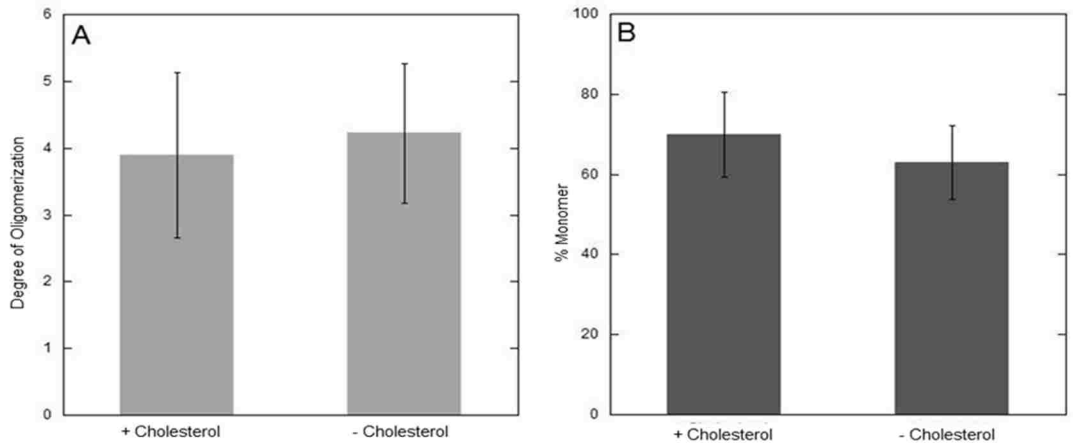

Figure 7-7. Comparison of A) the degree of oligomerization and B) the % monomer of caveolin-1 in the presence and absence of cholesterol (data collected by Sophia Miotto).

Conclusions

This chapter presents a novel homo-FRET assay to determine the oligomeric state of membrane proteins in liposomes in the presence of cholesterol. This method can detect the overall oligomeric state of membrane proteins (as seen in the case of GlyA) and also evaluate changes in oligomerization due to mutations. In this way, this technique can be used in a comparative manner. Preliminary studies on caveolin-1 indicate that the presence of cholesterol does not affect the oligomeric state of caveolin-1. Therefore, the high levels of cholesterol found in caveolae are not required for the formation of the network of oligomers thought to stabilize caveolae. Additionally, previous *in vitro* assays to determine the oligomeric state of caveolin-1 have shown that it is monomeric. This is the first in vitro analysis that suggests a higher order oligomeric state of caveolin-1 *in vitro*. However, further studies need to be conducted to establish the nature of this oligomeric state. Overall, homo-FRET utilizing mCherry as a fluorescent probe is an exciting new way to probe the oligomeric state of membrane proteins in native like bilayers.

Chapter 8 PFOA as a powerful tool to solubilize inclusion bodies

Abstract

The purification of membrane proteins can be challenging due to their low solubility in conventional detergents and/or chaotropic solutions. The introduction of fusion systems that promote the formation of inclusion bodies has facilitated the over-expression of membrane proteins. The protocol presented, describes the use of perfluorooctanoic acid (PFOA) as an aid in the purification of highly hydrophobic membrane proteins expressed as inclusion bodies. The advantage of utilizing PFOA is threefold: first, PFOA is able to reliably solubilize inclusion bodies, second, PFOA is compatible with nickel affinity chromatography, and third, PFOA can be efficiently dialyzed away to produce a detergent free sample. To demonstrate the utility of employing PFOA, a segment of the extremely hydrophobic membrane protein caveolin-1 was expressed and purified.

Introduction

Membrane proteins are major players in cellular biology. They are responsible for a plethora of cellular functions such as signal transduction and transport (168). Additionally, a large number of drug targets have been identified as membrane proteins, indicating that these proteins are heavily involved in normal cell function (169). However, the purification and analysis of these membrane proteins can be challenging because of their highly hydrophobic characteristics and strong propensity to aggregate (170). In addition, recombinant expression of membrane proteins usually results in low yields due to stresses put on the host membrane which results in toxicity. However, the over-expression of membrane proteins into inclusion bodies has emerged as a powerful tool to achieve high levels of protein in *E. coli* cells by eliminating the toxicity issues mentioned above which limit protein production (95).

Inclusion bodies can be isolated through a series of wash treatments that separate them from the soluble and membrane components of the host cell. While this insolubility is an attractive feature in aiding the isolation of the protein, it can be an obstacle when it comes to solubilizing the protein. Typically strong chaotropic solutions such as 8 M urea or 6 M guanadinium hydrochloride are utilized. However, for highly hydrophobic membrane proteins, these solutions are often not powerful enough to completely dissolve the inclusion bodies. Alternatively, strong detergents such as sodium dodecyl sulfate are attractive, but many of these detergents are not compatible with widely used purification techniques such as nickel affinity chromatography. Furthermore, it is often difficult, if not impossible, to remove these harsh detergents from the sample, which can be

problematic, as it is often desirable to acquire experimental results in the presence of a native-like detergent and lipid systems.

Perfluorooctanoic acid (PFOA) is a powerful detergent that has been shown to have the ability to solubilize membrane proteins (Figure 8-1) (171). In this report, the utility of PFOA is extended by showing that it can dissolve highly hydrophobic membrane proteins expressed as inclusion bodies. Furthermore, it is compatible with nickel affinity chromatography, and can be easily removed by dialysis, providing a detergent-free precipitate that can then be solubilized in a detergent or lipid system of choice. To demonstrate the usefulness of PFOA, we detail the purification of the integral membrane protein caveolin-1 from inclusion bodies. Caveolin-1 is the preeminent protein in membrane invaginations called caveolae, which have been shown to be crucial for caveolae formation, signal transduction, mechano-protection, and endocytosis; however studies of this protein have been hindered by its extremely hydrophobic character (35, 44, 113, 121). Because of this, caveolin-1 is an ideal candidate to demonstrate the utility of PFOA.

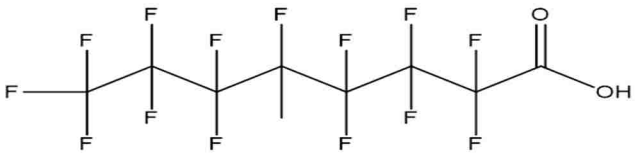

Figure 8-1. Structure of perfluorooctanoic acid (PFOA) (172).

Materials and methods

Protein expression

H9_TrpLE_caveolin-1_62-178 was cloned into the pET-24a vector, and transformed into BL21(DE3) cells. 1 mL of an overnight culture (20 hours) in MDG media was used to inoculate 1 L of ZYM-5052 media (105). The culture was shaken at 250 rpm on an orbital shaker at 37°C for 12-14 hours. Cells were harvested at 8200 x *g* for 15 min at 4°C, resuspended in 0.9% (w/v) NaCl, and re-centrifuged at 5000 x *g* for 30 min at 4°C. Pellets were stored at -80°C until needed.

Protein purification

1 L cell pellets were resuspended in 200 mL of a buffer containing 20% (w/v) sucrose, 10 mM Tris pH 8.0, 1 mM EDTA and 50 mM BME. Cells were lysed by sonication in a Branson Sonifier 450 for 15 minutes (power level 40 and duty cycle 5) with stirring at 4°C. Next, the lysis was centrifuged for 2 hours at 27,500 x *g* at 4°C. The supernatant was removed, and the pellet was resuspended in 200 mL of a buffer containing 1% (v/v) Triton X-100, 10 mM Tris pH 8.0 followed by sonication for 15 minutes with stirring at 4°C. The mixture was centrifuged at 27,500 x *g* for 1 hour at 4°C. The supernatant was discarded, and the remaining pellet contained the isolated inclusion bodies.

Solubilization of inclusion bodies

Isolated inclusion bodies were dissolved in 40 mL of 8% (w/v) PFOA, 25 mM phosphate pH 8.0 and homogenized using a dounce homogenizer. The solution was then centrifuged at 50,000 x *g* for 30 min at 22°C. The supernatant contained the solubilized inclusion bodies.

Ni-NTA purification

After solubilization into 8% (w/v) PFOA, the supernatant was filtered through a 0.2 μm filter and loaded onto a column containing 20 mL of Ni sepharose 6 resin. The column was washed with approximately 5 column volumes of 1% (w/v) PFOA, 25 mM phosphate pH 8.0, or until the absorbance at 280 nm was steady, to remove any unbound protein. Samples were eluted in the presence of 1% (w/v) PFOA, 25 mM phosphate pH 8.0, 250 mM imidazole.

Dialysis

The most concentrated column fractions were pooled, and placed in 10,000 MWCO dialysis tubing. Samples were dialyzed against 20 L of 50 mM ammonium sulfate for 24 hours at room temperature with stirring. Precipitated protein was isolated by centrifugation at 4000 x *g* for 30 min at 22°C. The pellet contained the purified precipitated protein.

Results and Discussion

Inclusion body production and solubilization

Inclusion bodies have emerged as a powerful tool to obtain high levels of membrane proteins expressed in *E. coli* cells. One of the challenges of membrane protein expression, especially of a non-native membrane proteins, is that the over-expressed protein can crowd the membrane and become toxic to the bacterial cell (173). This leads to low protein expression that can make protein isolation very challenging due to the high background of endogenous host proteins. However, the fusion of a membrane protein to particular proteins will cause the protein of interest to be rapidly expressed in an unfolded state, and incorporated into insoluble cytoplasmic aggregates (i.e. inclusion bodies). One of the common proteins utilized to promote inclusion body formation is trp leader (trpLE) which has been shown to result in significantly enhanced membrane protein expression (174). Advantageously, the properties of these aggregates can then be exploited to extract the protein of interest. First, the cells are lysed in a buffer containing sucrose which removes soluble cellular components. After centrifugation, this leaves a pellet that contains only the inclusion bodies and other hydrophobic membrane components. These hydrophobic membrane components can be removed via a second lysis step that utilizes a buffer containing a mild detergent (in this case Triton X-100). Since Triton X-100 will not solubilize the inclusion bodies, after centrifugation, the majority of the pellet contains inclusion bodies.

Normally, once the inclusion bodies have been isolated from the whole cell milieu, they are solubilized in either 8 M urea or 6 M guanidinium hydrochloride.

However, in the case of highly insoluble transmembrane domains, even solutions of these strong chaotropic agents cannot effectively solubilize the inclusion bodies. For example, when the membrane interacting domain of caveolin-1 (residues 62-178, GRAVY score 0.659) is expressed with the fusion protein trp leader, the inclusion body pellet is not soluble in either 8 M urea or 6 M guanidinium hydrochloride (data not shown) (175). For this reason, the conventional methodology for processing inclusion bodies was not applicable. However, it was determined that a solution of 8% (w/v) PFOA can efficiently and rapidly solubilize inclusion bodies (Figure8-2). Additionally, in some cases, the addition of 1% (w/v) PFOA to a solution containing 8 M urea can significantly enhance the ability of 8 M urea to solubilize hydrophobic inclusion bodies, thereby decreasing the need for a very high detergent concentration.

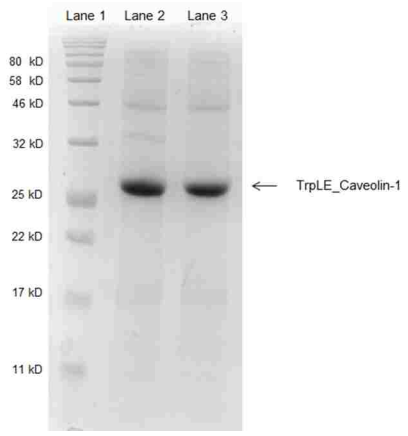

Figure 8-2. SDS-PAGE analysis of caveolin-1 (62-178) inclusion bodies dissolved in 8% (w/v) PFOA. Lane 1, Molecular weight ladder; lane 2, caveolin-1 in PFOA buffer pre-centrifugation; lane 3, caveolin-1 in PFOA buffer post-centrifugation (50,000 x *g*) (172).

The pKa of PFOA has been reported to be between 2.8 and 3. However, there is a study that has determined the pKa to be substantially lower, approximately -0.5 (176, 177). Whichever value is most representative, the low pKa of PFOA is an advantage because it will not interfere with typical buffering agents in the 4 to 12 range. It is also important to note that PFOA can form precipitates with potassium counterions, therefore, buffer conditions are limited to the use of sodium or ammonium counter ions. Additionally, it should be noted that due to the exclusionary fluorous nature of PFOA, it is incompatible with many other common detergents, such as Empigen BB, so caution should be taken when working with other detergents. Similarly, guanadinium hydrochloride is not compatible with PFOA as it forms a precipitate.

Purification

Nickel purification has arisen as a key tool for the purification of proteins. The hexa-histidine tag imparts specificity for binding to the nickel-bound nitrilotriacetic acid resin, but due to its small size it generally will not perturb the protein structure or its function (178). Most of the time, this eliminates the need to do additional cleavage steps to remove the affinity tag. The purification of membrane proteins using nickel affinity can be challenging. Membrane proteins need detergents for solubility, and not all detergents are compatible with the resin chemistry. Many milder detergents that are compatible with nickel affinity chromatography are not sufficient to keep the highly insoluble membrane proteins in solution much less solubilize them from an inclusion body state. In contrast, several stronger detergents (e.g. SDS) are able to solubilize inclusion bodies and keep the protein in solution, but interfere with the binding affinity of

the column. This makes PFOA an attractive choice as it is able to both solubilize membrane proteins, and is compatible with the nickel affinity column chemistry. In this case, the nickel chromatography trace of a nona-histidine tagged Trp leader fusion of caveolin-1 residues 62-178 is presented as an example of an insoluble membrane protein that can be purified using nickel affinity chromatography with PFOA buffers (Figure 8-3a). Although 8% (w/v) is needed to initially solubilize the inclusion bodies, the column can be run in 1% (w/v) PFOA which is sufficient to keep the protein in solution. In addition, the high ionic strength of the PFOA detergent mediates any ion exchange effects with the resin so the addition of NaCl to the buffer (typically 300 - 500 mM) is not needed. Imidazole can be added to the wash to enhance the purity of the finally product (0 mM - 40 mM), but the maximum tolerated level before there is significant protein loss must be determined for each protein individually. However, for caveolin-1 very high purities have been obtained without using imidazole in the wash step (Figure8-3b). Elution is accomplished using a 1% (w/v) PFOA solution containing 250 mM imidazole. The elution can also be done with a 1% (w/v) PFOA solution at a pH of 4.5. However it is important to keep in mind that the solubility of PFOA decreases dramatically below a pH of 4.0.

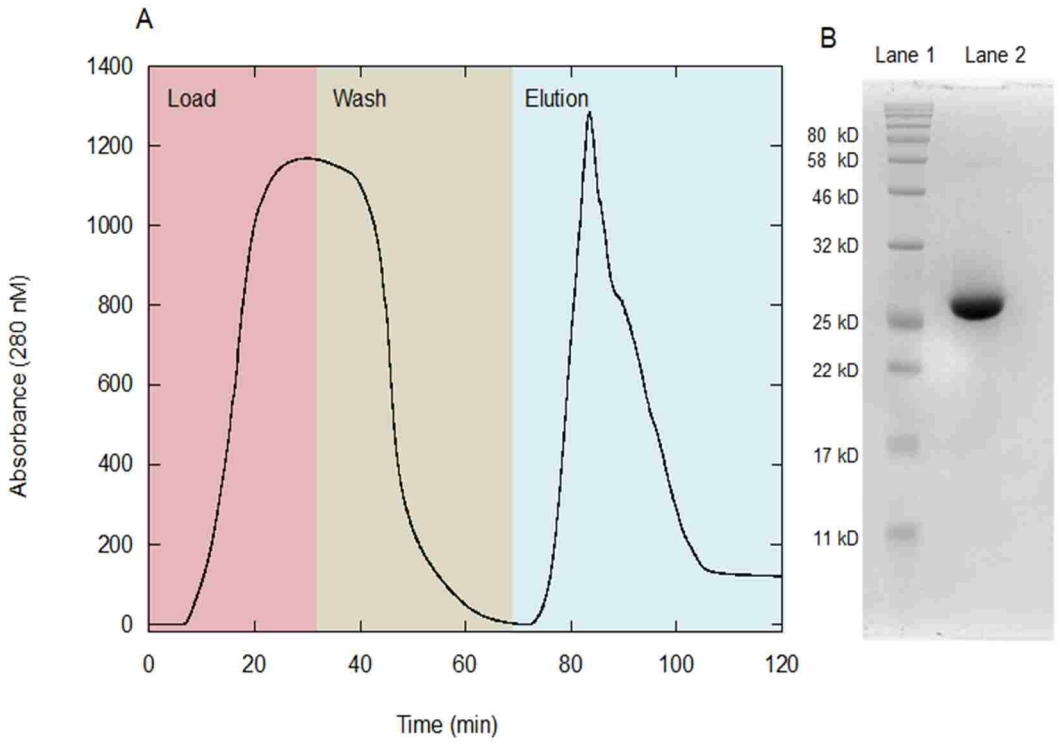

Figure 8-3. A) Representative chromatogram of the nickel affinity column purification of caveolin-1 (62-178). B) SDS-PAGE analysis of nickel purified caveolin-1 in PFOA. Lane 1, molecular weight ladder; lane 2, caveolin-1 (62-178) after elution (172).

Dialysis

One of the major challenges of membrane protein purification is that often times, the detergents that are necessary for purification are not desirable for the downstream characterization of the protein. For example, PFOA may be used for purification, but the final experiments are desired to be done in phospholipid vesicles. Also, there are cases where even the residual presence of even a few detergent molecules can cause erroneous

results (179). One common method for the removal of detergents is dialysis. However, many detergents that are commonly used in membrane protein expression have very low CMC values making them difficult if not impossible to remove using this method. This again highlights the need for a detergent that meets three fundamental requirements: protein solubilization, compatibility with purification techniques and the ability to be readily removed. PFOA has been shown to be removed by slow dialysis over time (171). This is due to the relatively high CMC of PFOA (reported as 13-30 mM, depending on the buffer system (171)). When the protein is loaded onto the nickel column, it can be washed into 1% (w/v) PFOA. This is advantageous as the 1% (w/v) PFOA can be more readily dialyzed than an 8% (w/v) solution. The dialysis of a 50 mL solution against 20 L of water at room temperature is sufficient to cause 100% precipitation of the protein (Figure 8-4). After precipitation, the protein is recovered by gentle centrifugation (4000 x *g*). Next, the precipitated protein can be washed several times to remove all traces of PFOA. Importantly the addition of 50 mM ammonium sulfate to the dialysis buffer significantly enhances the rate of protein precipitation. This precipitate is extremely easy to redissolve in whatever downstream detergents and/or lipids that are desired.

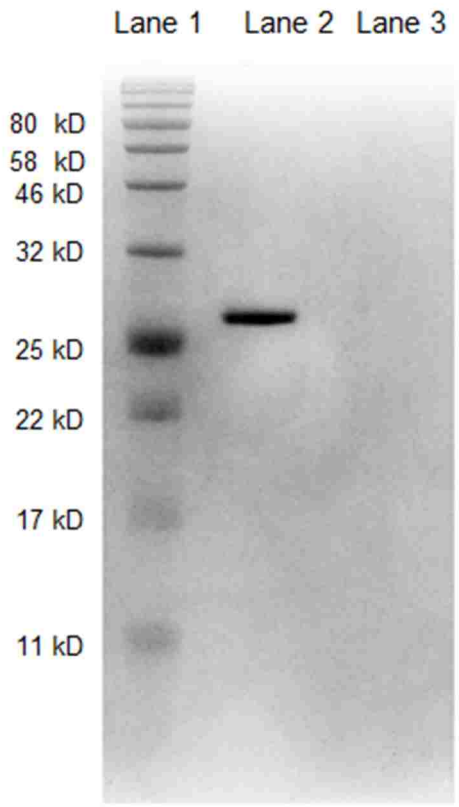

Figure 8-4. SDS-PAGE analysis of caveolin-1 after precipitation. Lane 1, molecular weight ladder; lane 2, caveolin-1 (62-178) after precipitation before centrifugation, lane 3, supernatant after centrifugation of precipitated caveolin-1 (172).

Conclusions

Obtaining sufficient amounts of insoluble membrane proteins at high levels is crucial to the understanding of protein structure and function through biophysical characterization. However, there are several challenges to obtaining high levels of purified membrane proteins, most notably the need for a detergent system that is compatible with both purification techniques and downstream characterization. In the procedure described herein, we demonstrate that PFOA has a threefold advantage when applied to the purification of membrane proteins. First, it is able to efficiently dissolve inclusion bodies. Second, it is compatible with Ni-NTA purification. Finally, it can be easily removed through dialysis, which produces a detergent free sample that can be carried through for additional purification such as cleavage of the fusion protein or incorporation into other membrane mimics.

References

1. Korn, E. D. (1968) Structure and Function of the Plasma Membrane : A Biochemical Perspective. *J. Gen. Physiol. 52,* 257-278.

2. Alenghat, F. J., and Golan, D. E. (2013) Chapter Three - Membrane Protein Dynamics and Functional Implications in Mammalian Cells. *Curr. Top. Membr.72,* 89-120.

3. Singer, S. J., and Nicolson, G. L. (1972) The Fluid Mosaic Model of the Structure of Cell Membranes. *Science. 175*, 720.

4. Goñi, F. M. (2014) The Basic Structure and Dynamics of Cell Membranes: An Update of the Singer-Nicolson Model. *Biochim. Biophys. Acta. 1838*, 1467-1476.

5. Bagatolli, L. A., and Mouritsen, O. G. (2013) Is the Fluid Mosaic (and the Accompanying Raft Hypothesis) a Suitable Model to Describe Fundamental Features of Biological Membranes? what may be Missing? *Frontiers in Plant Science. 4*, 457.

6. Palade, G. E. (1953) Fine Structure of Blood Capillaries. *J. Appl. Physiol. 24*, 1424.

7. Hayer, A., Stoeber, M., Bissig, C., and Helenius, A. (2010) Biogenesis of Caveolae: Stepwise Assembly of Large Caveolin and Cavin Complexes. *Traffic. 11*, 361-382.

8. Stan, R. (2005) Structure of Caveolae. *Biochim Biophys Acta. 1746*, 334-348.

9. Spisni, E., Tomasi, V., Cestaro, A., and Tosatto, S. C. (2005) Structural Insights into the Function of Human Caveolin 1. *Biochem. Biophys. Res. Commun. 338*, 1383-1390.

10. Sinha, B., Köster, D., Ruez, R., Gonnord, P., Bastiani, M., Abankwa, D., Stan, R. V., Butler-Browne, G., Vedie, B., Johannes, L., Morone, N., Parton, R. G., Raposo, G., Sens, P., Lamaze, C., and Nassoy, P. (2011) Cells Respond to Mechanical Stress by Rapid Disassembly of Caveolae. *Cell. 144*, 402-413.

11. Kiss, A. (2012) Caveolae and the Regulation of Endocytosis. *Adv. Exp. Med. Biol. 729*, 14-28.

12. Patel, H. H., Murray, F., and Insel, P. A. (2008) Caveolae as Organizers of Pharmacologically Relevant Signal Transduction Molecules. *Annu. Rev. Pharmacol. Toxicol. 48,* 351-391.

13. Thorn, H., Stenkula, K. G., Karlsson, M., Ortegren, U., Nystorm, F., Gustavsson, J., and Stralfors, P. (2003) Cell Surface Orifices of Caveolae and Localization of Caveolin to the Necks of Caveolae in Adipocytes. *Mol. Biol. Cell. 14*, 3967-3976.

14. Wheaton, K., Sampsel, K., Boisvert, F., Davy, A., Robbins, S., and Riabowol, K. (2001) Loss of Functional Caveolae during Senescence of Human Fibroblasts. *J. Cell. Physiol. 187*, 226-235.

15. Schwencke, C., Braun-Dullaeus, R. C., Wunderlich, C., and Strasser, R. H. (2006) Caveolae and Caveolin in Transmembrane Signaling: Implications for Human Disease. *Cardiovascular Research. 70,* 42-49.

16. Parton, G., and Simons, K. (2007) The Multiple Faces of Caveolae. *Nat. Rev. Mol. cell biol. 8*, 185-194.

17. Sonnino, S., and Prinetti, A. (2009) Sphingolipids and Membrane Environments for Caveolin. *FEBS Lett. 583,* 597-606.

18. Razani, B., Woodman, S. E., and Lisanti, M. P. (2002) Caveolae: From Cell Biology to Animal Physiology. *Pharmacol. Rev. 54,* 431-467.

19. Hailstones, D., Sleer, L. S., Parton, R. G., and Stanley, K. K. (1998) Regulation of Caveolin and Caveolae by Cholesterol in MDCK Cells. *J. Lipid Res. 39,* 369-379.

20. Walser PJ, , Ariotti N, , Howes M, , Ferguson C, , Webb R, , Schwudke D, , Leneva N, , Cho KJ, , Cooper L, , Rae J, , Floetenmeyer M, , Oorschot VM, , Skoglund U, , Simons K, , Hancock JF, , and Parton RG. (2012) Constitutive Formation of Caveolae in Bacterium. *Cell. 150,* 752-763.

21. Ortegren, U., Yin, L., Ost, A., Karlsson, H., Nystrom, F. H., and Stralfors, P. (2006) Separation and Characterization of Caveolae Subclasses in the Plasma Membrane of Primary Adipocytes; Segregation of Specific Proteins and Functions. *Febs Journal. 273*, 3381-3392.

22. Ortegren, U., Karlsson, M., Blazic, N., Blomqvist, M., Nystrom, F. H., Gustavsson, J., Fredman, P., and Stralfors, P. (2004) Lipids and Glycosphingolipids in Caveolae and Surrounding Plasma Membrane of Primary Rat Adipocytes. *Eur. J. Biochem. 271,* 2028-2036.

23. Hill, M., Bastiani, M., Luetterforst, R., Kirkham, M., Kirkham, A., Nixon, S., Walser, P., Abankwa, D., Oorschot, V., Martin, S., Hancock, J., and Parton, R. (2008) PTRF-Cavin, a Conserved Cytoplasmic Protein Required for Caveola Formation and Function.. *Cell. 132,* 113-124.

24. Ludwig, A., Howard, G., Mendoza-Topaz, C., Deerinck, T., Mackey, M., Sandin, S., Ellisman, M. H., and Nichols, B. J. (2013) Molecular Composition and Ultrastructure of the Caveolar Coat Complex. *PLoS Biol. 11,* e1001640.

25. Drab, M., Verkade, P., Elger, M., Kasper, M., Lohn, M., Lauterbach, B., Menne, J., Lindschau, C., Mende, F., Luft, F. C., Schedl, A., Haller, H., and Kurzchalia, T. V. (2001) Loss of Caveolae, Vascular Dysfunction, and Pulmonary Defects in Caveolin-1 Gene-Disrupted Mice. *Science. 293*, 2449-2452.

26. Scherer, P. E., Lewis, R. Y., Volonte, D., Engelman, J. A., Galbiati, F., Couet, J., Kohtz, D. S., vanDonselaar, E., Peters, P., and Lisanti, M. P. (1997) Cell-Type and

Tissue-Specific Expression of Caveolin-2 - Caveolins 1 and 2 Co-Localize and Form a Stable Hetero-Oligomeric Complex in Vivo. *J. Biol. Chem. 272*, 29337-29346.

27. Parolini, I., Sargiacomo, M., Galbiati, F., Rizzo, G., Grignani, F., Engelman, J. A., Okamoto, T., Ikezu, T., Scherer, P. E., Mora, R., Rodriguez-Boulan, E., Peschle, C., and Lisanti, M. P. (1999) Expression of Caveolin-1 is Required for the Transport of Caveolin-2 to the Plasma Membrane - Retention of Caveolin-2 at the Level of the Golgi Complex. *J. Biol. Chem. 274*, 25718-25725.

28. Horikawa, Y. T., Patel, H. H., Tsutsumi, Y. M., Jennings, M. M., Kidd, M. W., Hagiwara, Y., Ishikawa, Y., Insel, P. A., and Roth, D. M. (2008) Caveolin-3 Expression and Caveolae are Required for Isoflurane-Induced Cardiac Protection from Hypoxia and ischemia/reperfusion Injury. *J. Mol. Cell. Cardiol. 44*, 123-130.

29. Whiteley, G., Collins, R. F., and Kitmitto, A. (2012) Characterization of the Molecular Architecture of Human Caveolin-3 and Interaction with the Skeletal Muscle Ryanodine Receptor. *J. Biol. Chem.. 287(48)*, 40302-40316.

30. Stoppani, E., Rossi, S., Meacci, E., Penna, F., Costelli, P., Bellucci, A., Faggi, F., Maiolo, D., Monti, E., and Fanzani, A. (2011) Point Mutated Caveolin-3 Form (P104L) Impairs Myoblast Differentiation Via Akt and p38 Signalling Reduction, Leading to an Immature Cell Signature. *Biochim. Biophys. Acta. 1812*, 468-479.

31. Dietzen, D. J., Hastings, W. R., and Lublin, D. M. (1995) Caveolin is Palmitoylated on Multiple Cysteine Residues. Palmitoylation is Not Necessary for Localization of Caveolin to Caveolae. *J. Biol. Chem. 270*, 6838-6842.

32. Kurzchalia, T. V., Dupree, P., Parton, R. G., Kellner, R., Virta, H., Lehnert, M., and Simons, K. (1992) VIP21, a 21-kD Membrane Protein is an Integral Component of Trans-Golgi-Network-Derived Transport Vesicles. *J. Cell Biol. 118*, 1003-1014.

33. Rothberg, K. G., Heuser, J. E., Donzell, W. C., Ying, Y. S., Glenney, J. R., and Anderson, R. G. (1992) Caveolin, a Protein Component of Caveolae Membrane Coats. *Cell. 68*, 673-682.

34. Glenney, J. R. (1992) the Sequence of Human Caveolin Reveals Identity with VIP21, a Component of Transport Vesicles. *FEBS Lett. 314*, 45-48.

35. Root, K. T., Plucinsky, S. M., and Glover, K. J. (2015) Chapter Nine - Recent Progress in the Topology, Structure, and Oligomerization of Caveolin: A Building Block of Caveolae. *Curr. Top. Membr. 75*, 305-336.

36. Le, P., Guay, G., Altschuler, Y., and Nabi, I. (2002) Caveolin-1 is a Negative Regulator of Caveolae-Mediated Endocytosis to the Endoplasmic Reticulum. *J. Biol. Chem. 277*, 3371-3379.

37. Ju, H., Zou, R., Venema, V. J., and Venema, R. C. (1997) Direct Interaction of Endothelial Nitric-Oxide Synthase and Caveolin-1 Inhibits Synthase Activity. *J. Biol. Chem. 272*, 18522-18525.

38. Lee, H., Woodman, S. E., Engelman, J. A., Volonte, D., Galbiati, F., Kaufman, H. L., Lublin, D. M., and Lisanti, M. P. (2001) Palmitoylation of Caveolin-1 at a Single Site (Cys-156) Controls its Coupling to the c-Src Tyrosine Kinase - Targeting of Dually Acylated Molecules (GPI-Linked, Transmembrane, Or Cytoplasmic) to Caveolae Effectively Uncouples c-Src and Caveolin-1 (Tyr-14). *J. Biol. Chem. 276*, 35150-35158.

39. Couet, J., Sargiacomo, M., and Lisanti, M. P. (1997) Interaction of a Receptor Tyrosine Kinase, EGF-R, with Caveolins - Caveolin Binding Negatively Regulates Tyrosine and serine/threonine Kinase Activities. *J. Biol. Chem. 272*, 30429-30438.

40. Byrne, D. P., Dart, C., and Rigden, D. J. (2012) Evaluating Caveolin Interactions: Do Proteins Interact with the Caveolin Scaffolding Domain through a Widespread Aromatic Residue-Rich Motif? *PLoS One. 7*, e44879.

41. Collins, B. M., Davis, M. J., Hancock, J. F., and Parton, R. G. (2012) Structure-Based Reassessment of the Caveolin Signaling Model: Do Caveolae Regulate Signaling through Caveolin-Protein Interactions? *Dev. Cell. 23*, 11-20.

42. Plucinsky S, G. K. (2017) The C-Terminal Domain of Caveolin-1 and Pulmonary Arterial Hypertension: An Emerging Relationship. *J Rare Dis Res Treat. 2(3)*, 44-48.

43. Monier, S., Parton, R. G., Vogel, F., Behlke, J., Henske, A., and Kurzchalia, T. V. (1995) VIP21-Caveolin, a Membrane Protein Constituent of the Caveolar Coat, Oligomerizes in Vivo and in Vitro. *Mol. Biol. Cell. 6*, 911-927.

44. Rieth, M. D., Lee, J., and Glover, K. J. (2012) Probing the Caveolin-1 P132L Mutant: Critical Insights into its Oligomeric Behavior and Structure. *Biochemistry. 51*, 3911-3918.

45. Yang, G., Xu, H., Li, Z., and Li, F. (2014) Interactions of Caveolin-1 Scaffolding and Intramembrane Regions Containing a CRAC Motif with Cholesterol in Lipid Bilayers. *Biochim. Biophys. Acta. 1838*, 2588-2599.

46. Lee, H., Park, D. S., Razani, B., Russell, R. G., Pestell, R. G., and Lisanti, M. P. (2002) Caveolin-1 Mutations (P132L and Null) and the Pathogenesis of Breast Cancer. Caveolin-1 (P132L) Behaves in a Dominant-Negative Manner and Caveolin-1 (-/-) Null Mice show Mammary Epithelial Cell Hyperplasia. *Am. J. Pathol. 161*, 1357-1369.

47. Ahn, M., Kim, H., Matsumoto, Y., and Shin, T. (2006) Increased Expression of Caveolin-1 and-2 in the Hearts of Lewis Rats with Experimental Autoimmune Myocarditis. *Autoimmunity. 39*, 489-495.

48. Williams, T. M., Sotgia, F., Lee, H., Hassan, G., Di Vizio, D., Bonuccelli, G., Capozza, F., Mercier, I., Rui, H., Pestell, R. G., and Lisanti, M. P. (2006) Stromal and Epithelial Caveolin-1 both Confer a Protective Effect Against Mammary Hyperplasia and Tumorigenesis: Caveolin-1 Antagonizes Cyclin D1 Function in Mammary Epithelial Cells. *Am. J. Path. 169*, 1784-1801.

49. Chatterjee, M., Ben-Josef, E., Thomas, D. G., Morgan, M. A., Zalupski, M. M., Khan, G., Andrew Robinson, C., Griffith, K. A., Chen, C., Ludwig, T., Bekaii-Saab, T., Chakravarti, A., and Williams, T. M. (2015) Caveolin-1 is Associated with Tumor Progression and Confers a Multi-Modality Resistance Phenotype in Pancreatic Cancer. *Sci. Rep. 5*, 10867.

50. Bonuccelli, G., Casimiro, M. C., Sotgia, F., Wang, C., Liu, M., Katiyar, S., Zhou, J., Dew, E., Capozza, F., Daumer, K. M., Minetti, C., Milliman, J. N., Alpy, F., Rio, M. C., Tomasetto, C., Mercier, I., Flomenberg, N., Frank, P. G., Pestell, R. G., and Lisanti, M. P. (2009) Caveolin-1 (P132L), a Common Breast Cancer Mutation, Confers Mammary Cell Invasiveness and Defines a Novel Stem cell/metastasis-Associated Gene Signature. *Am. J. Pathol. 174*, 1650-1662.

51. Koike, S., Kodera, Y., Nakao, A., Iwata, H., and Yatabe, Y. (2010) Absence of the Caveolin-1 P132L Mutation in Cancers of the Breast and Other Organs. *J. Mol. Diagn. 12*, 712-717.

52. Lacroix-Triki, M., Geyer, F. C., and Reis-Filho, J. S. (2010) Caveolin-1 P132L Mutation in Human Cancers: 1 CAVeat to be Voiced. *J. Mol. Diagn. 12*, 562-565.

53. Parton, R. G., Hanzal-Bayer, M., and Hancock, J. F. (2006) Biogenesis of Caveolae: A Structural Model for Caveolin-Induced Domain Formation. *J. Cell. Sci. 119*, 787-796.

54. Dupree, P., Parton, R. G., Raposo, G., Kurzchalia, T. V., and Simons, K. (1993) Caveolae and Sorting in the Trans-Golgi Network of Epithelial Cells. *EMBO J. 12*, 1597-1605.

55. Sargiacomo, M., Sudol, M., Tang, Z., and Lisanti, M. P. (1993) Signal Transducing Molecules and Glycosyl-Phosphatidylinositol-Linked Proteins Form a Caveolin-Rich Insoluble Complex in MDCK Cells. *J. Cell Biol. 122*, 789-807.

56. Rui, H., Root, K. T., Lee, J., Glover, K. J., and Im, W. (2014) Probing the U-Shaped Conformation of Caveolin-1 in a Bilayer. *Biophys. J. 106*, 1371-1380.

57. Fernandez, I., Ying, Y., Albanesi, J., and Anderson, R. G. (2002) Mechanism of Caveolin Filament Assembly. *Proc. Natl. Acad. Sci. U. S. A. 99*, 11193-11198.

58. Machleidt, T., Li, W. P., Liu, P., and Anderson, R. G. (2000) Multiple Domains in Caveolin-1 Control its Intracellular Traffic. *J. Cell Biol. 148*, 17-28.

59. Parr, R. D., Martin, G. G., Hostetler, H. A., Schroeder, M. E., Mir, K. D., Kier, A. B., Ball, J. M., and Schroeder, F. (2007) A New N-Terminal Recognition Domain in Caveolin-1 Interacts with Sterol Carrier Protein-2 (SCP-2). *Biochemistry. 46*, 8301-8314.

60. Li, S. W., Seitz, R., and Lisanti, M. P. (1996) Phosphorylation of Caveolin by Src Tyrosine Kinases - the Alpha-Isoform of Caveolin is Selectively Phosphorylated by v-Src in Vivo. *J. Biol. Chem. 271*, 3863-3868.

61. Vainonen, J. P., Aboulaich, N., Turkina, M. V., Strålfors, P., and Vener, A. V. (2004) N-Terminal Processing and Modifications of Caveolin-1 in Caveolae from Human Adipocytes. *Biochem. Biophys. Res. Commun. 320*, 480-486.

62. Le Lan, C., Neumann, J. M., and Jamin, N. (2006) Role of the Membrane Interface on the Conformation of the Caveolin Scaffolding Domain: A CD and NMR Study. *FEBS Lett. 580*, 5301-5305.

63. Hoop, C. L., Sivanandam, V. N., Kodali, R., Srnec, M. N., and van der Wel, P. C. (2012) Structural Characterization of the Caveolin Scaffolding Domain in Association with Cholesterol-Rich Membranes. *Biochemistry. 51*, 90-99.

64. Lee, J., and Glover, K. J. (2012) The Transmembrane Domain of Caveolin-1 Exibits a Helix-Break-Helix Structure. *Biochim Biophys Acta. 1818*, 1158-1164.

65. Song, K. S., Tang, Z. L., Li, S. W., and Lisanti, M. P. (1997) Mutational Analysis of the Properties of Caveolin-1 - A Novel Role for the C-Terminal Domain in Mediating Homo-Typic Caveolin-Caveolin Interactions. *J. Biol. Chem.. 272*, 4398-4403.

66. Schlegel, A., and Lisanti, M. P. (2000) A Molecular Dissection of Caveolin-1 Membrane Attachment and Oligomerization. Two Separate Regions of the Caveolin-1 C-Terminal Domain Mediate Membrane Binding and oligomer/oligomer Interactions in Vivo. *J. Biol. Chem. 275*, 21605-21617.

67. Mir, K. D., Parr, R. D., Schroeder, F., and Ball, J. M. (2007) Rotavirus NSP4 Interacts with both the Amino- and Carboxyl- Termini of Caveolin-1. *Virus Res. 126*, 106-115.

68. Schubert, A., Schubert, W., Spray, D. C., and Lisanti, M. P. (2002) Connexin Family Members Target to Lipid Raft Domains and Interact with Caveolin-1â€ . *Biochemistry. 41*, 5754-5764.

69. Austin, E. D., Ma, L., LeDuc, C., Berman Rosenzweig, E., Borczuk, A., Phillips, J. A., Palomero, T., Sumazin, P., Kim, H. R., Talati, M. H., West, J., Loyd, J. E., and Chung, W. K. (2012) Whole Exome Sequencing to Identify a Novel Gene (Caveolin-1) Associated with Human Pulmonary Arterial Hypertension. *Circ. Cardiovas. Genet. 5*, 336-343.

70. Desai, A. A. (2012) Novel Inheritable Caveolin-1 Mutations in Pulmonary Arterial Hypertension. *Circ. Cardiovas. Genet. 5*, 706-707.

71. Wallin, E., and von Heijne, G. (1998) Genome-Wide Analysis of Integral Membrane Proteins from Eubacterial, Archaean, and Eukaryotic Organisms. *Protein Sci. 7*, 1029-1038.

72. Hendrickson, W. A. (2016) Atomic-Level Analysis of Membrane-Protein Structure. *Nat. Struct. Mol. Biol*. *23*, 464.

73. Miroux, B., and Walker, J. E. (1996) Over-Production of Proteins inEscherichia Coli: Mutant Hosts that Allow Synthesis of some Membrane Proteins and Globular Proteins at High Levels. *J. Mol. Biol. 260*, 289-298.

74. White, S. H. (2004) The Progress of Membrane Protein Structure Determination. *Protein Science. 13*, 1948-1949.

75. Carpenter, E. P., Beis, K., Cameron, A. D., and Iwata, S. (2008) Overcoming the Challenges of Membrane Protein Crystallography. *Curr. Opin. Struct. Biol. 18*, 581-586.

76. Palsdottir, H., and Hunte, C. (2004) Lipids in Membrane Protein Structures. *Biochim. Biophys. Acta. 1666*, 2-18.

77. Seddon, A. A., Curnow, P., and Booth, P. J. (2004) Membrane Proteins, Lipids and Detergents: Not just a Soap Opera. *Biochimica Et Biophysica Acta. 1666*, 105-117.

78. Moraes, I., Evans, G., Sanchez-Weatherby, J., Newstead, S., and Stewart, P. D. S. (2013) Membrane Protein Structure Determination the Next Generation. *Biochim. Biophys. Acta. 1838*, 78-87.

79. Therien, A. G., and Deber, C. M. (2002) Interhelical Packing in Detergent Micelles: folding of a cystic fibrosis transmembrane conductance regulator construct. *J. Biol. Chem. 277*, 6067-6072.

80. Sanders, C. R., Hoffmann, A. K., Grayn, D. N., Keyes, M. H., and Ellis, C. D. (2004) French Swimwear for Membrane Proteins. *Chembiochem. 5*, 423-426.

81. Prosser, R. S., Evanics, F., Kitevski, J. L., and Al-Abdul-Wahid, M. S. (2006) Current Applications of Bicelles in NMR Studies of Membrane-Associated Amphiphiles and Proteins, *Biochemistry. 45*, 8453-8465.

82. Sanders, C. R., Hare, B. J., Howard, K. P., and Prestegard, J. H. (1994) Magnetically Oriented Phospholipid Micelles as a Tool for the Study of Membrane Associated Molecules. *Progr. NMR Spectr. 26*, 421-444.

83. Sanders, C. R., and Prosser, R. S. (1998) Bicelles: A Model Membrane System for all Seasons? *Structure. 6*, 1227-1234.

84. Glover, K. J., Whiles, J. A., Wu, G., Yu, N., Deems, R., Struppe, J. O., Stark, R. E., Komives, E. A., and Vold, R. R. (2001) Structural Evaluation of Phospholipid Bicelles for Solution-State Studies of Membrane-Associated Biomolecules. *Biophys. J. 81*, 2163-71.

85. De Angelis, A.,A., and Opella, S. J. (2007) Bicelle Samples for Solid-State NMR of Membrane Proteins. *Nat. Protocols. 2*, 2332-2338.

86. Akbarzadeh, A., Rezaei-Sadabady, R., Davaran, S., Joo, S. W., Zarghami, N., Hanifehpour, Y., Samiei, M., Kouhi, M., and Nejati-Koshki, K. (2013) Liposome: Classification, Preparation, and Applications. *Nanoscale Research Letters. 8*, 102-102.

87. Greenfield, N. J. (2006) Using Circular Dichroism Spectra to Estimate Protein Secondary Structure. *Nature protocols. 1*, 2876-2890.

88. Kelly, S. M., Jess, T. J., and Price, N. C. (2005) How to Study Proteins by Circular Dichroism. *Biochim Biophys Acta. 1751*, 119-139.

89. Kim, H. J., Howell, S. C., Van Horn, W. D., Jeon, Y. H., and Sanders, C. R. (2009) Recent Advances in the Application of Solution NMR Spectroscopy to Multi-Span Integral Membrane Proteins. *Prog Nucl Magn Reson Spectrosc. 55*, 335-360.

90. Verardi, R., Traaseth, N. J., Masterson, L. R., Vostrikov, V. V., and Veglia, G. (2012) Isotope Labeling for Solution and Solid-State NMR Spectroscopy of Membrane Proteins. *Adv. Exp. Med. Biol. 992*, 35-62.

91. Loura, L., and Prieto, M. (2011) FRET in Membrane Biophysics: An Overview. *Frontiers in Physiology. 2*, 82.

92. Bader, A. N., Hofman, E. G., Voortman, J., van Bergen en Henegouwen, Paul,M.P., and Gerritsen, H. C. (2009) Homo-FRET Imaging Enables Quantification of Protein Cluster Sizes with Subcellular Resolution. *Biophys. J. 97*, 2613-2622.

93. Yeow, E. K. L., and Clayton, A. H. A. (2006) Enumeration of Oligomerization States of Membrane Proteins in Living Cells by Homo-FRET Spectroscopy and Microscopy: Theory and Application. *Biophys. J. 92*, 3098-3104.

94. Squire, A., Verveer, P. J., Rocks, O., and Bastiaens, P. I. H. (2004) Red-Edge Anisotropy Microscopy Enables Dynamic Imaging of Homo-FRET between Green Fluorescent Proteins in Cells. *J. Struct. Biol. 147*, 62-69.

95. Diefenderfer, C., Lee, J., Mlyanarski, S., Guo, Y., and Glover, K. J. (2009) Reliable Expression and Purification of Highly Insoluble Transmembrane Domains. *Anal Biochem. 384*, 274-8.

96. Marley, J., Lu, M., and Bracken, C. (2001) A Method for Efficient Isotopic Labeling of Recombinant Proteins. *J. Biomol. NMR. 20*, 71-75.

97. Song Y., Mittendorf K. , Lu Z. , and Sanders C. R. (2014) Impact of Bilayer Lipid Composition on the Structure and Topology of the Transmembrane Amyloid Precursor C99 Protein. *J Am Chem Soc. 136 (11)*, 4093-4096.

98. Ng, H. Q., Kim, Y. M., Huang, Q., Gayen, S., Yildiz, A. A., Yoon, H. S., Sinner, E., and Kang, C. (2012) Purification and Structural Characterization of the Voltage-Sensor Domain of the hERG Potassium Channel. *Protein Expr. Purif. 86*, 98-104.

99. Chen, L., Lai , C., Lai, J., and Tian, C. (2011) Expression, purification, Detergent Screening and Solution NMR Backbone Assignment of the Human Potassium Channel Accessory Subunit MiRP1. *Prot. Expr. Purif. 76*, 205-210.

100. Tian, C., Vanoye , C. G., Kang , C., Welch , R. C., Kim , H., George, J., A., and Sanders, C. R. (2007) Preparation, Functional Characterization, and NMR Studies of Human KCNE1, a Voltage-Gated Potassium Channel Accessory Subunit Associated with Deafness and Long QT Syndrome. *Biochemistry. 46 (41)*, 11459-11472.

101. Wishart, D., and Sykes, B. (1994) The C-13 Chemical-Shift Index - a Simple Method for the Identification of Protein Secondary Structure using C-13 Chemical-Shift Data. *J. Biomol. NMR. 4*, 171-180.

102. Sun, X., Flynn, D. C., Castranova, V., Millecchia, L. L., Beardsley, A. R., and Liu, J. (2007) Identification of a Novel Domain at the N Terminus of Caveolin-1 that Controls Rear Polarization of the Protein and Caveolae Formation. *J. Biol. Chem. 282*, 7232-7241.

103. Bucci, M., Gratton, J., Rudic, R. D., Acevedo, L., Roviezzo, F., Cirino, G., and Sessa, W. C. (2000) In Vivo Delivery of the Caveolin-1 Scaffolding Domain Inhibits Nitric Oxide Synthesis and Reduces Inflammation. *Nat. Med. 6*, 1362-1367.

104. Couet, J., Li, S. W., Okamoto, T., Ikezu, T., and Lisanti, M. P. (1997) Identification of Peptide and Protein Ligands for the Caveolin-Scaffolding Domain - Implications for the Interaction of Caveolin with Caveolae-Associated Proteins. *J. Biol. Chem.. 272*, 6525-6533.

105. Studier, F. W. (2005) Protein Production by Auto-Induction in High Density Shaking Cultures. *Prot. Expr. Purif. 41*, 207-34.

106. Truhlar, S. M., Cervantes, C. F., Torpey, J. W., Kjaergaard, M., and Komives, E. A. (2008) Rapid Mass Spectrometric Analysis of 15N-Leu Incorporation Fidelity during Preparation of Specifically Labeled NMR Samples. *Protein Sci. 17*, 1636-1639.

107. Nietlispach, D. (2005) Suppression of Anti-TROSY Lines in a Sensitivity Enhanced Gradient Selection TROSY Scheme. *J. Biomol. NMR. 31*, 161-166.

108. Yang, D. W., and Kay, L. E. (1999) Improved 1HN-Detected Triple Resonance TROSY-Based Experiments.. *J. Biomol. NMR. 13*, 3-10.

109. Delaglio, F., Grzesiek, S., Vuister, G. W., Zhu, G., Pfeifer, J., and Bax, A. (1995) NMRPipe: A Multidimensional Spectral Processing System Based on UNIX Pipes. *J. Biomol. NMR. 6*, 277-293.

110. Goddard, T. D., and Kneller, D. G. *Sparky 3*. University of California, San Francisco.

111. Shen, Y., Delaglio, F., Cornilescu, G., and Bax, A. (2009) TALOS+: A Hybrid Method for Predicting Protein Backbone Torsion Angles from NMR Chemical Shifts. *J. Biomol. NMR. 44*, 213-223.

112. Ziarek, J. J., Peterson, F. C., Lytle, B. L., and Volkman, B. F. (2011) Binding Site Identification and Structure Determination of Protein-Ligand Complexes by NMR. *Meth. Enzymol. 493*, 241-275.

113. Plucinsky, S. M., and Glover, K. J. (2015) Secondary Structure Analysis of a Functional Construct of Caveolin-1 Reveals a Long C-Terminal Helix. *Biophys. J. 109*, 1686-1688.

114. Kim, M. K., and Kang, Y. K. (1999) Positional Preference of Proline in Alpha-Helices. *Prot. Sci. 8*, 1492-1499.

115. Aoki, S., Thomas, A., Decaffmeyer, M., Brasseur, R., and Epand, R. (2010) The Role of Proline in the Membrane Re-Entrant Helix of Caveolin-1. *J Biol Chem. 285*, 33371-33380.

116. Bouras, T., Lisanti, M. P., and Pestell, R. G. (2004) Caveolin-1 in Breast Cancer. *Cancer Biology & Therapy. 3*, 931-941.

117. Hanson, C. A., Drake, K. R., Baird, M. A., Han, B., Kraft, L. J., Davidson, M. W., and Kenworthy, A. K. (2013) Overexpression of caveolin-1 is Sufficient to Phenocopy the Behavior of a Disease-Associated Mutant. *Traffic. 14(6)*, 663-667.

118. Weiss, N., Couchoux, H., Legrand, C., Berthier, C., Allard, B., and Jacquemond, V. (2008) Expression of the Muscular Dystrophy-Associated Caveolin-3(P104L) Mutant in Adult Mouse Skeletal Muscle Specifically Alters the Ca(2+) Channel Function of the Dihydropyridine Receptor. *Pflugers Arch. 457*, 361-75.

119. Beard, W. A., Stahl, S. J., Kim, H. R., Bebenek, K., Kumar, A., Strub, M. P., Becerra, S. P., Kunkel, T. A., and Wilson, S. H. (1994) Structure/function Studies of Human Immunodeficiency Virus Type 1 Reverse Transcriptase. Alanine Scanning Mutagenesis of an Alpha-Helix in the Thumb Subdomain. *J. Biol. Chem. 269*, 28091-28097.

120. Bernatchez, P. N., Bauer, P. M., Yu, J., Prendergast, J. S., He, P., and Sessa, W. C. (2005) Dissecting the Molecular Control of Endothelial NO Synthase by Caveolin-1 using Cell-Permeable Peptides. *Proc. Nat. Acad. Sci. U. S. A. 102*, 761-766.

121. Root, K. T., and Glover, K. J. (2016) Reconstitution and Spectroscopic Analysis of Caveolin-1 Residues 62-178 Reveals that Proline 110 Governs its Structure and Solvent Exposure. *Biochim. Biophys. Acta. 1858*, 682-688.

122. Capozza, F., Daumer, K., Minetti, C., Milliman, J., Alpy, F., Rio, M., Tomasetto, C., Mercier, I., Flomenberg, N., Frank, P., Pestell, R., and Lisanti, M. (2009) Caveolin-1 (P132L), a Common Breast Cancer Mutation, Confers Mammary Cell Invasiveness and Defines a Novel Stem cell/metastasis-Associated Gene Signature. *Am J Pathol. 174*, 1650-1662.

123. Frank, P. G., Cheung, M. W. C., Pavlides, S., Llaverias, G., Park, D. S., and Lisanti, M. P. (2006) Caveolin-1 and Regulation of Cellular Cholesterol Homeostasis. *Am. J. Physiol. 291*, H677-H686.

124. Sargiacomo, M., Scherer, P. E., Tang, Z., Kübler, E., Song, K. S., Sanders, M. C., and Lisanti, M. P. (1995) Oligomeric Structure of Caveolin: Implications for Caveolae Membrane Organization. *Proc. Nat. Acad. Sci. U. S. A. 92*, 9407-9411.

125. Shvets, E., Ludwig, A., and Nichols, B. J. (2014) News from the Caves: Update on the Structure and Function of Caveolae. *Curr. Opin. Cell Biol. 29*, 99-106.

126. Lamas, S., Marsden, P. A., Li, G. K., Tempst, P., and Michel, T. (1992) Endothelial Nitric Oxide Synthase: Molecular Cloning and Characterization of a Distinct Constitutive Enzyme Isoform. *Proc. Nat. Acad. Sci. U. S. A. 89*, 6348-6352.

127. Lai, Y., Potoka, K. C., Champion, H. C., Mora, A. L., and Gladwin, M. T. (2014) Pulmonary Arterial Hypertension: The Clinical Syndrome. *Circulation Research. 115*, 115-130.

128. Förstermann, U., and Münzel, T. (2006) Endothelial Nitric Oxide Synthase in Vascular Disease. *Circulation. 113*, 1708.

129. Zhao, Y., Zhao, Y. D., Mirza, M. K., Huang, J. H., Potula, H. S. K., Vogel, S. M., Brovkovych, V., Yuan, J. X. -., Wharton, J., and Malik, A. B. (2009) Persistent eNOS Activation Secondary to Caveolin-1 Deficiency Induces Pulmonary Hypertension in Mice and Humans through PKG Nitration. *J. Clin. Invest. 119*, 2009-2018.

130. Zhao, Y., and Malik, A. B. (2009) A Novel Insight into the Mechanism of Pulmonary Hypertension Involving Caveolin-1 Deficiency and eNOS Activation. *Trends Cardiovasc. Med. 19*, 238-242.

131. Förstermann, U., and Sessa, W. C. (2011) Nitric Oxide Synthases: Regulation and Function. *Eur. Heart J. 33*, 829-837.

132. Garcí-a-Cardeña, G., Fan, R., Stern, D. F., Liu, J., and Sessa, W. C. (1996) Endothelial Nitric Oxide Synthase is Regulated by Tyrosine Phosphorylation and Interacts with Caveolin-1. *J. Biol. Chem. 271*, 27237-27240.

133. Star, A., and Kuzmych, O. (2010) *Detection of Nitric Oxide*. Google Patents, .

134. Schubert, W., Frank, P. G., Woodman, S. E., Hyogo, H., Cohen, D. E., Chow, C. W., and Lisanti, M. P. (2002) Microvascular Hyperpermeability in Caveolin-1 (-/-) Knock-Out Mice - Treatment with a Specific Nitric-Oxide Synthase Inhibitor, L-Name, Restores Normal Microvascular Permeability in Cav-1 Null Mice. *J. Biol. Chem. 277*, 40091-40098.

135. Trane, A. E., Pavlov, D., Sharma, A., Saqib, U., Lau, K., van Petegem, F., Minshall, R. D., Roman, L. J., and Bernatchez, P. N. (2014) Deciphering the Binding of Caveolin-1 to Client Protein Endothelial Nitric-Oxide Synthase (eNOS): Scaffolding Subdomain Identification, Interaction Modeling, and Biological Significance. *J. Biol. Chem. 289*, 13273-13283.

136. Murata, T., Lin, M. I., Huang, Y., Yu, J., Bauer, P. M., Giordano, F. J., and Sessa, W. C. (2007) Reexpression of Caveolin-1 in Endothelium Rescues the Vascular, Cardiac, and Pulmonary Defects in Global Caveolin-1 Knockout Mice. *J. Exp. Med. 204*, 2373.

137. Krajewska, W. M., and Maslowska, I. (2004) Caveolins: Structure and Function in Signal Transduction. *Cell. Mol. Biol. Lett. 9*, 195-220.

138. Bernatchez, P., Sharma, A., Bauer, P. M., Marin, E., and Sessa, W. C. (2011) A Noninhibitory Mutant of the Caveolin-1 Scaffolding Domain Enhances eNOS-Derived NO Synthesis and Vasodilation in Mice. *J. Clin. Invest. 121*, 3747-3755.

139. Han, B., Tiwari, A., and Kenworthy, A. K. (2014) Tagging Strategies Strongly Impact the Fate of Overexpressed Caveolin-1. *Traffic. 16(4)*, 417-438.

140. Garci´a-Cardeña, G., Martasek, P., Masters, B. S. S., Skidd, P. M., Couet, J., Li, S., Lisanti, M. P., and Sessa, W. C. (1997) Dissecting the Interaction between Nitric Oxide Synthase (NOS) and Caveolin: Functional Significance of the NOS Caveolin Binding Domain *in vivo*. *J. Biol. Chem.. 272*, 25437-25440.

141. Aoki, S., and Epand, R. M. (2012) Caveolin-1 Hydrophobic Segment Peptides Insertion into Membrane Mimetic Systems: Role of Proline Residue. *Biochim. Biophys. Acta. 1818*, 12-18.

142. Epand, R. M., Sayer, B. G., and Epand, R. F. (2005) Caveolin Scaffolding Region and Cholesterol-Rich Domains in Membranes. *J. Mol. Biol. 345*, 339-350.

143. Zhu, Q., and Casey, J. R. (2007) Topology of Transmembrane Proteins by Scanning Cysteine Accessibility Mutagenesis Methodology. *Methods. 41*, 439-450.

144. Guan, X., and Fierke, C. A. (2011) Understanding Protein Palmitoylation: Biological Significance and Enzymology. *Science China.Chemistry. 54*, 1888-1897.

145. Rouser, G., Fleischer, S., and Yamamoto, A. (1970) Two Dimensional Thin Layer Chromatographic Separation of Polar Lipids and Determination of Phospholipids by Phosphorus Analysis of Spots. *Lipids. 5*, 494-496.

146. Volonte, D., Galbiati, F., Pestell, R. G., and Lisanti, M. P. (2001) Cellular Stress Induces the Tyrosine Phosphorylation of Caveolin-1 (Tyr(14)) Via Activation of p38 Mitogen-Activated Protein Kinase and c-Src Kinase - Evidence for Caveolae, the Actin Cytoskeleton, and Focal Adhesions as Mechanical Sensors of Osmotic Stress. *J. Biol. Chem. 276*, 8094-8103.

147. Decaffmeyer, M., Shulga, Y. V., Dicu, A. O., Thomas, A., Truant, R., Topham, M. K., Brasseur, R., and Epand, R. M. (2008) Determination of the Topology of the Hydrophobic Segment of Mammalian Diacylglycerol Kinase Epsilon in a Cell Membrane and its Relationship to Predictions from Modeling. *J. Mol. Biol. 383*, 797-809.

148. Yeagle, P. L. (1989) Lipid Regulation of Cell Membrane Structure and Function. *FASEB Journal. 3*, 1833-1842.

149. Fatmi, M. Q., and Chang, C. A. (2010) The Role of Oligomerization and Cooperative Regulation in Protein Function: The Case of Tryptophan Synthase. *PLOS Computational Biology. 6*, e1000994.

150. Hashimoto, K., and Panchenko, A. R. (2010) Mechanisms of Protein Oligomerization, the Critical Role of Insertions and Deletions in Maintaining Different Oligomeric States. *Pro. Nat. Acad. Sci. U. S. A. 107*, 20352-20357.

151. Patel, H. H., and Insel, P. A. (2008) Lipid Rafts and Caveolae and their Role in Compartmentation of Redox Signaling. *Antioxidants & Redox Signaling. 11*, 1357-1372.

152. Jiskoot, W., Teerlink, T., Beuvery, E. C., and Crommelin, D. J. A. (1986) Preparation of Liposomes Via Detergent Removal from Mixed Micelles by Dilution. *Pharm. Weekbl. 8*, 259-265.

153. Akrap, N., Seidel, T., and Barisas, B. G. (2010) Förster Distances for Fluorescence Resonant Energy Transfer between mCherry and Other Visible Fluorescent Proteins. *Anal. Biochem. 402*, 105-106.

154. Blackman, S. M., Piston, D. W., and Beth, A. H. (1998) Oligomeric State of Human Erythrocyte Band 3 Measured by Fluorescence Resonance Energy Homotransfer. *Biophys. J. 75*, 1117-1130.

155. Sharma, P., Varma, R., Sarasij, R. C., Ira, , Gousset, K., Krishnamoorthy, G., Rao, M., and Mayor, S. (2004) Nanoscale Organization of Multiple GPI-Anchored Proteins in Living Cell Membranes. *Cell. 116*, 577-589.

156. Day, R. N., and Davidson, M. W. (2009) The Fluorescent Protein Palette: Tools for Cellular Imaging. *Chem. Soc. Rev. 38*, 2887-2921.

157. Dennis, A. M., Sotto, D. C., Mei, B. C., Medintz, I. L., Mattoussi, H., and Bao, G. (2010) Surface Ligand Effects on Metal-Affinity Coordination to Quantum Dots: Implications for Nanoprobe Self-Assembly. *Bioconjugate Chem. 21*, 1160-1170.

158. Shaner, N. C., Campbell, R. E., Steinbach, P. A., Giepmans, B. N. G., Palmer, A. E., and Tsien, R. Y. (2004) Improved Monomeric Red, Orange and Yellow Fluorescent Proteins Derived from Discosoma Sp. Red Fluorescent Protein. *Nat Biotech. 22*, 1567-1572.

159. Fleming, K. G., Ren, C., Doura, A. K., Eisley, M. E., Kobus, F. J., and Stanley, A. M. (2004) Thermodynamics of Glycophorin A Transmembrane Helix Dimerization in C14 Betaine Micelles. *Biophys. Chem. 108*, 43-49.

160. Fisher, L. E., Engelman, D. M., and Sturgis, J. N. (2003) Effect of Detergents on the Association of the Glycophorin A Transmembrane Helix. *Biophys. J. 85*, 3097-3105.

161. Smith, S. O., Song, D., Shekar, S., Groesbeek, M., Ziliox, M., and Aimoto, S. (2001) Structure of the Transmembrane Dimer Interface of Glycophorin A in Membrane Bilayers. *Biochemistry. 40*, 6553-6558.

162. Sarabipour, S., and Hristova, K. (2013) Glycophorin A Transmembrane Domain Dimerization in Plasma Membrane Vesicles Derived from CHO, HEK 293T, and A431 Cells. *Biochim. Biophys. Acta. 1828*, 1829-1833.

163. Russ, W. P., and Engelman, D. M. (2000) The GxxxG Motif: A Framework for Transmembrane Helix-Helix Association. *J. Mol. Biol. 296*, 911-919.

164. Fleming, K. G., and Engelman, D. M. (2001) Specificity in Transmembrane Helix-Helix Interactions can Define a Hierarchy of Stability for Sequence Variants. *Proc. Natl. Acad. Sci. U. S. A. 98*, 14340-14344.

165. Lemmon, M. A., Flanagan, J. M., Hunt, J. F., Adair, B. D., Bormann, B. J., Dempsey, C. E., and Engelman, D. M. (1992) Glycophorin A Dimerization is Driven by Specific Interactions between Transmembrane Alpha-Helices. *J Biol Chem. 267*, 7683-9.

166. Mingarro, I., Whitley, P., Lemmon, M. A., and von Heijne, G. (1996) Ala-Insertion Scanning Mutagenesis of the Glycophorin A Transmembrane Helix: A Rapid Way to Map Helix-Helix Interactions in Integral Membrane Proteins. *Protein Sci. 5*, 1339-1341.

167. Fleming, K. G., Ackerman, A. L., and Engelman, D. M. (1997) The Effect of Point Mutations on the Free Energy of Transmembrane Alpha-Helix Dimerization. *J Mol Biol. 272*, 266-75.

168. Smart, E. J., Graf, G. A., McNiven, M. A., Sessa, W. C., Engelman, J. A., Scherer, P. E., Okamoto, T., and Lisanti, M. P. (1999) Caveolins, Liquid-Ordered Domains, and Signal Transduction. *Mol. Cell. Biol. 19,* 7289-7304.

169. Tang, X., Wang, Y., Li, D., Luo, J., and Liu, M. (2011) Orphan G Protein-Coupled Receptors (GPCRs): Biological Functions and Potential Drug Targets. *Acta Pharmacol. Sin. 33,* 363-371.

170. Molina, D. M., Cornvik, T., Eshaghi, S., Haeggstrom, J. Z., Norland, P., and Sabet, M. I. (2008) Engineering Membrane Protein Overproduction in Escherichia Coli. *Protein Science. 17,* 673-680.

171. Shepherd, F. H., and Holzenburg, A. (1995) The Potential of Fluorinated Surfactants in Membrane Biochemistry. *Anal. Biochem. 224*, 21-27.

172. Plucinsky, S. M., Root, K. T., and Glover, K. J. (2018) Efficient Solubilization and Purification of Highly Insoluble Membrane Proteins Expressed as Inclusion Bodies using Perfluorooctanoic Acid. *Protein Expr. Purif. 143*, 34-37.

173. Rosano, G. L., and Ceccarelli, E. A. (2014) Recombinant Protein Expression in Escherichia Coli: Advances and Challenges. *Frontiers in Microbiology. 5,* 172.

174. Hwang, P. M., Pan, J. S., and Sykes, B. D. (2014) Targeted Expression, Purification, and Cleavage of Fusion Proteins from Inclusion Bodies in Escherichia Coli. *FEBS Lett. 588*, 247-252.

175. Kyte, J., and Doolittle, R. F. (1982) A Simple Method for Displaying the Hydropathic Character of a Protein. *J. Mol. Biol. 157,* 105-132.

176. Burns, D. C., Ellis, D. A., Li, H., McMurdo, C. J., and Webster, E. (2008) Experimental pKa Determination for Perfluorooctanoic Acid (PFOA) and the Potential Impact of pKa Concentration Dependence on Laboratory-Measured Partitioning Phenomena and Environmental Modeling. *Environ. Sci. Technol. 42*, 9283-9288.

177. Goss, K. (2008) The pKa Values of PFOA and Other Highly Fluorinated Carboxylic Acids. *Environ. Sci. Technol. 42,* 456-458.

178. Hoffmann, A., and Roeder, R. G. (1991) Purification of His-Tagged Proteins in Non-Denaturing Conditions Suggests a Convenient Method for Protein Interaction Studies. *Nucleic Acids Res. 19,* 6337-6338.

179. Allen, T. M., Romans, A. Y., Kercret, H., and Segrest, J. P. (1980) Detergent Removal during Membrane Reconstitution. *Biochim. Biophys. Acta. 601,* 328-342.

Sarah M. Plucinsky

Department of Chemistry Lehigh University

Education

Bachelor of Science in Chemistry May 2011
Wagner College, GPA 3.55
Staten Island, NY
Advisor: Maria Gelabert, Ph.D.

Master of Science in Chemistry May 2013
Lehigh University, GPA 3.6
Bethlehem, PA
Advisor: Kerney J. Glover Ph.D.

Ph. D. in Chemistry January, 2018
Lehigh University,
Bethlehem, PA
Advisor: Kerney J. Glover Ph.D.

Research Experience

Undergraduate Research
Professor Roy Mosher, Ph.D. (Deceased): Wagner College, Staten Island, NY

- Worked on cloning the JadK gene found within streptomycine venezula using a vector within E.coli to over-express the gene. The gene was then used for medicinal purposes

Shire HGT- QC Cell Biology Intern Summer 2010
Butch Beckmann, Shire HGT: Waltham MA.

- Worked with the cell biology group to test drug substance and drug product samples using ELISA and Western blots

Lehigh University-Glover Lab Summer 2011
Professor K. Jebrell Glover, Ph.D.: Lehigh University, Bethlehem, PA

- Assisted on a project to determine the location of the putative membrane turn within caveolin-1 using site directed mutagenesis and NMR spectroscopy.

Dissertation August 2011-January 2018
Professor K. Jebrell Glover, Ph.D.: Lehigh University, Bethlehem, PA

- The main focus of this research was to use biophysical techniques to characterize the integral membrane protein caveolin-1. By using solution state NMR techniques and circular dichroism spectroscopy, the secondary structure of a functional construct was assigned. Additionally, alanine scanning mutagenesis

was employed to investigate the role of specific residues for the overall structure and function of caveolin-1. The overall goal of this research was to deepen the understanding of caveolin-1 structure, function and topology which will allow for further investigation into the proteins physiological role.

Technical Skills

- PCR, primer design, DNA sequencing, Site-directed mutagenesis
- Western blot and SDS-PAGE
- Membrane protein expression, purification, reconstitution
- Protein construct design
- NMR spectroscopy of membrane proteins
- Chromatography: RP-HPLC, Affinity Chromatography
- MALDI-TOF mass spectrometry
- Analytical Ultracentrifugation
- Circular Dichroism Spectroscopy
- Various protein labeling techniques
- Enzymatic assay design

Teaching experience

Teaching Assistant Fall 2011-Spring 2013**,** Spring 2014-Sping 2016

- Courses: Organic Chemistry I Lab, Fall 2011; Organic Chemistry II Lab Spring 2012; General Chemistry I Lab, Fall 2012; Organic Chemistry II Lab Spring 2013; General Chemistry I Lab Spring 2014; General Chemistry I Lab Fall 2014; General Chemistry I Lab Spring 2015; Organic Chemistry I Lab, Fall 2015; General Chemistry II Lab, Spring 2016

Publications

Sarah M. Plucinsky and Kerney Jebrell Glover. (2015). "Secondary Structure Analysis of a Functional Construct of Caveolin-1 Reveals a Long C-terminal Helix" *Biophysical Journal.* 2015, 109, 8, 1686-1688.

Kyle T. Root*, Sarah M. Plucinsky* and Kerney Jebrell Glover. (2015) "Recent Progress in the Topology, Structure and Oligomerization of Caveolin-1: A Building Block of Caveolae" *Current Topics in Membranes.* 75:305-36.
** Co-first author*

Sarah M. Plucinsky, Kerney J. Glover,(2017) "The C-terminal domain of caveolin-1 and pulmonary arterial hypertension: An emerging relationship". *Journal of Rare Disease Research and Treatment* 2(3): 44-48

Sarah M. Plucinsky, Kyle T. Root, and Kerney Jebrell Glover (2018). "Efficient solubilization and purification of highly insoluble membrane proteins expressed as inclusion bodies using perfluorooctanoic acid. *Protein expression and purification.*143: 34-37.

Sarah M. Plucinsky, Sophia A. Miotto, Maxim Chudaev, and Kerney Jebrell Glover (2017) "Effect of cholesterol on the oligomeric state of caveolin-1 reconstituted into lipid bilayers: An in vitro homo-FRET analysis". *Manuscript in preparation*.

Presentations

Delaware Membrane Protein Symposium
University of Delaware, Newark, DE May 2012
Poster entitled "Probing the structure of caveolin-1"

Federation of American Societies for Experimental Biology (FASEB)
"Molecular Biophysics of Membranes" June 2012
Poster entitled "Probing the structure of caveolin-1"

Bimolecular Structure, Dynamics, and Function: Membrane Proteins
Vanderbilt University, Nashville, TN May 2014
Poster entitled "Caveolin revealed: A mutagenesis study of caveolin-1"

Federation of American Societies for Experimental Biology (FASEB)
"Molecular Biophysics of Membranes" June 2014
Poster entitled "Caveolin revealed: A mutagenesis study of caveolin-1"

59th Annual Biophysical Society Meeting
Baltimore, Maryland February 2015
Poster entitled "Caveolin revealed: A mutagenesis study of caveolin-1"

Graduate Open House Lehigh University Annually since 2012
Presented several Posters: "Probing the structure of caveolin-1";
"Caveolin revealed: A mutagenesis study of caveolin-1";
"Secondary Structure analysis of caveolin-1"

Gordon Research Conference June, 2017
Stonehill College, Easton, MA
Membrane Protein Folding: Folding Biophysics, Design, and Stabilization with Applications to Disease
Poster entitled: "Biophysical Characterization of Caveolin-1"

Panel Discussions

Grad Study in STEM Disciplines: What? Why? How? When?
Lehigh University, Bethlehem PA November 11, 2014

- Answered questions about graduate studies in the STEM from undergraduate students

Graduate Student Admit weekend
Lehigh University, Bethlehem, PA February 27, 2016

- Panel discussion about the Chemistry graduate program at Lehigh University

Workshops

Rosetta Membrane Workshop April 2014
Vanderbilt University, Nashville, TN

- Attendee: Workshop on using computational modeling for membrane protein structure.

Awards

Lehigh University Chemistry Departmental Fellowship May 2016-May2017